

Alma Mater Studiorum - Università di Bologna

**DOTTORATO DI RICERCA
in CHIMICA
Ciclo XXIX**

Settore Concorsuale di afferenza: 03/A2

Settore Scientifico disciplinare: CHIM/02

**Conformational equilibria landscapes:
rotational spectroscopy and modeling
of isolated molecular systems**

CANDIDATA

Annalisa Vigorito

RELATORE

Dott.ssa Assimo Maris

COORDINATORE DOTTORATO

Chiar. mo prof. Aldo Roda

Esame finale anno 2017

MOTIVATION & ABSTRACT

One of the final target of a chemist is to design a molecule or a supramolecular system that have all features needed to perform a function in efficient and specific fashion.

For instance, in medicinal chemistry, an ideal drug must be effective, not toxic and devoid of side effects. To have these features, a ligand must have great affinity for a biological receptor, depending on the complementary of both the shape and electronic feature distributions of the binding site and the ligand.

To design a drug, that satisfy these requisites, molecular designers need exhaustive information on the energetic and structural factors that drive the conformational preferences at both free and bound states. These information can be inferred from structural analysis of molecules or model molecular systems.

Rotational spectroscopy analysis combined to theoretical methods provide a synergic approach to investigate, in detail, the structure and internal dynamics of both isolated molecules and weakly bound complexes.

In free-jet rotational spectroscopy, the experimental measurements are done by microwave and millimeter wave spectrometers operating in the unperturbed environment of a jet plume. While the interpretation of the experimental data is performed by theoretical methods that use semi rigid and coupled Hamiltonians, ab initio and DFT calculations and flexible models.

The rotational spectra are highly sensitive to the atomic masses distribution, so conformational and tautomeric equilibria and isotopologues species can be investigated.

Regarding internal dynamics, useful information, are obtained, when hyperfine structures, due to the tunnel effect, are observed in the spectra. Owed to these information, it is possible to model the potential energy surface governing these motions.

Furthermore, millimetre wave spectroscopy contributes significantly to the astrochemistry research area. A lot of information on circumstellar and interstellar medium results from the study of the electromagnetic radiation that reaches us. High resolution and sensitive radio-astronomy tools such as the telescopes Atacama Large Millimeter/submillimeter Array (ALMA), Herschel Space Observatory for the Far-Infrared, have been built to pick up these radiations. Laboratory rotational spectroscopy provides the basic physical parameters necessary for interpreting the astronomical spectra.

During my PhD, several molecules and weakly bound complexes have been characterized using the rotational spectroscopy technique and theoretical calculations.

The most of my work has been performed in the laboratory of rotational spectroscopy at UNIBO, while some objectives have been analyzed in the course of my visit at laboratory of prof. Sanz in

King's College Department in London.

Some of the studied systems will be deepened in the course of this thesis, while others, already published, will not be discussed further.

Below, the abstracts of the molecular systems described in this thesis are reported.

CHAPTER 1

MILLIMETER WAVE SPECTRUM OF 1,2-BUTANEDIOL: STRUCTURE, DYNAMICS AND IMPLICATIONS FOR ASTRONOMICAL SEARCH

Linear diols are substances of astrochemistry and biology interest. Ethylene glycol, the smallest member of this class, has been observed in several sections of interstellar species and it is highly possible that hydroxylated compounds with increasing carbon atom number could be synthesized on the parent bodies of the carbonaceous meteorites.

Rotational investigations on 1,2-butanediol provide the sets of spectroscopy parameters needed to verify its presence in the planetary atmosphere.

The conformational space of 1,2-butanediol was explored through the broadband rotational spectrum in the 59.6-103.6 GHz frequency range and density functional theory methods.

Six of the twenty-four more stable conformers, were identified. All of them are characterized by an intramolecular hydrogen bond between the hydroxyl groups. The identification of ^{13}C and deuterated isotopologues has allowed the determination of the structural parameters of the most abundant conformation.

CHAPTER 2

THE ROTATIONAL SPECTRUM OF 1,4-BUTANEDITHIOL

Although thiols are considered sulfurated analogues of diols, their properties change significantly due to the size, electronegativity and polarizability differences between oxygen and sulfur atoms. These differences affect also on conformational flexibility of molecules belonging to the two classes. In the case of 1,4-butanediol, the conformational preferences are driven from the formation of an intramolecular hydrogen bond between hydroxyl groups. While in 1,4-butanedithiol this interaction is not present and as a consequence the population is spread on a large number of conformers. Four of fifty-nine calculated conformers were identified.

CHAPTER 3

THE SHAPES OF SULFONILAMIDE: THE ROTATIONAL SPECTRA OF BENZENESULFONAMIDE, *ortho*-TOLUENSULFONAMIDE and *para*-TOLUENSULFONAMIDE

Compounds of the Sulfonamides class, in particular those containing the benzosulfonamide group, are of extreme interest in biologic field since many of them are active against a variety of diseases. In our work, structural investigations were done on pharmacophore group benzensulfonamide and its derivatives *para*-toluensulfonamide and *ortho*-toluensulfonamide

This study shows as weak intramolecular interactions are able to change the conformational preferences of the pharmacophore group.

In the compounds, benzensulfonamide and *para*-toluensulfonamide, where, there are not groups close to the sulfonamide tail, the conformational behaviour is similar. In both cases, the amino group lies perpendicular respect to the aromatic plane.

Instead in OTS, where a weak attractive interaction between the nitrogen lone pair and the methyl hydrogen atoms takes place, the amino group lies in *gauche*.

For the three species, the ^{14}N quadrupole coupling constants were assigned. In addition, for *ortho*-toluensulfonamide, also the methyl group rotation barrier was determined.

CHAPTER 4

INTERNAL DYNAMICS IN PHARMACOPHORE GROUPS: THE ROTATIONAL SPECTRA OF 2-PYRROLIDINONE AND 2-IMIDAZOLIDINONE

The lactams 2-imidazolidinone and 2-pyrrolidinone, show a pharmacological activity and are often inserted within drugs because they allow to control both the flexibility and electronic distribution of the molecular systems.

Since the biological interest toward these compounds, a detailed analysis on their structures and dynamics was undertaken.

The spectra of 2-imidazolidinone and 2-pyrrolidinone showed hyperfine structures, due to tunnel effect. These splittings revealed the existence of two twisted ring equivalent conformations connected by an inversion ring motion.

For 2-pyrrolidinone, the potential energy surface governing the motion was determined theoretically. The achieved double minimum potential energy surface show that the motion takes place through a planar transition state, lying at 2.63 kJ mol⁻¹.

While for IMI, the potential energy surface was modelled semi-experimentally using the Meyer's 1D-flexible model. To describe the interconversion between the two equivalent structures, two plausible paths were hypothesized: an inversion motion and pseudorotation motion.

CHAPTER 5

EXPLORING THE CONFORMATIONAL LANDSCAPE OF TERPENOID SYSTEMS: A MICROWAVE STUDY OF S-(-)-PERILLALDEHYDE

Terpenoids, have shown several biological properties. Detailed analysis of their structures could be helpful to elucidate the mechanism of action in the biological processes in which they are involved. In my case, the terpenoid, s-(-)-perillaldehyde, was analyzed.

In the spectrum of perillaldehyde, two equatorial and one axial conformational species were identified. The analysis of relative abundance between the species showed that the conformational equilibrium is sharply shifted toward the equatorial species.

The spectra of all ten ¹³C isotopologues species were identified for the two equatorial conformers. For one of two conformers, the experimental structure, using Kraitchman's substitution method, was determined.

CHAPTER 6

MILLIMETER WAVE SPECTRUM OF THE ACRYLONITRILE-METHANOL WEAKLY BOUND MOLECULAR COMPLEX

Investigations of gas phase molecular complexes by high resolution spectroscopic techniques provide accurate structural and dynamical information which can serve as a useful guide in the modeling intermolecular interactions.

For the acrylonitrile-methanol complex, the 1:1 adduct was characterized.

The complex shows a planar ring shaped geometry in which the two subunits are held together by two hydrogen bonds: a main OH_{CH₃OH}—N_{ACN} interaction and a weaker O_{CH₃OH} —HC_{ACN}

interaction. The methanol methyl group rotation barrier was determined. As observed, in other methanol complexes the barrier value was found lower than that observed for bare methanol methyl group rotation.

CHAPTER 7

MICROSOLVATION OF BIOMOLECULES

The microsolvation of biomolecules provides information on the water preferred binding sites in biology environments and a likely picture of first shell of solvation process in biology environments.

1) THE ROTATIONAL SPECTRUM OF MONOHYDRATE AND BIHYDRATE S-(-)-PERILLALDEHYDE

In the spectrum of s-(-)-perillaldehyde-water, the monohydrates and dehydrates clusters of the two equatorial species, observed for perillaldehyde monomer, were found.

Regarding the monohydrates clusters, three conformations were identified. All species show a ring-shaped geometry in which the two subunits are held together through two intermolecular bonds: a main hydrogen bond, $C=O_{\text{PERY}}-H_{\text{H}_2\text{O}}$, and a weaker interaction between the $CH_{\text{PERY}}-O_{\text{H}_2\text{O}}$.

For dehydrates clusters, two conformations are observed. These structures can be considered as the result of the one water molecule addition to two of the observed monohydrate clusters.

The observed structural differences in the hydrogen bond network between the, corresponding, heterodimers and heterotrimers prove the existence of cooperative effects in hydrogen bonded complexes.

2) MICROSOLVATION OF HETEROCYCLIC RINGS: THE ROTATIONAL SPECTRA OF IMIDAZOLIDINONE-WATER, PYRROLIDINONE-WATER AND OXAZOLIDINONE-WATER COMPLEXES

This study can be considered an excellent model for explaining the water binding preferences in proteins. In three molecular systems, imidazolidinone-water, pyrrolidinone-water and oxazolidinone-water, the water close a cycle with the amide group. The two subunits are held through two hydrogen bonds: $C=O-HO_{\text{H}_2\text{O}}$ and $NH-O_{\text{H}_2\text{O}}$, respectively. In spectrum of

oxazolidinone-water, the hyperfine structure due to the combination of ring and water inversion motions was observed. From the analysis of the tunneling splittings, the spacing between the vibrational energy sublevels was determined.

LIST OF PUBLICATIONS:

- A. Vigorito, L. Paoloni, C. Calabrese, L. Evangelisti, L. B. Favero, S. Melandri, A. Maris “Structure and Dynamic of Cyclic Amides: The Rotational Spectrum of 1,3-Dimethyl-2-imidazolidinone”, submitted paper.
- W. Li, A. Vigorito, C. Calabrese, L. Evangelisti, L. Favero, A. Maris, S. Melandri, “The microwave spectroscopy study of 1,2-dimethoxyethane”, DOI: [10.1016/j.jms.2017.02.015](https://doi.org/10.1016/j.jms.2017.02.015).
- A. Vigorito, C. Calabrese, E. Paltanin, S. Melandri, A. Maris “Regarding on the torsional flexibility of the dyhydrolipoic acid’s pharmacophore: 1,3-propanedithiol”, *Phys. Chem. Chem. Phys.* 2017, 19, 496-502.
- C. Calabrese, A. Vigorito, A. Maris, S. Mariotti, P. Fathi, W. Geppert, S. Melandri “Millimeter wave spectrum of the weakly bound complex CH₂=CHCN-H₂O:Structure, Dynamics, and implications for astronomical search”, *J. Phys. Chem. A.*, 2015, 119, 11674-11682.
- Vigorito, Q. Gou, C. Calabrese, S. Melandri, A. Maris, W. Caminati “How CO₂ interacts with carboxylic acids: a rotational study of formic acid-CO₂”, *Chem. Phys. Chem.*, 2015, 16, 2961-2967.
- C. Calabrese, A. Vigorito, G. Feng, L. Favero, A. Maris, S. Melandri, W.D. Geppert, W. Caminati, “ Laboratory rotational spectrum of acrylic acid and its isotopologues in the 6-18.5 GHz and 52-74.4 GHz frequency ranges”, *J. Mol. Spectr.*, 2014, 295, 37-43.

ACKNOWLEDGEMENTS

The rotational spectroscopy group in UNIBO is an enjoyable place to work, for this reason I wish to express my deep grateful to all members of group: prof. Sonia Melandri, prof. Walter Caminati, prof. Assimo Maris, dott. Camilla Calabrese, dott. Luca Evangelisti, and dott. L. B. Favero.

In particular, I'm very grateful to prof. Assimo Maris for all imparted teachings in the course of these three year and her deep humanity.

CHAPTER 1

MILLIMETER WAVE SPECTRUM OF 1,2-BUTANEDIOL: STRUCTURE, DYNAMICS AND IMPLICATIONS FOR ASTRONOMICAL SEARCH

Introduction

Linear diols are organic compounds of great relevance in biological, chemical and astrophysical field.

Owed to their amphipathic character and capability to form hydrogen bonds, diols play a fundamental role in biological field [1]. The two hydroxyl groups provide an exceptional hydrophilic character to diols systems, while the carbonaceous chain length adjusts their lipophilicity, conferring to diols analogue properties to some biological macromolecules. For this reason, they can be used for instance as building block in drugs. Another use of linear diols is in cryobiology where they have the role of cryoprotectant agent [2]. The cryobiology techniques have the aim to preserve the biological organs undergoing them at very low temperature. Cryoprotectant agents avoid the crystallization of water molecules within the biological tissues. The Diols, interacting with these water molecules through hydrogen bonds, disturb the crystallization process, inducing the formation of an amorphous solid state [3].

However linear diols are also an interest topic in astrochemistry. Diols are considered sugar alcohols and for this reason they are retained key organic species associated with the prebiotic synthesis of the sugars [4]. Ethylene glycol, the smallest member of diols class, has been found in several sections of the planetary atmosphere and it is retained highly possible that hydroxylated compounds and relative sugars with increasing carbon atoms number could be synthesized on the parent bodies of the carbonaceous meteorites [4]. 1,2-Ethenediol was detected in the massive and luminous Galactic center source Sagittarius B2(N) and Large Molecule Heimat Sgr B2(N-LMH) [4]. There is also strong evidence of 1,2-ethenediol in three less-evolved molecular clouds in the Galactic center [5]. Very recently, it was also detected in the hot corinos associated with the class 0 protostars NGC 1333-IRAS2A [6] and, tentatively, IRAS 16293-2422B [7]. Finally, 1,2-ethenediol was also found to be abundant in the outflows of comet Hale-Bopp [8].

In this work the conformational and dynamic behavior of a linear diol, 1,2-butanediol (hereafter BD), has been investigated by rotational spectroscopy and theoretical calculations. In addition in this study are also provided useful data to verify the presence of BD in the interstellar and circumstellar media.

A lot of information on the planetary atmosphere results from the study of the electromagnetic

radiation that reaches us. High resolution and sensitive radio-astronomy tools such as the telescopes Atacama Large Millimeter/submillimeter Array (ALMA), Herschel Space Observatory for the Far-Infrared, have been built to pick up these radiations.

Gas phase species in interstellar and circumstellar media emit millimeter and sub-millimeter spectra.

The rotational spectroscopy laboratory data allow to decode these information leading to qualitative and quantitative identification of the species.

From a structural point of view, linear diols are flexible molecules and their conformational landscape is enriched with increasing carbon atoms number. So far, all isomers of diols with chains lengths from C₂ to C₄ [9-14] except BD and 2,3-butanediol have been investigated by rotational spectroscopy. The rotational spectra of these systems reveal that although diols may exist in several distinct conformations, only the ones which exhibit an intramolecular hydrogen bond between the two hydroxyl groups (OH \cdots O) are stable. In addition in diols in which the two hydroxyl groups are bound to chain terminal Carbon atoms, also the potential energy governing the large amplitude motions due to the torsion of OH groups was described.

Experimental section

BD (purity 98%, molecular weight 90.121 g/mol) was purchased from Sigma-Aldrich and used without any further purification. The deuterated species for BD were obtained by passing D₂O in Ar over the sample. Both argon and helium, purchased from SIAD, were used as carrier gas. BD appears as a colorless, viscous liquid at ambient conditions. The melting point is -50 °C and the boiling point is 191-192 °C. The sample was heated to about 80 °C and a stream of the carrier gas (argon $P_0=20$ kPa or helium $P_0=40$ kPa) was flowed over it and then expanded to about $P_b=0.5$ Pa through a 0.3 mm diameter pinhole nozzle. The data reported in Steele et al. [15] and Verevkin [16] were used to extrapolate the BD vapour pressure at the working temperature: 0.545 kPa at 80°C. In this way the concentration of BD is estimated to be around 2.7% and 1.4% in argon and helium, respectively. Rotational spectra in the millimeter wave region (59.6-103.6 GHz) were recorded using a Stark-modulated free-jet absorption spectrometer. Details about the experimental setup can be found in ref. 17, 18, 19. The spectrometer has a resolution of about 300 kHz and an estimated accuracy of about 50 kHz.

Table 1: Theoretical results for 24 hydrogen bonded conformers of BD

	ΔE (kJ/mol)	A (MHz)	B (MHz)	C (MHz)	μ_a (D)	μ_b (D)	μ_c (D)
g'G'Ag	1.3	7826	1912	1664	0.3	1.9	1.6
aG'Ag	0.0	7838	1929	1674	1.4	2.0	0.5
gG'Aa	0.8	7682	1919	1659	2.8	0.2	0.4
gG'Ag'	2.8	7552	1917	1662	2.2	0.6	1.6
g'G'G'g	4.4	5503	2222	1713	0.8	2.1	1.3
aG'G'g	3.2	5535	2243	1722	0.2	2.5	0.8
gG'G'a	3.0	5427	2250	1715	2.5	1.4	0.5
gG'G'g'	4.7	5365	2258	1716	2.4	0.6	1.5
g'G'Gg	5.6	5958	2162	1906	0.3	1.4	1.9
aG'Gg	4.4	6017	2173	1911	0.8	2.4	0.2
gG'Ga	5.2	5870	2171	1895	2.4	1.0	1.0
gG'Gg'	8.3	5866	2156	1883	2.8	0.5	0.7
g'GAg	5.1	5948	2184	1915	0.7	1.3	1.9
g'GAa	3.8	5952	2182	1913	2.4	0.5	0.9
aGAg'	4.7	5985	2188	1925	1.8	1.6	0.9
aGAg'	5.8	6004	2158	1899	0.3	2.5	0.4
g'GG'g	6.6	4342	2700	2012	0.2	1.2	2.0
g'GG'a	3.8	4410	2666	2002	1.8	1.7	0.5
aGG'g'	6.4	4407	2668	2010	0.2	2.4	0.8
gGG'g'	8.3	4445	2608	1978	1.9	2.0	0.1
g'GGg	13.4	4153	2899	2353	0.2	2.1	1.2
g'GGa	10.8	4155	2906	2342	1.8	1.8	0.8
aGGg'	12.6	4183	2882	2347	1.5	1.6	1.5
aGGg'	13.8	4193	2858	2316	1.1	1.9	1.5

Theoretical conformational landscape and spectroscopic properties of 1, 2-butanediol

The structural landscape of BD is defined by the conformational arrangement and the configuration with respect to the stereogenic center *C2 (figure 1). Due to the presence of the chiral center two specular forms, R and S enantiomers, can exist. To simplify the discussion, hereinafter we will refer only to the R configuration since by conventional spectroscopy experiments the enantiomers cannot be distinguished.

The conformational arrangement is defined by four dihedral angles: two of them are relative to the backbone atoms arrangements (OCCO and CCCC), the other two describe the orientations of the hydroxyl groups (HOCC and CCOH). While the rotation of the methyl group does not contribute to the conformational space because it has C_{3V} local symmetry for which the rotation give rise to three equivalent minima. However it could lead to characteristic tunneling splittings if the corresponding barrier is sufficiently low.

Because of steric hindrance, only three staggered positions are possible for each dihedral angles (namely anti, gauche and gauche') giving place to a total $3^4=81$ possible rotamers. In this study the rotamers are identified by combinations of four letters (xXXX). The letters are related with the values of the dihedral angles: g/G (c.a. 60°) and g'/G' stand for gauche (c.a. -60°), t/T (c.a. 180°)

stand for trans. The capital letters (T, G, G') refer to the skeletal backbone atoms, while the lower-case letters (t, g, g') describe the positions of the OH groups.

Depending on the backbone orientation, the structures belong to nine "skeletal families": AA, AG, AG', GA, GG, GG', G'A, G'G and G'G'. Considering also the position of the two hydroxyl hydrogen atoms, each family has nine conformers. To have an overview of the conformers stability and internal rotation pathways, the internal rotation coordinates of the hydroxyl groups (HOCC and CCOH) for each family were explored. In this analysis we assumed that the reorientation of the hydroxyl hydrogen atoms does not induce a conformational change in the backbone structure. The PESs were calculated at B3LYP/6-311++G(d,p) level of theory, using the Gaussian 09 quantum chemistry package [20], whereas all the other internal coordinates were freely optimized. The optimizations were achieved for all families except for that GG, because in this case the rotation of the hydroxyl groups induced the rearrangement from GG to G'G. The obtained PESs are reported in Figure 2 as contour level maps.

Depending on the relative positions of the oxygen atoms, described by the OCCO dihedral angle, two kinds of behaviors can be distinguished. For the AA, AG, AG' families ($\text{OCCO} \approx 180^\circ$), where the hydroxyl groups cannot interact, all nine minima are present. Instead for those ones GA, GG', G'A, G'G and G'G' ($\text{OCCO} \approx \pm 60^\circ$), the almost "regular" landscape shown by the AX forms is strongly modified by the interaction between the hydroxyl groups. Twenty-four structures, showed in figure 1, are stabilized by the formation of an intramolecular hydrogen bond, whereas the remaining ones are destabilized by the repulsive interaction between the hydroxyl hydrogen atoms or between the oxygen lone pairs. It is worth noting that there are two kinds of hydrogen bond, depending on the proton donor or acceptor role of the two involved hydroxyl groups. In all GY and G'Y species the two more stable conformers exhibit the hydroxyl group acting as proton acceptor in anti with respect to the CC bond: in G'Y the lowest energy minimum is ag (OH proton acceptor) followed by ga (OH proton donor), whereas in GY the role of the hydroxyl groups is reversed and the lowest energy minimum is g'a (OH proton donor) followed by ag' (OH proton acceptor). In both GY and G'Y species the third and fourth minima are g'g (OH proton acceptor) and gg' (OH proton donor), respectively. The twenty-four most stable structures indicated from the PESs were furthermore optimized at the B3LYP/aug-cc-pVTZ level of calculation. Subsequent harmonic frequency calculations confirmed that the optimized geometries correspond to energetic minima. The obtained spectroscopic parameters and the relative electronic energies (kJ mol^{-1}) for twenty-four conformers are reported in table 1.

In addition the PESs in figure 2 indicated that the barriers connecting the hydrogen bonded species are between 1.5 and 4.8 kJ mol^{-1} , thus, according to Ruoff et al. [21], relaxation processes which

convert high energy conformers to more stable species can be expected during supersonic expansion experiments.

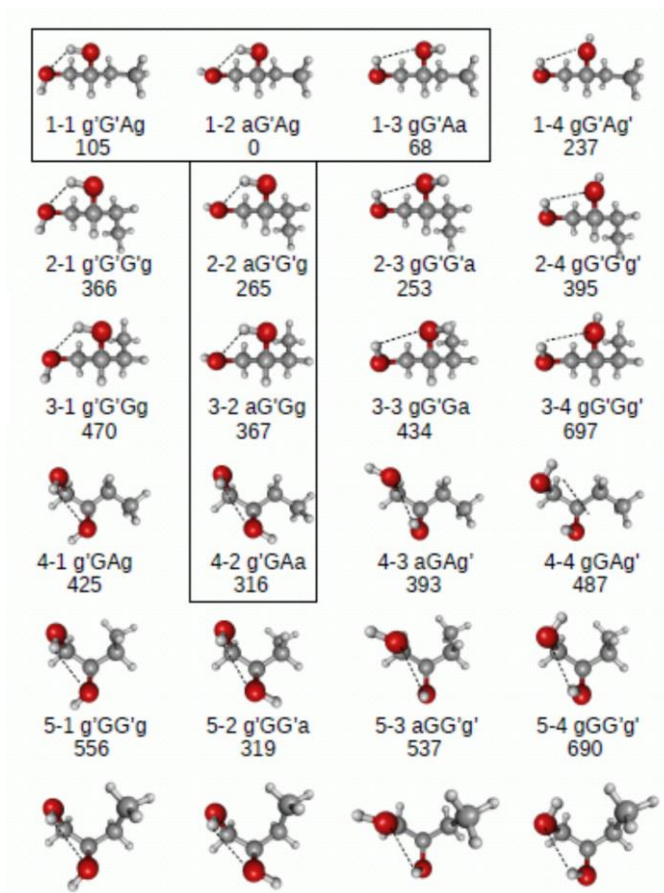


Figure 1: Calculated geometries and relative electronic energies (cm^{-1} , B3LYP/6-311++G(d,p)) of the 24 hydrogen-bonded conformers of R-BD.

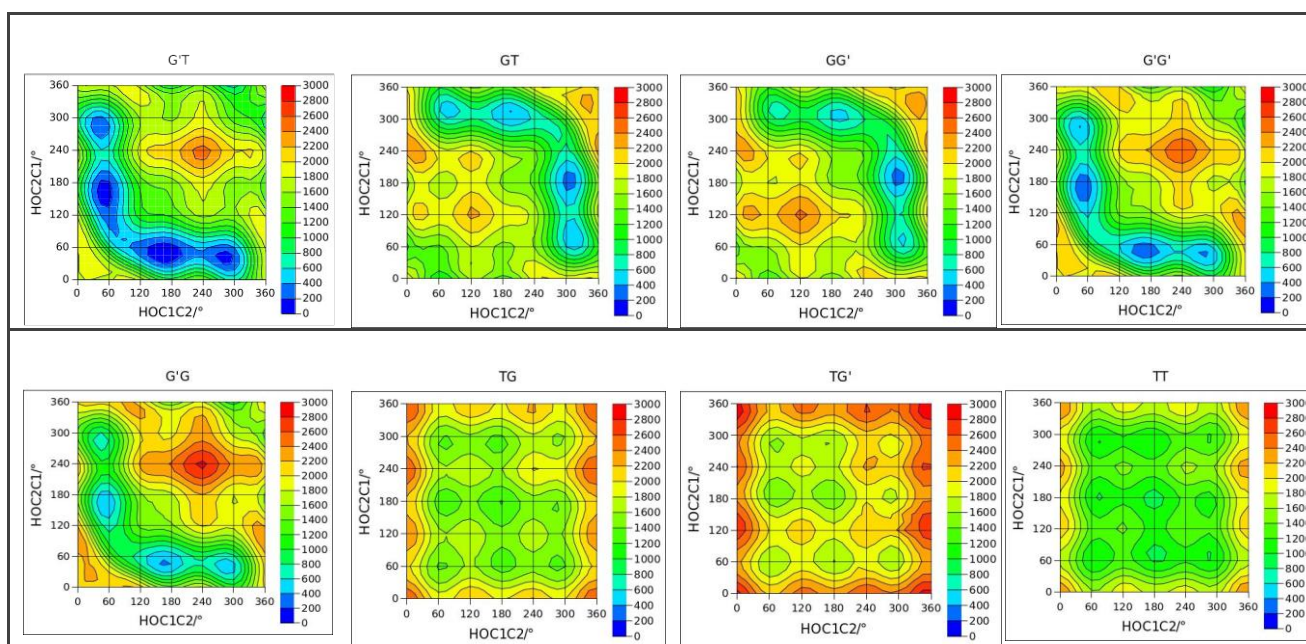


Figure 2: Theoretical 2D sections of the conformational PES (cm^{-1}) of BD.

Results

Rotational spectrum

To have an overview of the BD rotational spectrum, two fast scans were recorded in the 59.6-74.4 GHz frequency range using both argon and helium as carrier gas. In addition for the most stable conformers the experimental measures were extended furthermore up to 103.6 GHz in order to facilitate the identification of BD in the planetary atmosphere. The spectra appear in both cases very dense, reflecting the presence of several species. However many peaks are partially or totally depleted in argon suggesting that relaxation processes occur upon supersonic expansion. This is often observed when the barriers connecting different minima are of the order of $2kT$.

On the basis of the theoretical rotational constants, dipole moments, relative energies and interconversion barriers, the spectra of six species, aG'Ag, g'G'Ag, gG'Ag, aG'G'g, aG'Gg and g'GAa, were assigned. The obtained experimental spectroscopic parameters are reported in table 2. All measured transition lines were fitted to Watson's S -reduced semirigid asymmetric rotor Hamiltonian using the SPFIT program [22, 23].

In agreement both with the quantum mechanical results, that predict the aG'Ag conformer to be the global minimum, and the experimental findings on 1,2-ethanediol and 1,2-propanediol for which the common atom frame of the stablest form has the same shape (a G'g), most intense spectral lines, both in helium and argon expansions, belong to the R-branch μ_b and μ_c degenerate transitions of conformer aG'Ag. Globally for this species transitions of R-branch with J up to 25 and K_a up to 13 obeying to all three types of selection rules were identified. Besides R-branch transitions $K_a=6\leftarrow 5$ Q-branch band and several weaker Q-branch transitions with $\Delta K_a = 2$ and 0.

Additional weak lines, observed in argon, were assigned to the aG'G'g, aG'Gg and g'GAa species.

Regarding aG'G'g, the assignment was facilitated from the identification of a characteristic pattern, due to the asymmetry splitting, constituted by the μ_b and μ_c transitions with $K_a=5$ and $J=7\leftarrow 6$ within few MHz. Subsequently more b - and c -type transitions were measured. Transitions with J up to 15 and K_a up to 9 were assigned.

For aG'G g species only the μ_a and μ_b type transition lines were observed. Transitions with J up to 18 and K_a up to 7 were assigned. Besides the R-branch lines, it has been also possible to observe the $K_a=9\leftarrow 8$ Q-branch band.

While for the g'GAa species transitions with J up to 19 and K_a up to 7 obeying to all three types of selection rules were observed. The form corresponding to g'GAa (g'Ga), was observed also for the homologues 1,2-ethanediol and 1,2-propanediol.

Using helium as carrier gas also the additional lines relative to species $gG'Ag$ and $g'G'Ag$ were observed. Regarding $gG'Ag$, the theoretical calculations estimated only a substantial dipole moment component along a -axis and for this species the assignment was achieved speculating that the several little modulated lines, observed in the spectrum, could belong to μ_a -type transitions of a same species. A μ_a -type spectrum with transitions J up to 21 and K_a up to 12 was assigned. While for the species $g'G'Ag$ the assigned spectrum was constituted, mainly, from μ_b - and μ_c -type R -branch transition lines and only three a -type transitions were measured due to the small μ_a value. Transitions with J up to 21 and K_a up to 6 were assigned. Besides the R -branch lines, transitions of the Q -branch $K_a=6\leftarrow 5$ were observed.

No splittings due to internal rotation of the methyl group were observed for the conformers identified, suggesting that the barrier hindering the internal rotation were relatively high. This hypothesis was further confirmed by exploring the methyl group rotation at the B3LYP/6-311++G(d,p) level. The height barrier obtained was 963 cm^{-1} resulting in splittings A and E, predicted by XIAM program [24], very small, not resolvable in our spectrometer.

Table 2: Experimental spectroscopic parameters for the observed conformers of BD

	1BD	2BD	3BD	5BD	7BD	8BD
Exp.	aG'Ag	g'G'Aa	gG'Ag	aG'G'g	aG'Gg	g'GAa
A (MHz)	7830.099(1) ^a	7821.834(4)	7694.1(1)	5961.454(4)	5509.351(5)	5966.892(3)
B (MHz)	1945.1557(4)	1930.667(1)	1937.537(3)	2211.278(2)	2276.790(6)	2207.152(2)
C (MHz)	1687.5717(4)	1678.812(1)	1673.401(3)	1937.809(2)	1739.501(6)	1936.076(2)
D_J (kHz)	0.1613(4)	0.161(2)	0.157(1)	0.465(4)	0.410(1)	0.451(4)
D_{JK} (kHz)	1.984(3)	1.90(1)	1.890(4)	0	-0.920(4)	0.41(2)
D_K (kHz)	8.22(1)	7.86(9)	0	7.2(1)	9.2(5)	7.90(4)
d_1 (kHz)	-0.0182(1)	-0.0171(3)	-0.013(2)	-0.042(1)	-0.174(7)	-0.0598(9)
d_2 (kHz)	-0.0041(1)	-0.0032(3)	0.0023(7)	0.0028(5)	-0.022(2)	0.0063(6)
N^b	247	82	69	56	46	57
σ (kHz) ^c	38	51	59	48	39	57
$\mu_a/\mu_b/\mu_c^d$	y/y/y	y/y/y	y/n/n	y/y/y	n/y/y	y/y/n

^a Standard error in parentheses in the units of the last digit. ^b Number of transitions. ^c Root mean square deviation of the fit. ^d Yes (y) or no (n) observation of a -, b -, and c -type transitions, respectively.

Relative abundance of conformers

The measured intensities match a rotational temperature of 3 and 5 K when using argon and helium as carrier gas, respectively. As example a portion of the He- and Ar-spectra comparing the $K_a=6\leftarrow 5$ Q -branch transitions of aG'Ag and g'G'Ag conformers is shown in Figure 3. The lines intensity ratio between g'G'Ag and aG'Ag conformers is about 1:3. This value, weighted on the theoretical

$\mu_b^2 + \mu_c^2$ values leads to $g'G'Ag:aG'Ag=1:4$ population ratio. Assuming that the equilibrium pre-expansion population at 353K is not modified this population ratio correspond to a relative energy of 3.9 kJ/mol. Regarding the $gG'Aa$ conformer, the intensity of the μ_a -type transition lines are similar to those of $aG'Ag$. Although, due to an incomplete Stark-modulation of the lines transitions, it is not possible to determine a reliability intensity ratio, considering that the $(\mu_a, g'GAa/ \mu_a, aG'Ag)^2=4$ we can state that the $g'GAa$ conformer is less populated than the $aG'Ag$ one.

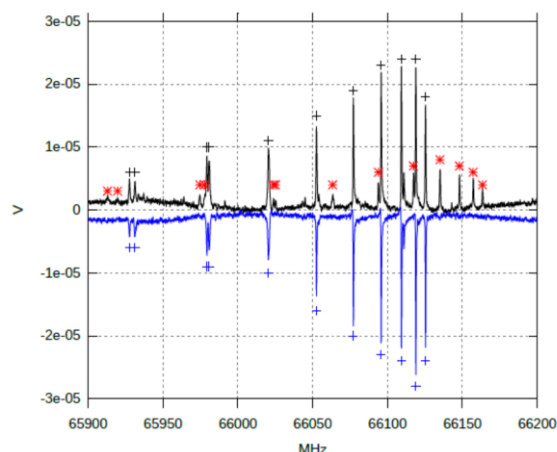


Figure 3: Portion of the spectra recorded using He (upper side) and Ar (lower side) as carrier gas. The $K_a=6\ 5$ Q-branch transitions of $aG'Ag$ and $g'G'Ag$ of 12 BD are indicated by plus and asterisk signs, respectively.

Table 3: Experimental spectroscopic constants of isotopomers of BD

	$^{13}C_1$	$^{13}C_2$	$^{13}C_3$	$^{13}C_4$	OH--OD	OD--OH	OD--OD
A (MHz)	7758.648(3) ^a	7823.889(3)	7764.090(3)	7822.821(3)	7813.493(1)	7511.109(1)	7493.483(1)
B (MHz)	1933.875(3)	1944.864(3)	1932.313(3)	1896.984(3)	1875.4496(5)	1940.292(1)	1871.395(1)
C (MHz)	1676.288(3)	1687.691(3)	1675.606(3)	1651.511(2)	1634.6389(5)	1668.450(1)	1616.935(1)
D_J (kHz)	[0.1613] ^b	[0.1613]	[0.1613]	[0.1613]	[0.1613]	0.146(2)	0.137(3)
D_{JK} (kHz)	[1.984]	[1.984]	[1.984]	[1.984]	[1.984]	[1.984]	[1.984]
D_K (kHz)	[8.22]	[8.22]	[8.22]	[8.22]	[8.22]	[8.22]	[8.22]
d_1 (kHz)	[-0.0182]	[-0.0182]	[-0.0182]	[-0.0182]	[-0.0182]	[-0.0182]	[-0.0182]
d_2 (kHz)	[-0.0041]	[-0.0041]	[-0.0041]	[-0.0041]	[-0.0041]	[-0.0041]	[-0.0041]
N^c	15	12	14	16	42	51	42
σ (kHz) ^d	49	51	64	52	44	46	49

^a Standard error in parentheses in the units of the last digit. ^b Values in squared brackets are fixed to the parent species ones. ^c Number of transitions. ^d Root mean square deviation of the fit.

Rotational spectra of the isotopologues

In order to determine the experimental structure of the aG'Ag species also the isotopologues species were identified.

Owed to the strong intensity of the peaks of the parent species the rotational spectra of the four ^{13}C isotopologues were observed in natural abundance. The rotational constants of all four ^{13}C were assigned while the centrifugal distortion constants were fixed to the values of the parent species. The deuterated isotopologues species were obtained by passing D_2O on BD. All three possible deuterated species to the hydroxyl groups were identified (OD--OH, OH--OD and OD--OD). The fittings were performed using the same Hamiltonian described for the parent species. The spectroscopic parameters for all isotopologues species are reported in table 3.

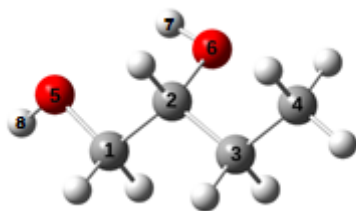


Figure 4: Picture of conformer aG'Ag, numbering of the atoms used through the text.

Experimental structure

From the assigned rotational constants for the parent species and for its ^{13}C and OD--OH, OH--OD and OD--OD isotopologues, a partial experimental structure was determined.

First, the substitution coordinates, r_s , were found using the Kraitchman's equations [25] and uncertainties estimated according to Constain's rule [26] implemented in the KRA program. These equations, exploiting the changes in the inertia momenta of singly substituted species respect to those ones of the parent species, provide the coordinates of the substituted nuclei in the principal axis system. Owed to this approach the experimental structures can be built atom-by atom on the basis of a series of single isotopic substitutions. Indeed the position of a substituted atom is free from other assumptions about the molecular structure. However the method has some limitations, for example, only the absolute values of the substitution coordinates can be determined, and it does not allow to determine the atoms coordinates close to the principal axis system, returning imaginary

values. In addition, the use of effective rotational constants, namely those ones determined experimentally, in the Kraitchman's equations provides r_s structures, that are intermediate values between the geometries of effective ground state and equilibrium those ones. The obtained r_s coordinates for the aG'Ag species of BD are reported in table 4 and there compared to the theoretical coordinates. The r_s structure confirms the conformational assignment. The method returns two imaginary values for the a and b coordinates of C₂ atom and they were set to zero.

Table 4: Comparison between experimental substitution (r_s absolute values in Å) and theoretical equilibrium (r_e , Å) principal axis system coordinates of the C and H atoms for the observed conformer aG'Ag.

	atoms	r_e (Å) ^b	r_s (Å)
a (Å)	C ₁	1.2206	1.214(1) ^a
b (Å)	C ₁	-0.7472	-0.745(2)
c (Å)	C ₁	0.2224	0.220(7)
a (Å)	C ₂	-0.0321	[0]i ^c
b (Å)	C ₂	-0.0136	[0]i
c (Å)	C ₂	-0.2285	-0.237(6)
a (Å)	C ₃	-1.3025	-1.291(1)
b (Å)	C ₃	-0.6900	-0.698(2)
c (Å)	C ₃	0.2669	0.265(6)
a (Å)	C ₄	-2.5797	-2.5665(6)
b (Å)	C ₄	-0.0347	-0.03(6)
c (Å)	C ₄	-0.2554	-0.248(6)
a (Å)	H ₇	0.8521	0.815(2)
b (Å)	H ₇	1.691	1.6689(9)
c (Å)	H ₇	0.054	0
a (Å)	H ₈	-3.1456	3.1062(5)
b (Å)	H ₈	-0.3179	0.306(5)
c (Å)	H ₈	0.1550	0.225(7)

^aConstrain's errors expressed in units of the last decimal digits. ^bFrom B3LYP/aug-cc-pVTZ geometry.

^cImaginary value.

Conclusion

The conformational space of 1,2-Butanediol was explored through the broadband rotational spectrum in the 59.6-74.4 GHz frequency range and functional density theory calculations. Six of the 81 possible non-equivalent isomers, (namely: aG'Ag, g'G'Aa, gG'Ag, aG'G'g, aG'Gg and g'GAa) were observed. The spectroscopic data needed to verify the presence of BD in the planetary atmosphere are provided.

For the populated conformer aG'Ag also the ¹³C in natural abundance and enriched-OD isotopologues were identified. Moreover, the interconversion dynamics among the conformers has been elucidated via quantum mechanical calculations.

References

- [1] C. Blundell, T. Nowak, M. Watson “Measurement, Interpretation and Use of Free Ligand Solution Conformations in Drug Discovery”, *Prog. Med. Chem.*, 2016, 55, 45-147
- [2] G. Fahy, D. Levy, *Cryob.* 1987, 24
- [3] P. Mehl, P. Boutron, *Cryob.* 1987, 24
- [4] J. Hollis, F. Lovas, P. Jewell, L. Coudert, *Astroph. J.* 2002, 571
- [5] M. Requena-Torres, J. Martin-Pintado, S. Martin, Morris, *Astrophys J.* 2008, 672
- [6] A. Maury, A. Belloche, P. André, *Astron. and Astroph.*, 2014, 12
- [7] J. Jorgensen, C. Favre, S. Bisschop, *ApJL*, 2012, L4
- [8] J. Crovisier, D. Bockelé-Morvan, N. Bivier, *Astron and Astroph.*, 2004, L35
- [9] J.-B. Bossa, M. H. Ordu, H. S. P. Müller, F. Lewen, S. Schlemmer, *Astron. and Astroph.* 2014, A12
- [10] D. Plusquellic, F. Lovas, B. Pate, J. Neill, M. Muckle, A. Remijan, *J. Phys. Chem. A*, 2009, 46
- [11] B. Velino, L. Favero, A. Maris, W. Caminati, *J. Phys. Chem. A*, 2011, 115
- [12] L. Evangelisti, Q. Gou, L. Spada, G. Feng, W. Caminati, *Chem. Phys. Lett.*, 2013, 55
- [13] W. Caminati, *J. Mol. Spectros.*, 1981, 83
- [14] W. Caminati, G. Corbelli, *J. Mol. Struct.*, 1982, 78
- [15] W. Steele, R. Chirico, S. Knimeyer, A. Nguyen, *J. Chem. Phys.*, 1996, 41
- [16] S. Verevkin, *Fluid Phase Equil.*, 2004, 23
- [17] S. Melandri, W. Caminati, L. Favero, A. Millemaggi and P. Favero, *J. Mol. Struct.*, 1995, 352/353
- [18] S. Melandri, G. Maccaferri, A. Maris, A. Millemaggi, W. Caminati, and P. Favero, *Chem. Phys. Lett.*, 1996, 261
- [19] C. Calabrese, A. Maris, L. Evangelisti, L. Favero, S. Melandri, W. Caminati, *J. Phys. Chem. A.* 2013, 117
- [20] M.J. Frisch, G.W. Trucks, H.B. Schlegel, G.E. Scuseria, M.A. Robb, J.R. Cheeseman, G. Scalmani, V. Barone, B. Mennucci, G. A. Petersson, H. Nakatsuji, M. Caricato, X. Li, H.P. Hratchian, A.F. Izmaylov, J. Bloino, G. Zheng, J.L. Sonnenberg, M. Hada, M. Ehara, K. Toyota, R. Fukuda, J. Hasegawa, M. Ishida, T. Nakajima, Y. Honda, O. Kitao, H. Nakai, T. Vreven, J.A. Montgomery Jr., J.E. Peralta, F. Ogliaro, M. Bearpark, J.J. Heyd, E. Brothers, K.N. Kudin, V.N. Staroverov, T. Keith, R. Kobayashi, J. Normand, K. Raghavachari, A. Rendell, J. C. Burant, S.S. Iyengar, J. Tomasi, M. Cossi, N. Rega, J. M. Millam, M. Klene, J.E. Knox, J.B. Cross, V. Bakken, C. Adamo, J. Jaramillo, R. Gomperts, R.E. Stratmann, O. Yazyev, A.J. Austin, R. Cammi, C. Pomelli, J. Ochterski, R.L. Martin, K. Morokuma, V.G. Zakrzewski, G.A. Voth, P. Salvador, J.J. Dannenberg, S. Dapprich, A.D. Daniels, O. Farkas, J.B. Foresman, J.V. Ortiz, J. Cioslowski, D. Fox, Gaussian 09, Revision D.01, Gaussian, Inc., R. Wallingford, CT

- [21] Ruoff, T. Klots, T. Emilson, H. Gutowski, *J. Chem. Phys.* 1990, 93
- [22] H. M. Pickett, *J. Mol. Spectrosc.* 148 (1991) 371-377.
- [23] J.K.G. Watson, in *Vibrational Spectra and Structure*; Durig, J.R., Ed.; Elsevier: Amsterdam, 1977; Vol. 6, pp 1-89.
- [24] H. Hartwig, H. Dreizler, *Z. Naturforsch.*, 1996, 51a
- [25] J. Kraitchman, *Am. J. Phys.*, 1953, 21
- [26] C. Constain, G. Srivastava, *J. Chem. Phys.*, 1961, 35

CHAPTER 2

THE ROTATIONAL SPECTRUM OF 1,4-BUTANEDITHIOL

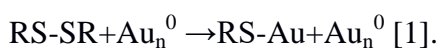
Introduction

Dithiols are organic compounds containing two sulfhydryl groups (SH bond). Although they are considered sulfurated analogues of diols their properties change significantly due to the size, electronegativity and polarizability differences between oxygen and sulfur atoms. Since the difference in electronegativity between S and H is small the SH bond presents low polarity and forms hydrogen bonds weaker than those formed by the OH. Dithiols sulfur atoms tend to coordinate with metals that behave as soft Lewis acids such as silver, copper, platinum, mercury, iron, colloidal gold particles. This strong binding affinity is invoked in the explanation of several processes involving dithiols such as smells detection and nanostructured microelectronics devices [1].

Dithiols and thiols are extremely potent odorant substances by humans; for example the natural gas odorant 2-methyl-2propanethiol is detected at 0.3 parts per billion (ppb). To this day, the action mechanism of any odorant compounds on respective nasal receptors is not understood and there aren't still structural studies of these substances with their biological targets performed by crystallography. In the case of thiols, it have been proposed that for mediating thiols odor perception, odorant receptors have to function as metalloproteins involving transition metal ions such as Cu(I) [2].

However in order to understand the key factors of smelling perception produced from these substances, researchers have given rise to a great number of studies to correlate their activities with their structures [3]. Detailed structural investigations of such compounds are therefore of fundamental importance.

Dithiols are also used as self-assembled monolayers on a gold surface. Nanostructures of gold such as nanoparticles and monolayer protected clusters have a key role in various applications ranging from microelectronics, sensors, catalysis to biomedical field. Thiol self-assembled monolayers provide stabilization, decoration and functionalization of nanostructures. The sulfur-gold interaction is semi-covalent and has a strength of approximately 188 kJ/mol. Chemisorption of thiols on gold gives indistinguishable monolayers probably forming the Au(1) thiolate (RS-) species. The reaction may be considered formally as an oxidative addition of S-S bond to the gold surface, namely:



However relating the microscopic (atomic, molecular and supramolecular) structure of a surface to its macroscopic physical, chemical, biological properties (corrosion, resistance, adhesive, strength, biocompatibility) is not trivial. For this reason models in which the surface structure is controlled on atomic scale play an important role. In this work we focused our attention on the structural features of 1,4-butanedithiol in isolated phase (hereafter BT). The study has been performed by rotational spectroscopy combined to theoretical calculations that provide a synergic approach for determining the conformational preferences of the system on the potential energy surface. This is the first study on an isomer of butanedithiol to be performed. BT is a very flexible molecule, its conformational landscape is described by 5 dihedral angles giving place to $3^5=243$ conformers. Among these rotamers several equivalent forms that can interconvert are possible. In our previous study on the conformational behaviour of 1,3-propanedithiol we observed 5 of the possible 25 non-equivalent isomers and showed that the conformational preferences arise from a balance of electronic and steric effects and as a consequence the population is spread on a larger number of conformers [4].

Theoretical conformational landscape and spectroscopic properties of BT

For a complete conformational analysis of BT, a 5-dimensional space defined by three skeletal torsional angles (SCCC, CCCC, CCCS) and two sulfhydryl dihedral angles (HSCC and CCSH) has to be considered. Because of the steric hindrance, only three staggered positions are possible for each dihedral angle (namely anti, gauche and gauche'), giving place to a total of $3^5=243$ possible rotamers. In this study the rotamers are identified by the combinations of five letters. The letters are related with the values of the dihedral angles: g or G (c.a. 60°), g' or G' (c.a. -60°) stand for gauche, t or T (c.a. 180°) stand for trans. The capital letters (T, G, G') refer to the backbone atoms while the lower-case letters (t, g, g') describe the positions of the SH groups. Considering only the backbone orientations, the structures can be grouped in 27 'skeletal families'. However due to the symmetry of the molecule the number of non-equivalent backbone structures decreases to 10, namely: TTT, TTG, TGG, TGT, TGG', GTG, G'TG, GGG, GG'G and G'G'G. Then, taking into account also the orientation of the SH groups, 70 non-equivalent rotamers can be distinguished. They are listed in Table 1 with the symmetry group and degeneracies.

Each rotamer was fully optimized at B3LYP level using 6-311++G(d,p) basis set achieving 59 conformers [5]. The not reported conformers could not be optimized. Illustrative purposes, pictures of the most stable conformer of each family are reported in figure 1. The list of relative energy values, rotational constants and electric dipole moment components is given in table 1. The

computational results report 17 conformers below 5 kJ mol⁻¹. The most stable is gTTGg, while the conformers of the family TGG', GG'G and G'G'G lie above 9.6 kJ mol⁻¹.

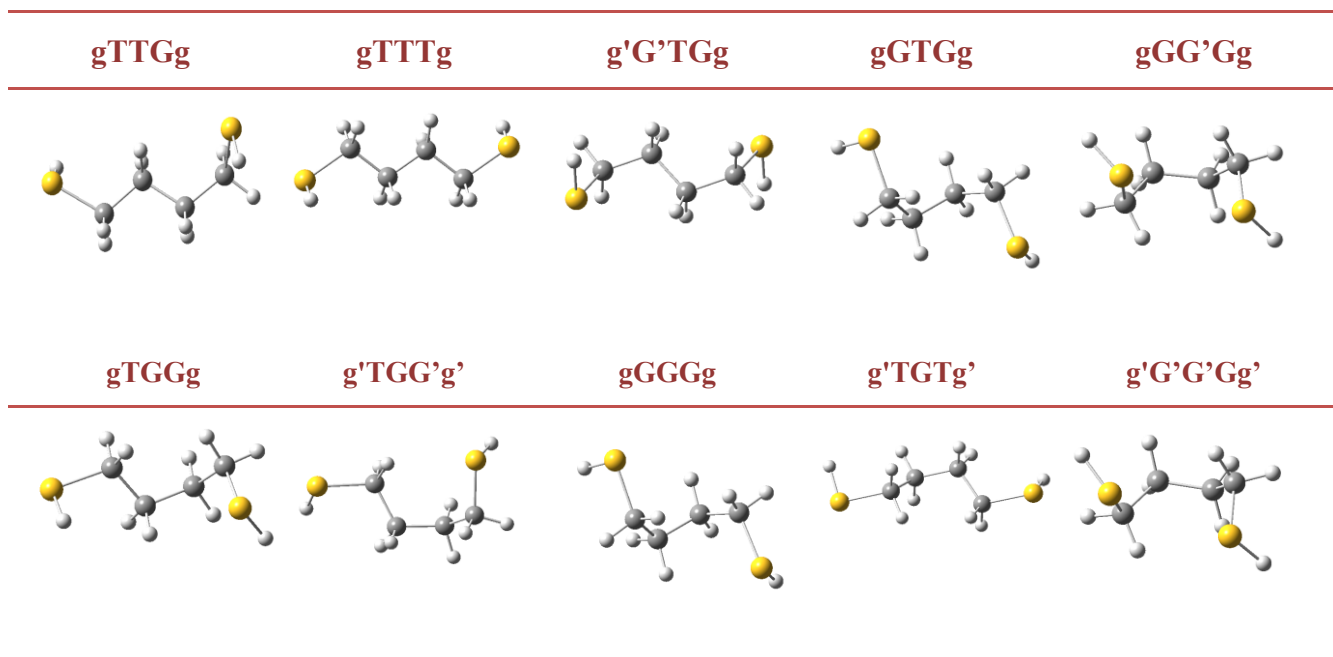


Figure 1: Pictures of the most stable conformer of each family.

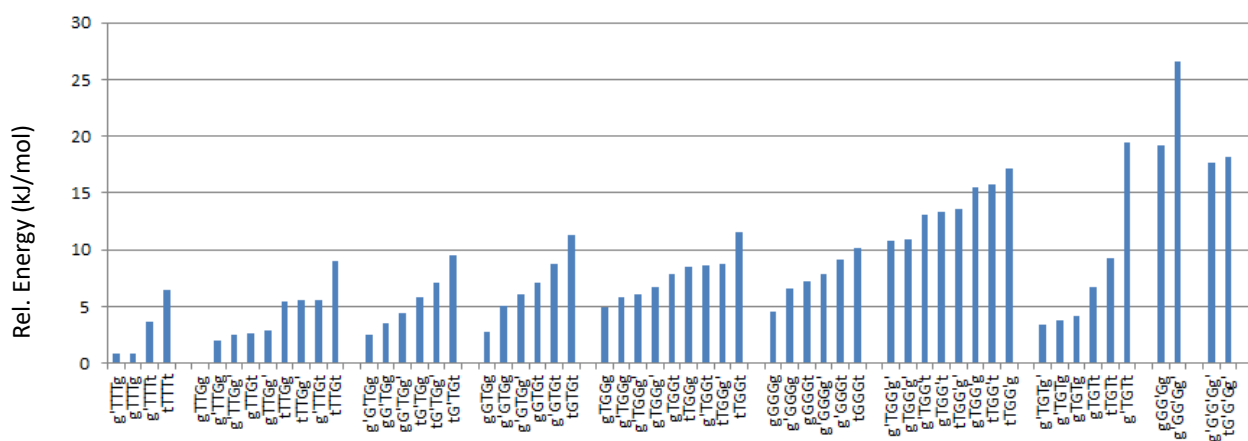


Figure 2: Conformers theoretical relative energies (kJ mol⁻¹)

Table 1: Theoretical spectroscopic parameters

Conf.	Γ	g	ΔE (cm ⁻¹)	A (MHz)	B (MHz)	C (MHz)	μ_a (D)	μ_b (D)	μ_c (D)	B+C (MHz)
4 TTT										
g'TTTg	C ₁	2	67	14488	543	533	0	0	0	1076
g'TTTg	C ₂	2	72	14470	543	533	0	0	-1.45	1076
g'TTTt	C ₁	4	305	14391	549	537	-0.52	-1.18	0.68	1086
t'TTTt	C _{2h}	1	544	14324	555	542	0	0	0	1097
9 TTG										
g'TTGg	C ₁	4	0	5719	698	650	0.81	2.56	0.03	1348
g'TTGg	C ₁	4	167	5778	698	649	1.13	1.68	-0.97	1347
g'TTGg'	C ₁	4	212	5902	692	643	0.38	1.08	0.08	1335
g'TTGt	C ₁	4	217	5710	707	657	0.18	2.48	1.17	1364
g'TTGg'	C ₁	4	239	5845	693	645	0.10	1.91	1.19	1337
t'TTGg	C ₁	4	455	5706	707	657	0.18	2.82	-1.17	1365
t'TTGg'	C ₁	4	465	5813	703	652	-0.53	2.16	-0.03	1354
g'TTGt	C ₁	4	470	5858	706	655	1.67	1.60	0.17	1361
t'TTGt	C ₁	4	753	5769	717	663	0.75	2.72	0.00	1380
6 G'TG										
g'G'TGg	C _i	2	207	7577	713	679	0	0	0	1392
g'G'TGg	C ₁	4	296	7605	712	676	0.41	0.58	-1.19	1388
g'G'TGg'	C _i	2	371	7674	709	672	0	0	0	1380
tG'TGg	C ₁	4	482	7512	728	689	-0.52	-0.46	-1.02	1417
tG'TGg'	C ₁	4	589	7582	724	685	-0.95	-0.97	0.10	1409
tG'TGt	C _i	2	798	7525	738	696	0	0	0	1434
6 GTG										
gGTGg	C ₂	2	233	4384	852	786	0	-1.53	0	1638
g'GTGg	C ₁	4	427	4717	812	766	-0.06	-1.98	-1.25	1578
g'GTGg'	C ₂	2	510	4871	793	754	0	-2.57	0	1547
gGTGt	C ₁	4	597	4579	845	786	-1.03	-2.19	0.54	1631
g'GTGt	C ₁	4	729	4785	819	773	-1.13	-2.80	-0.73	1593
tGTGt	C ₂	2	941	4748	843	791	0	-2.95	0	1633
9 TGG										
gTGGg	C ₁	4	416	4557	828	757	1.52	-1.72	0.15	1585
g'TGGg	C ₁	4	487	4527	831	759	0.90	-2.96	0.19	1589
g'TGGg'	C ₁	4	505	4500	832	757	-0.22	-2.25	-0.35	1590
gTGGg'	C ₁	4	557	4652	818	748	0.42	-0.98	-0.48	1566
gTGGt	C ₁	4	657	4503	850	775	1.69	-1.20	-1.13	1625
tTGGg	C ₁	4	712	4615	829	762	0.89	-2.14	-1.01	1591
g'TGGt	C ₁	4	716	4455	857	779	1.08	-2.43	-1.09	1636
tTGGg'	C ₁	4	727	4552	835	763	-0.24	-1.55	-1.64	1597
tTGGt	C ₁	4	966	4561	852	781	1.11	-1.59	-2.28	1633
6 GGG										
gGGGg	C ₂	2	378	5131	862	857	0	0	-1.91	1720
g'GGGg	C ₁	4	548	5249	850	842	-0.85	-0.79	-0.93	1692
gGGGt	C ₁	4	606	4970	892	886	0.02	0.15	0.60	1779
g'GGGg'	C ₂	2	656	5247	848	838	0	0	-0.09	1686
g'GGGt	C ₁	4	769	5072	880	871	-0.85	-1.01	0.28	1751
tGGGt	C ₂	2	847	4885	915	908	0	0	0.82	1824
9 TGG'										
g'TGG'g'	C ₁	4	904	4044	906	777	-1.28	-2.67	1.20	1684
gTGG'g'	C ₁	4	908	4043	905	781	-1.79	-1.75	0.32	1686
g'TGG't	C ₁	4	1093	4120	915	784	1.71	2.31	0.12	1699
gTGG't	C ₁	4	1116	4122	914	785	2.26	1.71	1.13	1699
tTGG'g'	C ₁	4	1138	4199	895	772	1.56	1.11	0.97	1667
gTGG'g	C ₁	4	1301	4320	858	746	-0.47	-1.66	-1.12	1604
tTGG't	C ₁	4	1315	4225	910	782	-1.95	-0.86	-0.41	1692
tTGG'g	C ₁	4	1435	4379	865	750	0.43	0.60	0.20	1615
6 TGT										
g'TGTg'	C ₂	2	289	9670	609	591	0	-1.61	0	1201
g'TGTg	C ₁	4	320	9886	605	590	0.25	-0.86	1.13	1195
gTGTg	C ₂	2	348	10127	600	588	0	0.02	0	1188
gTGTt	C ₁	4	562	10260	606	591	-0.31	0.78	-1.19	1197
tTGTt	C ₂	2	773	10374	611	595	0	1.43	0	1206

g'TGTt	C ₁	4	1622	9998	610	593	-0.05	-0.08	-0.05	1204
6 GG'G										
gGG'Gg	C ₂	2	1608	2641	1579	1122	0	-3.24	0	2702
g'GG'Gg'	C ₁	2	2224	2787	1332	1007	0.02	-2.32	-0.04	2339
9 G'G'G										
g'G'G'G'	C ₁	4	1479	2945	1290	994	1.38	-2.99	0.16	2284
tG'G'Gg'	C ₁	4	1524	2915	1350	1033	1.29	-2.15	1.32	2384

Experimental section

Commercial samples of BT (C₄S₂H₁₀, MW=122.25 g/mol, 97%) was purchased from Alfa Aesar and used as received, carrier gases (Ar and He) were purchased from SIAD. BT is smelling, it appears as a pale yellow liquid at ambient conditions. The boiling point is 105-106 °C and vapour pressure is 30 mmHg at room condition.

The spectrum of BT was recorded in the 59.6-74.4 GHz frequency range by a free-jet Stark modulated millimeter wave absorption spectrometer. Briefly, a stream of carrier gas (Ar at P₀ 20 kPa, He at P₀ 40 kPa) was bubbled through the sample and then expanded to about 0.5 Pa through a 0.3 mm diameter pinhole nozzle. The resolution and the estimated accuracy of the frequency measurements are about 300 kHz and 50 kHz, respectively [6-8].

Results

Rotational spectrum

To have an overview of the BT rotational spectrum, two fast scans were recorded using both helium and argon as carrier gases. The two spectra were differently populated, few lines are observed in the spectrum recorded in argon while the spectrum in helium appears very peaks dense reflecting the presence of several species. Guided by the values of the theoretical rotational constants (A, B and C, table 1) which are directly related to the molecular mass distribution of each conformer, and those of the electric dipole moment components which give rise to the selection rules and intensities of rotational transitions, the spectra of four species were assigned. All measured transition lines were fitted to Watson's *S*-reduced semirigid asymmetric rotor Hamiltonian [9] using the SPFIT program [10]. The determined spectroscopic parameters for the four species labeled as BT1, BT2, BT3 and BT4 are reported in table 2.

BT1 was the alone species observed in argon. For this species both *b*-type and *c*-type transitions with *J* from 6 to 25 and *K_a* from 3 to 7 were assigned. The *b*-type spectra of the species BT2, BT3 and BT4 were observed only in helium. For both BT2 and BT3 species, transitions with *J* from 6 to

27 and K_a from 3 to 7 were assigned. For BT4, transitions with J from 6 to 19 and K_a from 5 to 7 were assigned.

For all species, using the determined rotational constants, also a -type transitions were predicted but they were not found in no case.

Table 2: Experimental spectroscopic parameters

	BT1	BT2	BT3	BT4
A (MHz)	5780.24(1) ^a	5738.76(2)	5883.76(1)	5851.64(2)
B (MHz)	718.148(5)	717.977(4)	712.941(4)	712.397(8)
C (MHz)	666.267(6)	667.052(5)	660.112(5)	661.136(8)
D_J (kHz)	0.091(3)	0.096(2)	0.091(3)	0.088(5)
D_{JK} (kHz)	-2.48(1)	-2.41(1)	-2.48(1)	-2.49(4)
D_K (kHz)	33.8(2)	33.1(2)	34.6(3)	34.4(3)
d_1 (kHz)	-0.025	-0.023(1)	-0.19(1)	0
d_2 (kHz)	0	0	0	0
$\mu_a/\mu_b/\mu_c$ ^d	no/yes/yes	no/yes/no	no/yes/no	no/yes/no
N ^b	45	38	42	25
σ (kHz) ^c	54	44	32	89

^a Standard error in parentheses in the units of the last digit. ^b Number of transitions. ^c Root mean square deviation of the fit. ^d Yes or no observation of a -, b -, and c -type transitions, respectively.

Conformational identification

Unfortunately the determined rotational constants for the species BT1, BT2, BT3 and BT4 are very similar between them and for this reason the structural identification is not immediate. In addition, because the intensity of signal of this species is not so strong, the spectra of their isotopologues in natural abundance, which would allowed to discriminate between the species, were not detectable in natural abundance. However by some considerations a partial identification was achieved.

The missing of the signals relative to the BT2, BT3 and BT4 species in the spectrum recorded in gas Argon indicates that these species relax easily (barriers <400 cm⁻¹ [11]) on the alone species observed in Argon, BT1. Usually pathways at so low energy barriers take place between conformers differing for the orientation of H atoms rather than between those involving skeletal rearrangements. From this consideration springs that all observed species belong to only one of the ten possible skeletal families pinpointed by theoretical calculations.

The comparison between the B and C values, obtained theoretically and experimentally, suggests that the assigned species could belong to the family TTG or G'TG, while from the value of A it is established that they are part of TTG family.

However to distinguish unambiguously between which of the nine possible conformers of the family TTG have been observed is a task more challenging. Certainly, the fact of not having observed *a*-type is not a discriminating factor because the lack of these lines could be attributed both to small μ_a value of one conformation but also to the fact that these lines were predicted to high J , so they were expected very weak.

Regarding the species BT1, taking into account both whether it has *b*-type and *c*-type transitions and, being the only one species observed in Argon, it should be the most stable species of the family TTG, it is possible to conclude that the species BT1 is the structure g'TTGg.

Considering the theoretical relative energy values, other species were expected to be observed, but they were not found. The lack of other TTG conformers is probably due to a conformational relaxation effects upon supersonic expansions. This is often observed when the barriers connecting different minima are less than $2KT$. While TTT conformers were not identified because having *A* very large few lines were expected in our frequency range.

Conclusion

The conformational space of 1, 4-butanedithiol was explored through the broadband rotational spectrum in the 59.6-74.4 GHz frequency range and density functional theory calculations. Four of the fifty-nine possible non-equivalent rotamers predicted were assigned to the TTG skeletal family. The experimental findings in agreement with theoretical calculations show the conformational behavior of 1,4-butanedithiol is different from that observed for alcohol analogue, 1,4-butanediol [12].

In the case of 1,4-butanediol the conformational preferences are driven from formation of a intramolecular hydrogen bond between hydroxyl groups, two conformers belonging to the families GG'G and G'G'G were observed. While in 1, 4-butanedithiol due to the lower strength of the SH hydrogen bond with respect to OH one, the conformational preferences arose from a balance of electronic and steric effects.

References

- [1] C. Vericat, M. Vela, G. Benitez, P. Carro, R. Salvarezza, *Chem Soc. Rev.*, 2010, 39
- [2] X. Duan, E. Block, Z. Li, T. Connelly, J. Zhang, Z. Huang, X. Su, Y Pan, L. Wu, Q. Chi, S. Thomas, S. Zhang, M. Ma, H. Matsunami, G.-Q. Chen, H. Zhuang, *PNAS*, 2012, 109, (9)
- [3] M. Chastrette, *SAR and QSAR in Environmental Research*, 1997, 6
- [4] A. Vigorito, C. Calabrese, E. Paltanin, S. Melandri, A. Maris, *Phys. Chem. Chem. Phys.*, 2017, 19

- [5] M.J. Frisch, G.W. Trucks, H.B. Schlegel, G.E. Scuseria, M.A. Robb, J.R. Cheeseman, G. Scalmani, V. Barone, B. Mennucci, G. A. Petersson, H. Nakatsuji, M. Caricato, X. Li, H.P. Hratchian, A.F. Izmaylov, J. Bloino, G. Zheng, J.L. Sonnenberg, M. Hada, M. Ehara, K. Toyota, R. Fukuda, J. Hasegawa, M. Ishida, T. Nakajima, Y. Honda, O. Kitao, H. Nakai, T. Vreven, J.A. Montgomery Jr., J.E. Peralta, F. Ogliaro, M. Bearpark, J.J. Heyd, E. Brothers, K.N. Kudin, V.N. Staroverov, T. Keith, R. Kobayashi, J. Normand, K. Raghavachari, A. Rendell, J. C. Burant, S.S. Iyengar, J. Tomasi, M. Cossi, N. Rega, J. M. Millam, M. Klene, J.E. Knox, J.B. Cross, V. Bakken, C. Adamo, J. Jaramillo, R. Gomperts, R.E. Stratmann, O. Yazyev, A.J. Austin, R. Cammi, C. Pomelli, J. Ochterski, R.L. Martin, K. Morokuma, V.G. Zakrzewski, G.A. Voth, P. Salvador, J.J. Dannenberg, S. Dapprich, A.D. Daniels, O. Farkas, J.B. Foresman, J.V. Ortiz, J. Cioslowski, D. Fox, Gaussian 09, Revision D.01, Gaussian, Inc., Wallingford, CT
- [6] S. Melandri, W. Caminati, L. Favero, A. Millemaggi and P. Favero, *J. Mol. Struct.*, 1995, 352/353
- [7] S. Melandri, G. Maccaferri, A. Maris, A. Millemaggi, W. Caminati, and P. Favero, *Chem. Phys. Lett.*, 1996, 261
- [8] C. Calabrese, A. Maris, L. Evangelisti, L. Favero, S. Melandri, W. Caminati, *J. Phys. Chem. A*. 2013, 117
- [9] H. M. Pickett, *J. Mol. Spectrosc.* 148 (1991) 371-377.
- [10] J.K.G. Watson, in *Vibrational Spectra and Structure*; Durig, J.R., Ed.; Elsevier: Amsterdam, 1977; Vol. 6, pp 1-89.
- [11] R. Ruoff, T. Klots, T. Emilson, H. Gutowski, *J. Chem. Phys.*, 1990, 93
- [12] L. Evangelisti, Q. Gou, L. Spada, G. Feng, *W. Caminati, Chem. Phys. Lett.*, 2013, 556

CHAPTER 3

THE SHAPES OF SULFONILAMIDE: THE ROTATIONAL SPECTRA OF BENZENESULFONAMIDE, ortho-TOLUENSULFONAMIDE and para-TOLUENSULFONAMIDE

Introduction

In biological chemistry the structural characterization of a ligand within its biological target is of extreme importance. For instance, in the approach of the ligand-based drug design the ligands bioactive conformation is used to infer the necessary characteristics that a molecule must possess to bind to the target. These features allow to define a pharmacophore model that may be used to design new molecular entities interacting with the target. However if on one side the role of the ligand bioactive conformation is well recognized on the other side the free ligand conformation is often considered of secondary importance. Nevertheless in a recent study [1, 2], it stands out that: *“For a drug ligand to bind strongly to its target and have a strong effect, it needs to be able to adopt the right shape to fit into the target binding site. If a molecule has to change shape a lot to bind to its target, it is likely to bind poorly and therefore be unsuitable as a drug. In contrast, if a molecule is already the right binding shape (the ‘bioactive conformation’) a lot of the time, it is likely to bind strongly to the target and be a good drug. Knowledge of the 3D-shape of the free ligand is therefore extremely valuable in guiding the design of the best drug molecules.”*

Compounds of the Sulfonamides class, in particular those containing the benzosulfonamide group ($\text{Ph-SO}_2\text{NH}_2$), are of extreme interest in biologic field since many of them are found active against a variety of diseases.

Sulfanilamide was the first antibacterial drug useful clinically [3]. Today, sulfamethoxale is used largely for treating urinary tract infections, bronchitis and prostatitis and it is effective against both Gram negative and positive bacteria such as *Listeria monocytogenes* and *Escherichia coli*. This compound exerts its antimicrobial action targeting by enzyme dihydropteroate synthase [3]. In the receptor binding site it acts as analogue of natural substrate, para-aminobenzoic acid, providing the folate production resulting bacterial death. The X-ray crystal structure is available and catalogued in the RCSB Protein data Bank with the code 3TZF.

In addition, recent investigations have found that the arylsulfonamides are extremely potent inhibitors of the metalloenzyme family, carbonic anhydrase [4]. These enzymes catalyse the reversible hydration of carbon dioxide to bicarbonate ion and proton, a crucial equilibrium involved in many physiological processes such as respiration, pH balance and ion transport, and their

inhibition is useful to treat a multitude of diseases [4-6]. Several arylsulfonamides acting as antagonist ligands of these enzymes have been FDA-approved as anti-glaucoma, anti-inflammatory [7], anti-tumor [8], anti-viral HIV and for the treating Alzheimer's disease. X-ray crystal structures are available for arylsulfonamides compounds in isoenzymes carbonic anhydrase are catalogued in the PDB with the codes: 4COQ, 2HL4, 1JSV, 4JSA, 3K34.

Since the profound biological interest toward the sulfonamides class, in this work the structural characterization of their main pharmacophore group, benzenesulfonamide (hereafter BSA) and its methyl derivatives ortho-toluensulfonamide (hereafter OTS) and para-toluensulfonamide (hereafter PTS) (figure 1) in isolate phase has been performed. The chosen investigative method is the rotational spectroscopy technique because by their rotational spectra the conformational preferences of the compounds BSA, OTS, PTS can be determined with extraordinary accuracy. Indeed, these spectra may show typical hyperfine structures due to the ^{14}N quadrupole nucleus leading to determination of the ^{14}N quadrupole coupling constants, that in addition to the rotational constants, constitute a tool to identify unambiguously different conformers.

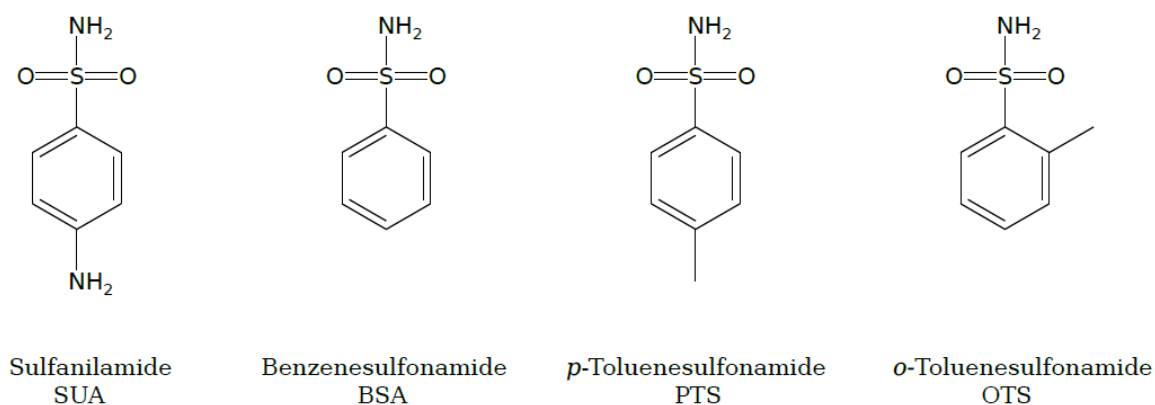


Figure 1: Sketch of SUA, BSA, PTS and OTS compounds

Previous studies done by rotational spectroscopy show that flexible chains, constituted from different atoms C, O, N, or S, attached to an aromatic ring give place to several configurations. The structural variability is observed also in systems with short side chains. In the prototype compound of this series, ethylbenzene [9], the ethyl group is perpendicular to the ring plane, while in anisole [10] the side chains lie in the plane of the aromatic ring. In Benzylamine [11], two conformations were observed: in one of them, the amino group is in gauche position with respect to the aromatic plane, with the nitrogen lone pair pointing toward the hydrogen atom, while in the second conformer the amino group lies perpendicular to the aromatic plane with the amino hydrogens pointing toward the π cloud. In the first conformer also the inversion motion of the $-\text{CH}_2\text{NH}_2$ group, above and below the phenyl plane, was modeled. In the case of the benzyl alcohol [12], four

equivalent conformers in which the alcohol group is in gauche position respect to the aromatic plane were determined.

Regarding the benzenesulfones compounds, only benzene sulfonyl chloride has been investigated by rotational spectroscopy [13]. In this case the Cl atom lies perpendicular at benzene plane.

Experimental section

Commercial samples of BSA, OTS and PTS were purchased from Alfa Aesar and used as received. BSA ($C_6H_7NO_2S$, 157.19 g/mol, 98%), OTS ($C_7H_9NO_2S$, 171.22 g/mol, 99%) and PTS ($C_7H_9NO_2S$, 171.22 g/mol, 98%) appear as white crystalline solids at ambient conditions. The corresponding melting points are 151-154°C, 156°C and 136-139°C, respectively.

The spectra of BSA, OTS and PTS were recorded by two different spectrometers in two different frequency ranges.

At “G. Ciamician” department, the BSA, OTS, PTS spectra were recorded in the 59.6 to 74.4 GHz frequency range by free jet Stark modulated absorption millimeter wave spectrometer (FJ-AMMW) [14-16]. The resolution and the estimated accuracy of the frequency measurements are about 300 kHz and 50 kHz, respectively. To obtain a suitable concentration of the samples, the substances were warmed: BSA at 140-150°C while OTS and PTS at 130-140°C. Successively the samples were expanded in gas argon from a pressure of 20 kPa to about 0.5 Pa through a 0.3 mm diameter pinhole nozzle. The deuterated isotopologues species for the compound BSA have been obtained by passing D_2O in Ar over the sample heated.

At “King’s College department”, the BSA, OTS, PTS spectra were recorded in the 2-8 GHz frequency range by pulsed jet chirped pulse Fourier transform microwave spectrometer (PJ-CP-FTMW) [17-18]. BSA, PTS and OTS were placed in a bespoke heating reservoir attached to the nozzle at temperature of 168°, 165° and 167°, respectively. The compounds were seeded in neon gas at backing pressures of ca. 5 bars. Typical molecular pulses of 1100 μs were used to produce the supersonic jet in vacuum chamber. Microwave chirped pulses of 4 μs were applied with a delay of 1400 μs with respect to the start of the molecular pulse. Molecular relaxation signals were collected for 15 μs using the digital oscilloscope and converted into the frequency domain through a fast Fourier-transform algorithm. The resolution is ca. 110 kHz.

Computational results

For the three compounds BSA, PTS and OTS different rotamers are generated by the rotation of the sulfonamide and the amino groups, the which orientations are defined by two dihedral angles: CCSN and CSNH, respectively (figure 1).

Rotation of the methyl group in PTS and OTS is not relevant to describe different rotamers because it gives place to three equivalent minima. However this motion must be taken in account because it could be generate splittings of the rotational transitions due to tunnel effect.

On the possible rotamers full geometry optimizations and subsequent harmonic frequency calculations, to characterize the stationary points, were run at the B3LYP/6-311++G** level of theory, using the Gaussian09 programs package [19].

The calculations indicated that the conformational behaviour of the BSA and PTS compounds is very similar. For both compounds two conformers, having a symmetry plane along the *a* and *c* principal axes (CCSN=90°) and differing for the amino group hydrogen atoms position, that can be oriented in way to eclipse or stagger the oxygen atoms of the SO₂ group, were predicted. The depiction of the structures, the corresponding spectroscopic parameters and the relative electronic energies are shown in tables 1 and 2, the conformers are labelled as BSA1, BSA2 and PTS1 and PTS2.

While for the compound OTS, different configurations were obtained. It were predicted four conformers in which the amino group can be oriented in gauche or in planar position with respect to the benzene plane, CCSN=60° and CCSN=0°, respectively. In both arrangements the amino group hydrogen atoms can be oriented in way to eclipse or stagger the O atoms of the SO₂ group. In OTS the methyl internal rotation pathway was explored varying the dihedral angle corresponding by 10° steps, whereas all the other internal coordinates were freely optimized. The obtained structures with the corresponding spectroscopic parameters and the relative electronic energies (ΔE) and internal rotation barrier (V_3) are reported in table 3, conformers are labelled as OTS1, OTS2 and OTS3 and OTS4.

Results

Analysis of the rotational spectra

The rotational spectra of three compounds BSA, OTS and PTS were initially recorded in the 59.6-74.4 GHz frequency range by FJ-AMMW. Guided from the values of the spectroscopic constants reported in table 1-3 all the spectra were assigned in this frequency range leading to determination of rotational constants and centrifugal distortion constants.

Subsequently additional experimental measurements were performed in the 2-8 GHz frequency range by PJ-CP-FTMW. The superior resolving capacity of this spectrometer allowed to observe the hyperfine structures due to the ^{14}N atom presence determining the ^{14}N nuclear quadrupole coupling constants (χ_{gg} , $g=a, b, c$).

Since the ^{14}N nucleus has a spin quantum number greater than $1/2$ ($I=1$) it has a non-spherical charge distribution and so a non-vanishing nuclear quadrupole moment ($Q=20.44(3)$ mb). The interaction between Q and the electric field gradient of the molecule (q_{gg} , $g=a, b, c$) provides a mechanism through which I and the molecular rotational angular momentum (J) interact producing a splitting of the rotational transitions. The analysis of these patterns yields the nuclear quadrupole coupling constants ($\chi_{gg}=Qq_{gg}e$, e =electron charge).

The BSA rotational spectra

In the spectrum of BSA, peaks relative to only one conformational species were identified. Overall in the two frequencies ranges were assigned: a -type and c -type transitions with J up to 31 and K_a up to 18.

A global fitting of all transition lines was done with Pickett's SPFIT program [20, 21], using a semirigid rotor Hamiltonian (H_R) in the S-reduction and I^r representation supplemented with a H_Q term to account for the nuclear quadrupole coupling contribution [25]. The Hamiltonian was set up in the coupled basis set $I + J = F$ and diagonalized in blocks of F . The energy levels involved in each transition are thus labelled with the quantum numbers $J, K-I, K+I, F$. A depiction of ^{14}N quadrupole hyperfine structure observed for the transition $2_{21}-2_{11}$ is given in figure 2. The obtained spectroscopic parameters are given in tables 1-2.

To obtain supplemental structural information, for BSA compound, also the rotational spectrum of the its deuterated isotopologues species were recorded in the frequency range 59.6-74.4 GHz. The monodeuterated and bideuterated species to amino group, ND and ND₂ respectively, were assigned. Measured transition lines were fitted to Watson's S-reduced semirigid asymmetric rotor Hamiltonian achieving the spectroscopic constants, reported in tables 1-2.

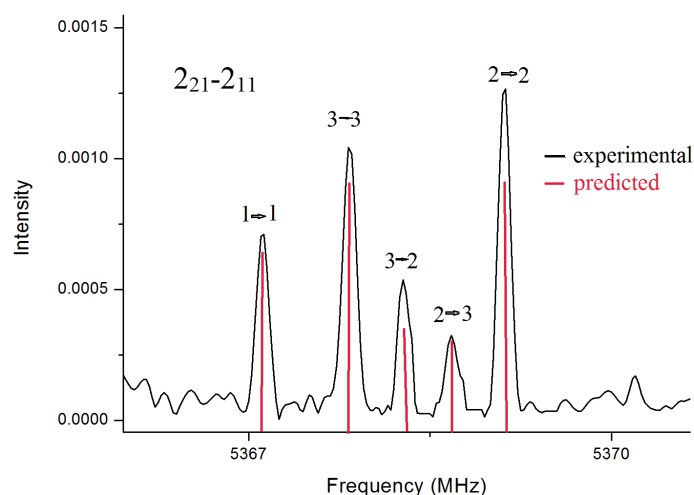


Figure 2: ^{14}N quadrupole hyperfine structure for the transition $2_{21}-2_{11}$

Conformational Assignment and structure for BSA

The determined rotational constants are quite in agreement with those of the conformational species predicted in table 1. In addition, the lack of μ_b -transitions confirms the presence of a symmetry plane along a and c axes.

However from the rotational constants it is not possible to discriminate between the two calculated conformers because these structures differing only the H atoms position, with small mass, have rotational constants very similar.

In compounds containing a ^{14}N atom, a valid help to carry on a structural identification is provided from the ^{14}N nuclear coupling constants because these parameters depend critically on the electronic environment around the ^{14}N nucleus and principal inertial axis system. Comparison between the experimental quadrupole coupling constants with those calculated in table 1 indicate that the species assigned for BSA is BSA1.

In addition from the assigned rotational constants for the isotopologues ND and ND₂ of BSA, supplemental information on the structure are obtained.

Using Kraitchman's equations and uncertainties estimated according to Constrain's rule implemented in Kra program [22, 23], the substitution coordinates for the amino group atom hydrogens were calculated. The obtained r_s coordinates are compared to the theoretical coordinates r_e of BSA1 and BSA2 in table 4. The r_s coordinates confirm the assignment of the species BSA1.

The PTS rotational spectrum

In the PTS spectrum were identified *a*-type and *c*-type transitions with J up to 31 and K_a up to 14. The fitting was done using a Watson's S-reduced semirigid rotor Hamiltonian implemented in SPFIT program. The lack of *b*-type transitions indicates the presence of a plane C_s , suggesting that the observed conformer is one of the two calculated structures reported in table 2.

As for BSA, also for PTS, the determination of the ^{14}N quadrupole coupling constants allowed the structural identification of PTS1 species.

The OTS rotational spectrum

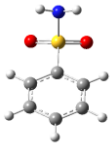
The spectrum of OTS in the frequency range 59.6 to 74.4 GHz showed splittings of the rotational transitions in two components, A and E, due to the methyl internal rotation coupling to overall molecular rotation.

A first assignment was performed for the components A, that follow the usual selection rules for a pseudo rigid rotor, obtaining a preliminary set of experimental rotational constants. The fitting was done using a Watson's S-reduced semirigid rotor Hamiltonian implemented in SPFIT program.

The analysis of hyperfine structure due to methyl rotation was performed by XIAM program of Hartwig and Dreizler [24]. A software that allows the simultaneous analysis of internal rotation and nuclear quadrupole couplings. The input data used were the rotational constants determined previously and the parameters of internal rotation such as the potential barrier (V_3), the moment of inertia of the CH_3 top (I_a) and the angles ($\angle \text{CC}, g$; where $g=a, b, c$) between the internal rotation axis (CC) and the principal axis (g) calculated for the most stable species OTS1. From the analysis the rotational and quartic centrifugal distortion constants the V_3 were obtained while the angles $\angle \text{CC}, g$ and I_a were held fixed. Additional measurements in the range 2-8 GHz allowed to determine the ^{14}N quadrupole couplings constants. Overall *a*-type and *c*-type transitions with J up to 31 and K_a up to 18 were assigned. All parameters are reported in table 3.

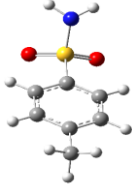
The V_3 height was determined to be $6.35(6) \text{ kJ mol}^{-1}$. Comparisons with other ortho methyl substituted benzene show that this value is between those of ortho-fluorotoluene 2.7 kJ mol^{-1} [25], anti-*o*-cresol $4.426(1) \text{ kJ mol}^{-1}$ and that one of syn-*o*-cresol $7.91(5) \text{ kJ mol}^{-1}$ [26], while it is more closer to the value of [^{35}Cl]-*o*-Chlorotoluene $5.580(5) \text{ kJ mol}^{-1}$ and [^{37}Cl]-*o*-Chlorotoluene $5.58(2) \text{ kJ mol}^{-1}$ [27].

Table 1: Theoretical and experimental spectroscopic parameters of BSA.

	BSA1	BSA2		exp. NH ₂	exp. NDH	exp. ND ₂
						
A (MHz)	2570	2572.99	A (MHz)	2627.659(1) ^a	2577.4061(7)	2531.2916(7)
B (MHz)	822	820.64	B (MHz)	838.2808(3)	826.662(6)	815.30(1)
C (MHz)	718	716.27	C (MHz)	730.4886(3)	724.128(5)	717.64(1)
μ_a (D)	2.61	4.83	D _J (kHz)	0.0430(7)	[0.043] ^c	[0.043]
μ_b (D)	0	0	D _{JK} (kHz)	0.09(2)	[0.09]	[0.09]
μ_c (D)	3.01	3.72	D _K (kHz)	-	-	-
χ_{aa} (MHz)	-2.92	-4.97	d ₁ (kHz)	-0.0024(2)	[-0.0024]	[-0.0024]
χ_{bb} (MHz)	1.61	1.78	d ₂ (kHz)	0.01202(6)	[0.01202]	[0.01202]
χ_{cc} (MHz)	1.32	3.19	χ_{aa} (MHz)	-2.62(1)	-	-
ΔE_e (cm ⁻¹)	0	232	χ_{bb} (MHz)	1.37(3)	-	-
			χ_{cc} (MHz)	1.24(3)	-	-
			$\mu_a/\mu_b/\mu_c$ ^d	yes/no/yes	no/no/yes	no/no/yes
			N ^b	152	45	27
			σ (kHz) ^c	63	69	59

^a Standard error in parentheses in the units of the last digit. ^b Number of transitions. ^c Root mean square deviation of the fit. ^d Yes or no observation of *a*-, *b*-, and *c*-type transitions, respectively. ^e Values in squared brackets are fixed to the parent species ones.

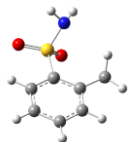
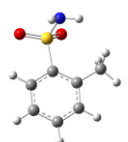
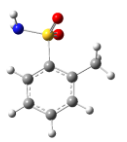
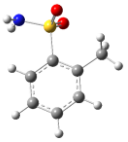
Table 2: Theoretical and experimental spectroscopic parameters of PTS.

	PTS1	PTS2		exp.
				
A (MHz)	2538.74	2539.13	A (MHz)	2634.331(3) ^a
B (MHz)	554.16	553.11	B (MHz)	563.2094(4)
C (MHz)	504.93	504.04	C (MHz)	512.8024(5)
μ_a (D)	3.27	5.55	D _J (kHz)	0.0263(4)
μ_b (D)	0	0.08	D _{JK} (kHz)	[0]
μ_c (D)	2.94	3.66	D _K (kHz)	0.139(8)
χ_{aa} (MHz)	-2.94	-4.99	d ₁ (kHz)	-0.022(4)

χ_{bb} (MHz)	1.62	1.78	d_2 (kHz)	-1.3(2)
χ_{cc} (MHz)	1.32	3.21	χ_{aa} (MHz)	-2.62(1)
ΔE_e (cm ⁻¹)	0	183	χ_{bb} (MHz)	1.35(1)
			χ_{cc} (MHz)	1.27(1)
			$\mu_a/\mu_b/\mu_c^d$	yes/no/yes
			N^b	89
			σ (kHz) ^c	38

^a Standard error in parentheses in the units of the last digit. ^b Number of transitions. ^c Root mean square deviation of the fit. ^d Yes or no observation of *a*-, *b*-, and *c*-type transitions, respectively.

Table 3: Theoretical and experimental spectroscopic parameters of OTS.

	OTS1	OTS2	OTS3	OTS4		exp.
						
A (MHz)	1726.71	1721.98	1729.13	1734.64	A (MHz)	1755.075(2) ^a
B (MHz)	811.75	806.77	809.12	804.82	B (MHz)	827.0307(5)
C (MHz)	627.5	623.95	625.84	624.29	C (MHz)	637.1196(5)
μ_a (D)	2.46	4.54	2.08	3.83	D_J (kHz)	0.0207(8)
μ_b (D)	1.26	1.65	2.64	3.44	D_{JK} (kHz)	0.058(4)
μ_c (D)	2.9	3.4	0.01	0.02	D_K (kHz)	0.009(3)
χ_{aa} (MHz)	-2.08	-4.88	-2.36	-4.68	d_1 (kHz)	0.013(2)
χ_{bb} (MHz)	-0.27	1.87	0.73	2.72	d_2 (kHz)	-
χ_{cc} (MHz)	2.35	3.01	1.63	1.96	χ_{aa} (MHz)	-2.030(9)
V_3 (cm ⁻¹)	472				χ_{bb} (MHz)	0.442579(5)
ΔE_e (cm ⁻¹)	0	569	429	1140	χ_{cc} (MHz)	1.587(1)
					$\mu_a/\mu_b/\mu_c^d$	yes/no/yes
					V_3 (cm ⁻¹)	531.4(5)
					F_0 (GHz)	[159.7784] ^c
					δ (rad)	[1.12810]
					ϵ (rad)	[-0.009362]
					$\langle(CC, a)^\circ$	[64.6358]
					$\langle(CC, b)^\circ$	[25.3695]
					$\langle(CC, c)^\circ$	[90.4847]
					N^b	137
					σ (kHz) ^c	21

^a Standard error in parentheses in the units of the last digit. ^b Number of transitions. ^c Root mean square deviation of the fit. ^d Yes or no observation of *a*-, *b*-, and *c*-type transitions, respectively. ^e Values in squared brackets are fixed to the theoretical values.

Table 4: Theoretical and experimental principal axes system coordinates of the amino hydrogen atoms in BSA.

	exp. NH	exp. NH		NH _{BSA1} ^b	NH _{BSA2} ^b
a _s (Å)	2.313(1) ^a	2.362(2)	a _e (Å)	-2.4144	-1.7345
b _s (Å)	0.813(3)	0.816(5)	b _e (Å)	-0.8428	-0.8479
c _s (Å)	1.768(1)	1.715(2)	c _e (Å)	-1.7369	-1.9853

^aConstrain's errors expressed in units of the last decimal digits. ^bFrom B3LYP/6-311++G** geometry.

Conformational Assignment of OTS

In the spectrum of OTS a population of lines relative to an only conformer was identified. The determined rotational constants are in agreement with those of the conformational species reported in table 2. However the similarity of rotational constants between the four calculated structures doesn't allow the immediate structural identification.

If the criterion that the most stable conformer obtained from the calculations must be the more likely to be observed is used, the assigned conformational species must be OTS1.

However some experimental considerations can be done to verify the validity of this statement.

The observation of μ_c -transitions in the spectrum makes possible to exclude the shapes OTS3 and OTS4. If ¹⁴N quadrupole coupling constants are compared with those calculated for OTS1 and OTS2, the assigned species must be OTS1. The superior stability of shape OTS1 can be ascribed to a weak attractive interaction between the nitrogen lone pair and the methyl hydrogen atoms.

Conclusion

In this work the conformational preferences of the compounds BSA, PTS, OTS were analyzed through their rotational spectra recorded by FJ-AMMW and PJ-CP-FTMW spectrometers in the 59.6-74.4 GHz and 2-8 GHz frequency ranges, respectively. For all the ¹⁴N quadrupole coupling constants were determined. For OTS also the hindering barrier of the methyl group rotation was determined.

This study shows as weak intramolecular interactions are able to change the conformational preferences of the pharmacophore group, benzensulfonamide.

In the compounds BSA and PTS, where there are not groups close to the sulfonamide tail, the conformational behaviour is similar. In both cases, the amino group lies perpendicular to the aromatic plane.

Instead in OTS, where a weak attractive interaction between the nitrogen lone pair and the methyl hydrogen atoms takes place, the amino group lies in gauche.

Indeed, in all cases, it is observed that the amino group hydrogen atoms are directed in way to eclipse the O's of the SO₂ group. This trend can be due to electrostatic interactions between O and H atoms.

References

- [1] www.c4xdiscovery.com;
- [2] C. Blundell, T. Nowak, M. Watson "Measurement, Interpretation and Use of Free Ligand Solution Conformations in Drug Discovery", *Prog. Med. Chem.*, 2016, 55, 45-147
- [3] A. Achari, D. Somers, J. Champness, P. Bryant, J. Rosemond, D. Stammers, *Nat. Struct. Biol.* 1997, 6
- [4] V. Krishnamurthy, G. Kaufman, A. Urbach, et al., *Chem. Rev.* 2008, 108,3
- [5] S. Zimmerman, A. Innocenti, A. Casini, J. Ferry, A.Scozzafava, C. Supuran, *Bioorg. Med. Chem. Lett.* 2004, 14, 24
- [6] A. Alsughayer, A. Elassar, S. Mustafa and F. Sagheer, *J. Biom. and Nanobiot.*, 2011, 2, 2
- [7] A. Scozzafava, T. Owa, A. Mastrolorenzo, C. Supuran, *Curr. Med. Chem.* 2003, 10, 11
- [8] A. Weber, A. Casini, A. Heine, D. Kuhn, C. Supuran, A. Scozzafava, G. Klebe, *J. Med. Chem.*, 2004, 47, 3
- [9] W. Caminati, D. Damiani, G. Corbelli, B. Velino, C. Bock, *Mol. Phys.* 1991, 74, 4
- [10] M. Onda, A. Toda, S. Mori, Ichiro Yamaguchi, *J. Mol. Struct.* 1986, 144, 1-2
- [11] H. Im, E. Bernstein, I. Seeman, H. Secor, *J. Am. Chem. Soc.*, 1991, 113
- [12] K. Utzat, R. Bohn, J. Montgomery, H. Michels, W. Caminati, *J. Phys. Chem.*, 2010, 114, 25
- [13] W. Caminati, A. Maris, A. Millemaggi, P. Favero, *Chem. Phys. Lett.* 1995, 243
- [14] S. Melandri, W. Caminati, L. Favero, A. Millemaggi, P. Favero, *J. Mol. Struct.*, 1995, 352/353
- [15] S. Melandri, G. Maccaferri, A. Maris, A. Millemaggi, W. Caminati, and P. Favero, *Chem. Phys. Lett.*, 1996, 261
- [16] C. Calabrese, A. Maris, L. Evangelisti, L. Favero, S. Melandri, W. Caminati, *J. Phys. Chem. A.* 2013, 117
- [17] J. Neill, S. Shipman, L. Alvarez-Valtierra, A. Lesarri, Z. Kisiel, B. Pate, *J. Mol. Spectrosc.* 2011, 269
- [18] D. Loru, M. Bermudez, M. Sanz, *J. Chem. Phys.*, 2016, 145
- [19] M.J. Frisch, G.W. Trucks, H.B. Schlegel, G.E. Scuseria, M.A. Robb, J.R. Cheeseman, G. Scalmani, V. Barone, B. Mennucci, G. A. Petersson, H. Nakatsuji, M. Caricato, X. Li, H.P. Hratchian, A.F. Izmaylov, J. Bloino, G. Zheng, J.L. Sonnenberg, M. Hada, M. Ehara, K. Toyota, R. Fukuda, J. Hasegawa, M. Ishida, T. Nakajima, Y. Honda, O. Kitao, H. Nakai, T. Vreven, J.A. Montgomery Jr., J.E. Peralta, F. Ogliaro, M.

Bearpark, J.J. Heyd, E. Brothers, K.N. Kudin, V.N. Staroverov, T. Keith, R. Kobayashi, J. Normand, K. Raghavachari, A. Rendell, J. C. Burant, S.S. Iyengar, J. Tomasi, M. Cossi, N. Rega, J. M. Millam, M. Klene, J.E. Knox, J.B. Cross, V. Bakken, C. Adamo, J. Jaramillo, R. Gomperts, R.E. Stratmann, O. Yazyev, A.J. Austin, R. Cammi, C. Pomelli, J. Ochterski, R.L. Martin, K. Morokuma, V.G. Zakrzewski, G.A. Voth, P. Salvador, J.J. Dannenberg, S. Dapprich, A.D. Daniels, O. Farkas, J.B. Foresman, J.V. Ortiz, J. Cioslowski, D. Fox, Gaussian 09, Revision D.01, Gaussian, Inc., Wallingford, CT

[20] H. M. Pickett, *J. Mol. Spectrosc.* 148 (1991) 371-377.

[21] J.K.G. Watson, in *Vibrational Spectra and Structure*; Durig, J.R., Ed.; Elsevier: Amsterdam, 1977; Vol. 6, pp 1-89.

[22] J Kraitichman, *Am. J. Phys.* 1953, 21

[23] C. Constain, G. Srivastava, *J. Chem. Phys.* 1961, 35

[24] H. Hartwig, H. Dreizler, *Z. Naturforsch. 51A*, 1996, 923-932

[25] J. Susskind, *J. Chem. Phys.*, 1970, 53, 6

[26] A. Welzel, A. Hellweg, I. Merke, W. Stahl, *J. Mol. Spectr.*, 2002, 215, 1

[27] D. Gerhard, A. Hellweg, I. Merke, W. Stahl, M. Baudalet, D. Petitprez, G. Wlodarczack, *J. Mol. Spectr.* 2003, 220

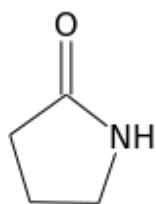
CHAPTER 4

INTERNAL DYNAMICS IN PHARMACOPHORE GROUPS: THE ROTATIONAL SPECTRA OF 2-PYRROLIDINONE AND 2-IMIDAZOLIDINONE

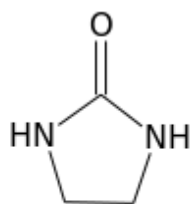
Introduction

Small cyclic structures are an important benchmark for the molecular designers. These structures can be inserted within of a molecule in order to manipulate the molecular electronic distribution and to handle the molecular conformational flexibility. In particular, heterocyclic rings are, often, used as building blocks in drugs. Among them, the five-membered lactams have attracted considerable interest in the biological field because, besides to have electronic and dynamic regulatory functions, they have pharmacological activity.

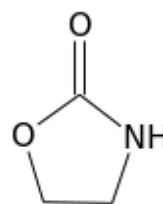
For instance, 2-oxazolidinone, 2-pyrrolidinone and 2-imidazolidinone are found in a great number of drugs. The 2-oxazolidinone is the main pharmacophore group of a whole antibiotic class, known as oxazolidinones. Oxazolidinones are active against a series of Gram-positive bacteria: they inhibit the protein synthesis by targeting the bacterial ribosomal subunit. The most known compound of this class is linezolid, sold with the name Zyvox [1]. The crystal structures of the linezolid assembled in the ribosomal subunit of several bacteria have been characterized and catalogued in the RCSB Protein Data Bank with the codes: 4WFA, 4K7Q, 3DLL and 3CPW.



2-pyrrolidinone



2-imidazolidinone



2-oxazolidinone

2-imidazolidinone derivatives are compounds useful for the therapy of senile dementia. While the 2-pyrrolidinone ring is found in many drugs active against a great variety of diseases: i) Piracetam, is able to improve the cognitive functions such as memory, creativity, or motivation and in addition it is used in UK to combat the discomfort of the Myoclonus, that is a brief and involuntary twitching of a muscle, or a group of muscles [2], ii) Cytisine, is used as a treatment against depression, PTSD, schizophrenia, Alzheimer's disease and Parkinson's disease [3]; iii) Doxapram hydrochloride (marketed as Dopram, Stimulex or Respiram) that acts as respiratory stimulant by

stimulation of the chemoreceptors in the carotid bodies of the carotid arteries, which in turn, stimulate the respiratory center in the brain stem [4].

Since the biological importance of five membered lactams, in this work a detailed analysis on the dynamic and structures of the rings: 2-imidazolidinone and 2-pyrrolidinone (hereafter IMI and PYR, respectively) have been performed by rotational spectroscopy.

Due to a delicate balancing between angular strain and torsional forces, saturated and partially saturated five member rings have puckered structures connected by large amplitude motions.

The two possible puckered geometries are known as envelope and twist. In the envelope form, four of the atoms are coplanar and a fifth is out of the plane, while, in the twist form, three atoms are coplanar and two are displaced, alternately above and below the plane.

Rotational spectroscopy investigations have contributed enormously to characterize the structures and the motions that occur between equivalent conformations. Information on the internal dynamics are obtained when hyperfine structures, due to tunnel effect, are observed in the spectra. The tunnel effect splits the vibrational levels in two sublevels (0 and 1), from which rotational transitions doublings are generated. The transitions can occur within the same sublevels or between different sublevels, labeled as intrastate ($0 \rightarrow 0$, $1 \rightarrow 1$) and interstate transitions ($0 \rightarrow 1$, $1 \rightarrow 0$), respectively. The interpretation of these tunneling splittings allows to determine the energy difference between vibrational sublevels (ΔE_{01}). Since this value depends on the reduced mass and barrier of the motion it can be used as parameter to model the potential energy surfaces governing the molecular motion. For instance, the hyperfine structures observed in the microwave spectrum of 1-chloro cyclopentene revealed the presence of two equivalent envelope conformations, connected by ring puckering motion. From the determined ΔE_{01} , the hindering motion barrier was evaluated, using Meyer's Flexible model, to be $V=2.89 \text{ kJ mol}^{-1}$ [5].

Fully saturated five-membered cycles are very floppy. In the prototype system, cyclopentane [6], the two, twisted and enveloped, arrangements have energy values very similar. The structures interconvert freely, passing through ten equivalent envelope and ten equivalent twisted structures, a path known as pseudorotation. In heterocyclic saturated systems as tetrahydrofuran [7] the twisted and enveloped arrangements have different energy and the pseudorotation barriers are more high.

In the case of saturated ring, containing sp^2 hybridized carbon atom, the conformational behaviour is still different. For instance the hyperfine structures, due to the effect tunnel, observed in the rotational spectra of cyclopentanone [8], ethylene carbonate [9], IMI [10] and oxazolidinone [11], indicated the existence of two equivalent twisted structures connected by ring inversion motion. Indeed for ethylene carbonate and cyclopentanone also the motion

hindering barrier was determined. To describe the interconversion between two equivalent structures, two plausible paths were hypothesized. In a first guess, it is supposed that the motion takes place through a planar configuration, the barriers were found 2.8 kJ mol^{-1} and 1.9 kJ mol^{-1} , respectively. In the other model, a pseudorotation path, through an envelope conformation, was hypothesized, the barriers were 14.3 kJ mol^{-1} and $0.478 \text{ kJ mol}^{-1}$, respectively [8, 9].

In this work, a furthermore study on IMI has been performed, in order to model the potential energy surface governing the ring inversion motion.

Experimental section and computational details

Commercial samples of PYR and IMI hemihydrate were purchased from Alfa Aesar and used as received. PYR ($\text{C}_4\text{H}_7\text{NO}$, m.w. 85.11, 99%) is a liquid substance, the melting point is $23\text{-}25^\circ\text{C}$ at ambient conditions. IMI ($\text{C}_3\text{H}_6\text{N}_2\text{O}\cdot 0.5\text{H}_2\text{O}$, m.w 95.10, 98+%) is a white crystalline solid, melting point is 55°C at ambient conditions. To obtain a suitable concentration of the samples, PYR and IMI were warmed at $85\text{-}90^\circ\text{C}$ and $120^\circ\text{-}130^\circ\text{C}$, respectively. The gas mixtures in argon were expanded from a pressure of 20 kPa to about 0.5 Pa through a 0.3 mm diameter pinhole nozzle. The isotopologues species of PYR and IMI have been obtained by passing D_2O in Ar over the heated samples. The spectra were recorded in the 52.5 to 74.4 GHz frequency range by the free-jet Stark modulated millimeter wave absorption spectrometer [12-14]. The resolution and the estimated accuracy of the frequency measurements are about 300 kHz and 50 kHz, respectively.

Full geometry optimizations were run applying appropriate options for the search of the minimum and the transition state. Subsequent harmonic frequency calculations were performed to characterize the stationary points. All computations were run at B3LYP/6-311++G(d,p) employing the Gaussian09 suite of program [15].

Results of PYR

Theoretical calculations indicated the existence of two equivalent non-planar conformations. The cycle is predicted in a twisted conformation in which the $\text{CC}(=\text{O})\text{N}$ frame is planar. From the structure, trial spectroscopic constants (table 1) were obtained and used for the search of the rotational transitions in the laboratory spectrum.

The spectrum showed hyperfine structure arising from ring inversion motion and ^{14}N quadrupole coupling interactions. Intrastate *a*-type and *b*-type transitions ($0 \rightarrow 0$, $1 \rightarrow 1$) and interstate *c*-type transitions ($0 \rightarrow 1$, $1 \rightarrow 0$) were identified (figure 1).

The rotational transitions patterns were fit using a coupled Hamiltonian:

$$H = H_{0,R} + H_{1,R} + H_{CD} + H_{Int} + H_Q$$

$$H_{Int} = \Delta E_{01} + F_{bc} (P_b P_c + P_c P_b) + F_{ac} (P_a P_b + P_b P_a)$$

where $H_{0,R}$ and $H_{1,R}$ are the rigid Hamiltonian relative to the vibrational sublevels 0 and 1, H_{CD} is the Watson *S*-reduced centrifugal distortion Hamiltonian [16, 17], H_Q is the quadrupole coupling Hamiltonian and H_{Int} is the interaction Hamiltonian between two sublevels, in which ΔE_{01} is the energy separation between the sublevels 0 and 1 and F_{bc} and F_{ac} are the Coriolis's interaction constants, that take in account the coupling of the two sublevels. The obtained rotational constants, quartic centrifugal distortion constants, ΔE_{01} and F_{bc} and F_{ac} are reported in table 1.

From rotational constants, the inertial planar momentum P_{cc} ($6.31 \text{ u}\text{\AA}^2$) was determined, acquiring an experimental indication of the planarity of the system. Direct comparison to the calculated values for the minimum ($5.96 \text{ u}\text{\AA}^2$) and planar structure ($4.95 \text{ u}\text{\AA}^2$) evidences that the experimental structures is not planar.

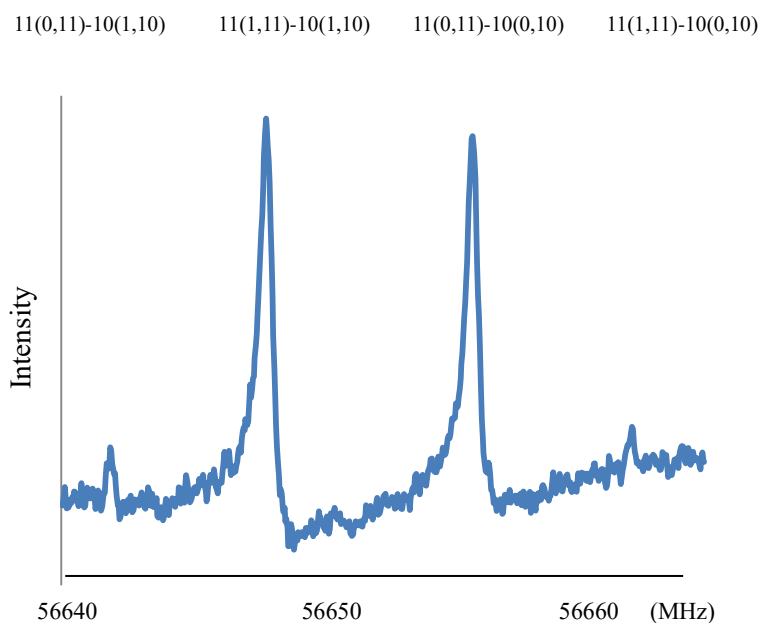


Figure 1: Portion of the spectrum of PYR

Deuterated isotopologues

Also the spectrum of the N-deuterated species (PYR-D) was analyzed. Measured transition lines were fitted using the same Hamiltonian, employed for the parent species. Intrastate *a*-type and *b*-type transitions with *J* up to 11 and *K_a* 9 were observed. The obtained rotational constants, centrifugal distortion constants, ΔE_{01} , F_{ac} and quadrupole couplings constants are reported in table 1.

Table 1. Theoretical and experimental spectroscopic parameters of PYR.

	B3LYP/6-311++G(d,p)	EXP. (NH)	EXP. (ND)
<i>A</i> (MHz)	7172.52	7175.131(6) ^a	6794.408(5)
<i>B</i> (MHz)	3440.21	3457.879(1)	3453.436(2)
<i>C</i> (MHz)	2459.92	2477.733(5)	2428.508(3)
<i>D_J</i> (kHz)	4.29	0.230(4)	0.199(6)
<i>D_{JK}</i> (kHz)	0.61	1.16(1)	1.14(1)
<i>D_K</i> (kHz)	0.36	1.21(8)	0.3(1)
<i>d₁</i> (kHz)	-	-0.028(2)	-
$\mu_a/\mu_b/\mu_c$ (D)	4.29/0.61/0.36	yes/yes/yes ^d	yes/yes/no
χ_{aa} (MHz)	2.39	2.2(1)	2.0(3)
χ_{bb} (MHz)	2.14	1.9(2)	1,7(0)
χ_{cc} (MHz)	-4.53	-4.1(2)	-3.7(0)
ΔE_{01} (MHz)		220.96(2)	206(1)
F_{bc} (MHz)		10.92(3)	11.11(9)
F_{ca} (MHz)		35.5(3)	[35.5] ^e
σ (kHz) ^c		110	130
<i>N^b</i>		204	78

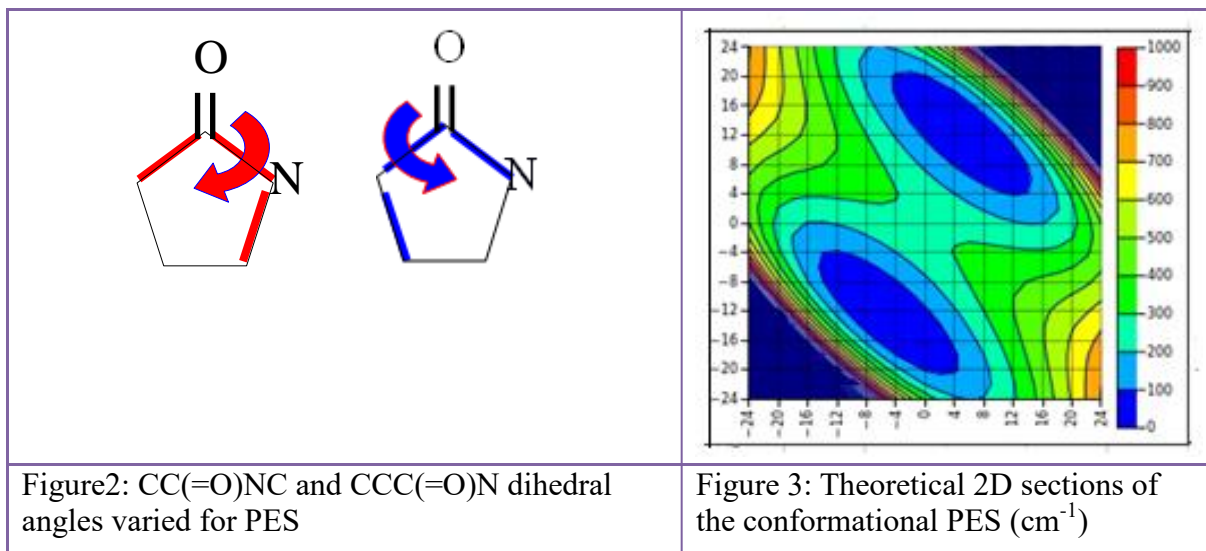
^a Standard error in parentheses in the units of the last digit. ^b Number of transitions. ^c Root mean square deviation of the fit. ^d Yes or no observation of *a*-, *b*-, and *c*-type transitions, respectively. ^e Values in squared brackets are fixed to the parent species ones.

Ring inversion potential energy surface

The rotational spectra of both PYR and PYR-D showed a hyperfine structures, arising from a ring inversion motion. The vibrational spacing was determined as 220.96(2) and , 206(1) (cm⁻¹) for PYR and PYR-D, respectively. The lowering of ΔE_{01} , in going from NH to ND species, is ascribed to the reduced mass effect.

In order to characterize the inversion motion, theoretical calculations aimed to the exploration of the conformational space were run. The CC(=O)NC and CCC(=O)N dihedral angles (figure 2) were

varied from -24° to $+24^\circ$, whereas all the other internal coordinates were freely optimized at the B3LYP/6-311++G(d,p) level of calculation. The achieved double minimum potential energy surface (figure 3) show that the motion takes place through a planar transition state, lying at 2.63 kJ mol^{-1} .



Results of IMI

Quantum mechanical calculations indicated that IMI exists in two equivalent non-planar structures belonging to the C_2 symmetry point group. The NC(=O)N frame is planar and the cycle is predicted in a twisted conformation with the C_2 axis passing through the CO bond. Since the C_2 symmetry axis coincides with the a inertial axis, a pure μ_a -type rotational spectrum is expected to be observed. The depiction of the structure, with the calculated spectroscopic parameters is reported in table 2.

The spectrum showed hyperfine structure arising from both the ring inversion and the ^{14}N nuclear quadrupole coupling to overall molecular rotation.

Using the experimental rotational constants previously reported in rif. 10, ΔE_{01} , F_{bc} and ^{14}N quadrupole coupling constants were obtained (table 2). Only intrastate a -type transitions with J up to 13 and K_a 9 were observed. The IMI spectrum showing some intrastate a -type transitions is reported in figure 4.

Comparison of experimental P_{cc} ($4.851 \text{ u}\text{\AA}^2$) with those calculated values for the minimum ($4.63 \text{ u}\text{\AA}^2$) and planar structure ($3.161 \text{ u}\text{\AA}^2$) evidences that the experimental structures is not planar.

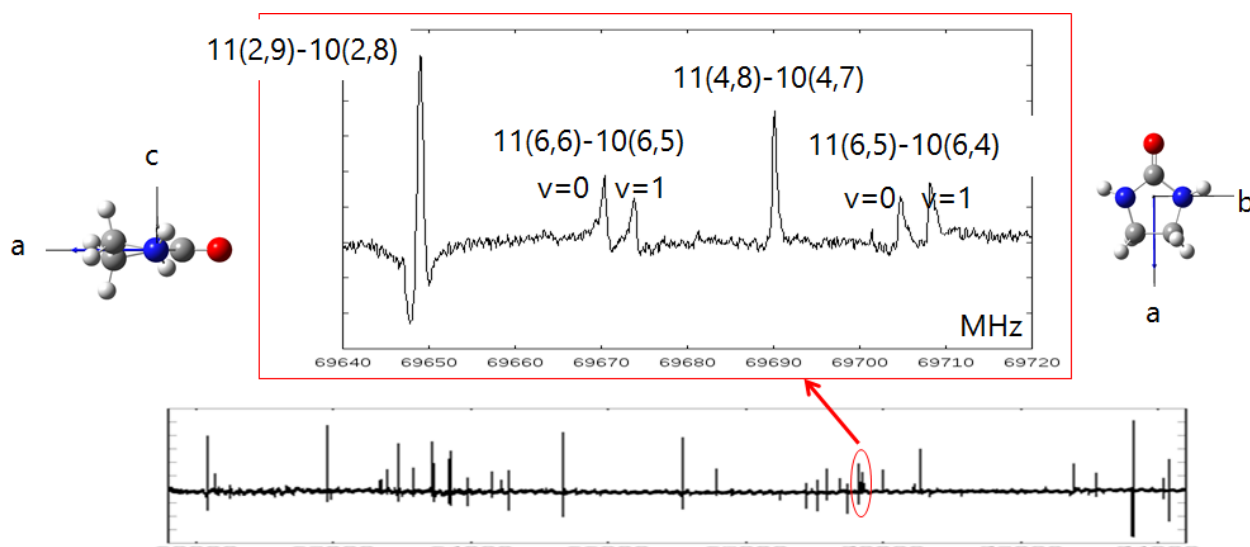


Figure 4: IMI spectrum showing some intrastate *a*-type transitions.

Deuterated isotopologues

In order to obtain more information on the ring inversion motion, also the spectra of deuterated isotopologues species (IMI-D and IMI-DD) were analyzed. In both cases intrastate *a*-type transitions with *J* up to 13 and *K_a* 9 were observed. The obtained rotational constants, centrifugal distortion constants, ΔE_{01} , F_{ac} are reported in table 2.

Table 2. Theoretical and experimental spectroscopic parameters of IMI.

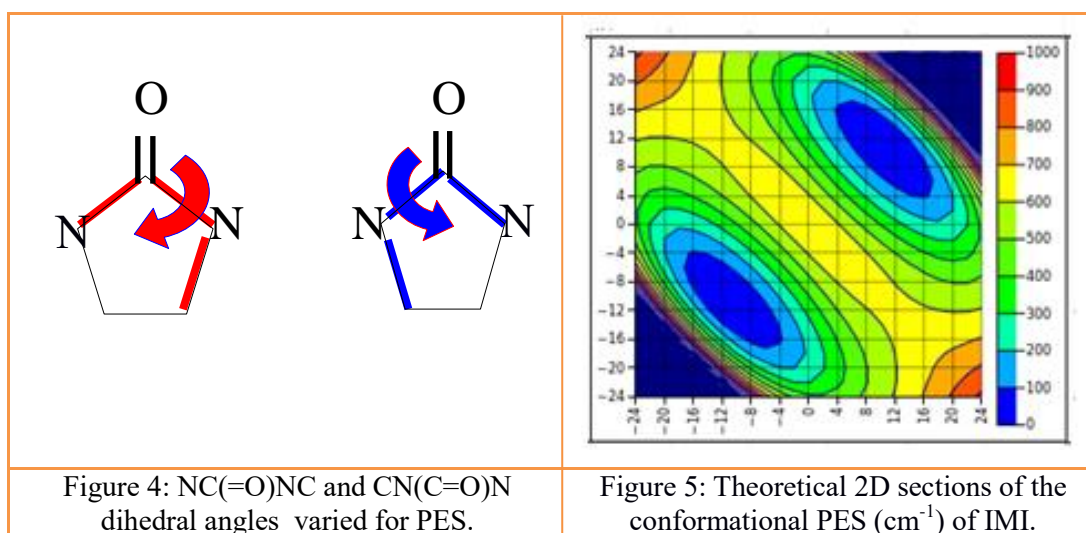
	B3LYP/6-311++G(d,p)	EXP. IMI	EXP. IMI-D	EXP. IMI-DD
<i>A</i> (MHz)	7696.94	7696.500(1) ^a	7260.930(2)	6861.636(5)
<i>B</i> (MHz)	3603.70	3619.287(4)	3615.989(6)	3613.18(1)
<i>C</i> (MHz)	2570.10	2583.799(5)	2531.958(7)	2480.98(1)
<i>D_J</i> (kHz)		0.29(1)	0.22(1)	0.19(2)
<i>D_{JK}</i> (kHz)		1.33(2)	1.29(2)	0.92(3)
<i>D_K</i> (kHz)		0	[0] ^c	[0]
<i>d₁</i> (kHz)		-0.05(3)	-0.057(3)	-0.075(3)
<i>d₂</i> (kHz)		-0.024(2)	[-0.024]	[-0.024]
$\mu_a/\mu_b/\mu_c$	4.61/ 0 /0	yes/no/no ^d	yes/no/no	yes/no/no
χ_{aa} (MHz)	-5.06	2.51(4)	[2.51]	[2.51]
χ_{bb} (MHz)	2.79	2.0(3)	[2.0]	[2.0]
χ_{cc} (MHz)	2.27	-4.5(3)	[-4.5]	[-4.5]
ΔE_{01} (MHz)		73.42(2)	51.19(3)	36.29(4)
F_{bc} (MHz)		-27.64(6)	27.6(1)	-27.3(2)
σ (kHz) ^c		46	56	58
<i>N</i> ^b		101	74	41

^a Standard error in parentheses in the units of the last digit. ^b Number of transitions. ^c Root mean square deviation of the fit. ^d Yes or no observation of *a*-, *b*-, and *c*-type transitions, respectively. ^e Values in squared brackets are fixed to the parent species ones.

Ring inversion potential energy surface

The rotational spectra of IMI, IMI-D and IMI-DD showed rotational transitions splittings, due to the tunnel effect, indicating the presence of a ring inversion motion. For the three species, the vibrational sublevels spacings are 73.43 (2), 51.18(3) and 36.31(4) cm^{-1} , respectively.

In order to determine the motion path, theoretical calculations were done. A bi-dimensional potential energy surface was obtained, varying at fixed values the $\text{NC}(=\text{O})\text{NC}$ and $\text{CN}(\text{C}=\text{O})\text{N}$ dihedral angles, (figure 5). The calculations showed a double minimum potential energy function, in which two almost isoenergetic interconversion paths can be recognized: the interconversion could take place passing through a planar structure by a ring puckering motion or an envelope configuration by a pseudorotation motion (figure 6).



Both paths were used to model a semi-experimental PES by Meyer's flexible model. [18]

The flexible model is a numerical method used to solve the vibrational problem for one- or two-dimensional internal motions.

The program calculates the rotational and vibrational wavefunctions and the corresponding eigenvalues, leaving from structural relaxations and energy profiles.

To describe the structural relaxations and energy trend are used analytic functions depending on one or two independent variables, in the case of one- or two-dimensional model, respectively.

The coefficients used in the potential energy potential function are varied until the spectroscopic constants (i.e. rotational constants, ΔE_{01}) of the investigated species are reproduced.

To describe the IMI ring inversion motion, one-dimensional model was used.

Two plausible paths were hypothesized. In both cases the structural parameters and potential energy paths were extracted by theoretical calculations.

In a first guess, it was supposed that the motion takes place through a planar configuration. The proposed model takes in account of the molecule C_2 symmetry. The chosen variable (r) was the dihedral angle $CNC(=O)N$.

The potential energy function with respect to the variable is: $V(r)=B_2*[1-(r/r_{eq})^2]^2$, in which r_{eq} and B_2 are the equilibrium r value and the barrier height, respectively.

In the second model, a pseudorotation motion through an envelope configuration of the ring was supposed. The potential energy V against the pseudorotation coordinate φ is described by: $V(\varphi)=V_2[1+\cos(2\varphi)]/2+V_4[1-\cos(4\varphi)]/2$.

For both models, the experimental data of parent species and the two isotopologues have been reproduced satisfying (table 3) and the achieved energy parameters are summarised in table 3.

Table 3: Results of the flexible model

Ring puckering	IMI	IMI-D	IMI-DD	Pseudo-rotation	IMI	IMI-D	IMI-DD
A_0 / MHz	7698	7259	6857	A_0	7697	7253	6848
B_0 / MHz	3611	3608	3604	B_0	3604	3600	3598
C_0 / MHz	2589	2536	2483	C_0	2567	2514	2463
E_{10} / MHz	73.44	51.24	37.46	E_{10}	74.37	55.18	40.68
r_{eq} / Å	13°			V_2 / cm^{-1}	465.12		
B_2 / cm^{-1}	455			V_4 / cm^{-1}	-83.6		

Conclusion

In this work, the dynamic and conformational behavior of the pharmacophore groups: 2-pyrrolidinone and 2-imidazolidinone has been investigated by their rotational spectra and theoretical methods such as functional density theory and Meyer's flexible model.

The compounds have two equivalent forms which can interchange by inversion motion.

In 2-pyrrolidinone, the motion is described by double minimum potential surface that takes place through a planar transition state, with a calculated barrier of 2.63 $kJ mol^{-1}$.

While for 2-imidazolidinone, the double minima potential energy surface was determined using the Meyer's 1D-flexible model.

To describe the interconversion between two equivalent structures, two plausible paths were hypothesized. In a first guess, it is supposed that the motion takes place through a planar configuration: $V(r)=B_2*[1-(r/r_{eq})^2]^2$. In the other model, a pseudorotation motion through an envelope configuration of the ring is supposed: $V(\varphi)=V_2[1+\cos(2\varphi)]/2+V_4[1-\cos(4\varphi)]/2$. The experimental data of all isotopologues are reproduced with $B_2=5.4 kJ mol^{-1}$, $r_{eq}=13^\circ$, and $V_2=5.65$, $V_4=1.00 kJ mol^{-1}$, respectively.

References

- [1] B. Bozdogan, P. Appelbaum., *Int. J. Antimicrob. Agents.*, 2004, 23, 2
- [2] L. Flicker, J. Evans, *Cochrane Database of Systematic Reviews*, 2004
- [3] J. Buccafusco, A. Terry, *Bioch. Pharm.*, 2009, 78, 7
- [4] R. Lugliani, B. Whipp, K. Wasserman, *Chest*, 1979, 76, 4
- [5] W. Caminati, R. Danieli, A.C. Fantoni, J.C. Lopez, *J. Mol. Spectr.*, 1997, 181
- [6] D. Cremer, J. Pople, *J. Am. Chem. Soc.*, 1975, 97, (6)
- [7] A. Mamleev, L. Gunderova, R. Galeev, *J. Struct. Chem.*, 2001, 42
- [8] H. Kim., W. Gwinn, *J. Chem. Phys.*, 1969, 51
- [9] J. Alonso, R. Cervellati, A. Degli Esposti, D. Lister, P. Palmieri, *J. Chem. Soc. Faraday Trans. 2*, 1986, 82
- [10] R. Cervellati, A. Degli Esposti, D. Lister, P. Palmieri, *J. Mol. Struct.* 1988, 189
- [11] working in progress at our laboratory
- [12] S. Melandri, W. Caminati, L. Favero, A. Millemaggi and P. Favero, *J. Mol. Struct.*, 1995, 352/353
- [13] S. Melandri, G. Maccaferri, A. Maris, A. Millemaggi, W. Caminati, and P. Favero, *Chem. Phys. Lett.*, 1996, 261
- [14] C. Calabrese, A. Maris, L. Evangelisti, L. Favero, S. Melandri, W. Caminati, *J. Phys. Chem. A.*, 2013, 117
- [15] M.J. Frisch, G.W. Trucks, H.B. Schlegel, G.E. Scuseria, M.A. Robb, J.R. Cheeseman, G. Scalmani, V. Barone, B. Mennucci, G. A. Petersson, H. Nakatsuji, M. Caricato, X. Li, H.P. Hratchian, A.F. Izmaylov, J. Bloino, G. Zheng, J.L. Sonnenberg, M. Hada, M. Ehara, K. Toyota, R. Fukuda, J. Hasegawa, M. Ishida, T. Nakajima, Y. Honda, O. Kitao, H. Nakai, T. Vreven, J.A. Montgomery Jr., J.E. Peralta, F. Ogliaro, M. Bearpark, J.J. Heyd, E. Brothers, K.N. Kudin, V.N. Staroverov, T. Keith, R. Kobayashi, J. Normand, K. Raghavachari, A. Rendell, J. C. Burant, S.S. Iyengar, J. Tomasi, M. Cossi, N. Rega, J. M. Millam, M. Klene, J.E. Knox, J.B. Cross, V. Bakken, C. Adamo, J. Jaramillo, R. Gomperts, R.E. Stratmann, O. Yazyev, A.J. Austin, R. Cammi, C. Pomelli, J. Ochterski, R.L. Martin, K. Morokuma, V.G. Zakrzewski, G.A. Voth, P. Salvador, J.J. Dannenberg, S. Dapprich, A.D. Daniels, O. Farkas, J.B. Foresman, J.V. Ortiz, J. Cioslowski, D. Fox, Gaussian 09, Revision D.01, Gaussian, Inc., Wallingford, CT
- [16] H. M. Pickett, *J. Mol. Spectrosc.*, 148 (1991) 371-377.
- [17] J.K.G. Watson, in *Vibrational Spectra and Structure*; Durig, J.R., Ed.; Elsevier: Amsterdam, 1977; Vol. 6, pp 1-89.
- [18] R. Meyer, *J. Mol. Spectr.*, 1979, 76, 266-300

CHAPTER 5

EXPLORING THE CONFORMATIONAL LANDSCAPE OF TERPENOID SYSTEMS: A MICROWAVE STUDY OF S-(-)-PERILLALDEHYDE

Introduction

Terpenes are a class of organic compounds, containing multiples unit of isoprene: $(C_5H_8)_n$. The isoprene units are linked together "head to tail" to form linear chains or rings, giving place to thousands of terpene compounds. If heteroatoms (O and N) are also contained in the terpenes structures, they are called terpenoids.

Terpenes and terpenoids are produced by many types of plants and flowers. Most of them are odorant substances and for this reason they are used largely in perfume and fragrance industries. However surprisingly terpenes and terpenoids are also atmosphere pollutions because, after being released in the atmosphere by the trees and plants, they react with other airborne chemicals forming air pollutants [1-3].

In addition terpenes have attracted considerable interest also in pharmaceutical field because they have shown notable biological activity such as antimicrobial, antitumor, and anti-inflammatory [4-10]. However structural studies of these substances within their biological targets are not available yet and the mechanism of action of these compounds is not elucidated.

In order to understand the key factors of their biological action, researchers have given rise to a great number of studies to correlate their activities with their structures [11].

Detailed structural investigations of such compounds are therefore of fundamental importance.

Rotational spectroscopy is a powerful tool to study in detail the structure and dynamic of molecular systems in gas phase. The rotational spectrum of a species is highly sensitive to its atom masses distribution and for this reason different conformers, tautomers and isotopologues can be identified unambiguously in a same mixture.

The focus of this work is the dynamics and structural characterization of the terpenoid, s-(-)-perillaldehyde (4-isopopenylcyclohex-1-ene-1-carbaldehyde, hereafter PERY), by its rotational spectrum recorded using a pulsed jet chirped pulse Fourier transform microwave spectrometer operating in the 2-8 GHz frequency range (PJ- CP-FTMW) [12, 13].

PERY is constituted from a cyclohexene ring with a carbaldehyde group in position 1 and a isopropenyl group in positions 4. Different rotamers of PERY arise from the flexibility of the cyclohexene ring, (giving place to equatorial and axial conformers), and the internal rotations of the isopropenyl and carbaldheyde side chains.

In a previous rotational study performed on PERY using pulsed jet Fourier transform microwave spectrometer two equatorial forms were observed [14].

However, a further investigation using PJ- CP-FTMW could bring to light other stable conformational species.

Indeed, PJ-CP-FTMW is a vanguard spectrometer that combines the main advantages of those spectrometers, that for decades, have had the hegemony in the field of rotational spectroscopy as the pulsed jet Fourier transform microwave spectrometer (PJ-FTMW) [15,16] and the free jet Stark modulated absorption millimeter wave spectrometer (FJ-MMWA) [17-19].

As PJ-FTMW, PJ- CP-FTMW has high sensibility and resolving capacity. For instance, the rotational spectra of little concentrated systems, such as isotopologues species in natural abundance, are often observed.

While as FJ-MMWA, PJ-CP-FTMW is a broadband spectrometer therefore the assignment of the spectra is facilitated. In addition, with PJ-CP-FTMW, the rotational spectra can be acquired simultaneously in full 2-8 GHz frequency range.

Calculations results

The conformational landscape of PERY is determined from the flexibility of the cyclohexene ring and the orientation of the carbaldheyde and isopropenyl groups with respect to the cyclohexene ring described from dihedral angles $O_8C_7C_1C_2$ and $C_3C_4C_9C_{10}$, respectively (figure 1).

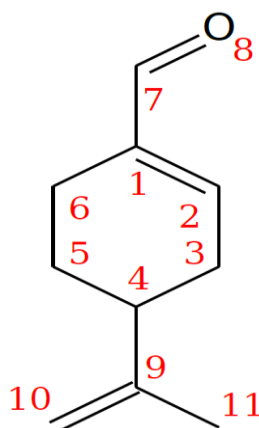


Figure 1: Sketch of perillaldehyde, numbering of the atoms used through the text.

The ring interconversion gives place to two conformational families in which the isopropenyl group lies in ring equatorial (EQ) or axial (AX) position. For each of them, carbaldheyde can be s-cis ($O_8C_7C_1C_2=0^\circ$) or s-trans ($O_8C_7C_1C_2=180^\circ$) oriented with respect to the ring double bond, whereas

isopropyl can assume three orientations ($C_3C_4C_9C_{10} \approx 0^\circ, 120^\circ$, and 240°). Thus, in principle, 12 rotamers can be considered.

On the likely rotamers, full geometry optimizations and subsequent harmonic frequency calculations, to characterize the stationary points, were performed by functional density method (B3LYP) and the Moller –Plesset second order perturbation theory (MP2) in combination with the 6-311++G(d,p) Pople’s basis set. All the calculations were done using the Gaussian 09 programs package [20].

A depiction of the obtained conformers is given in figure 2. The structures of the equatorial and axial families are labelled by EQn and AXn, respectively. The run index n can be 1,2,3 or 4,5,6 to indicate the three positions of the isopropenyl group and the C=O group in s-trans or in s-cis position, respectively. The corresponding spectroscopic parameters and the relative electronic energies are shown in table 1 and table 2.

The theoretical data both at B3LYP and MP2 level indicate that in the conformers in which the C=O group is oriented in s-trans are more stable of those in s-cis. This behavior is in agreement with experimental data reported for instance in acrolein where the abundance of s-cis conformer were only 2% of that s-trans at room conditions [21].

For the conformers belonging at the same family the stability order is $EQ1 > EQ2 > EQ3$ and $AX1 > AX2 > AX3$.

However the two methods are not in agreement in saying whether the conformers of equatorial family are more stable of those in axial, as can be noted in figure 3.

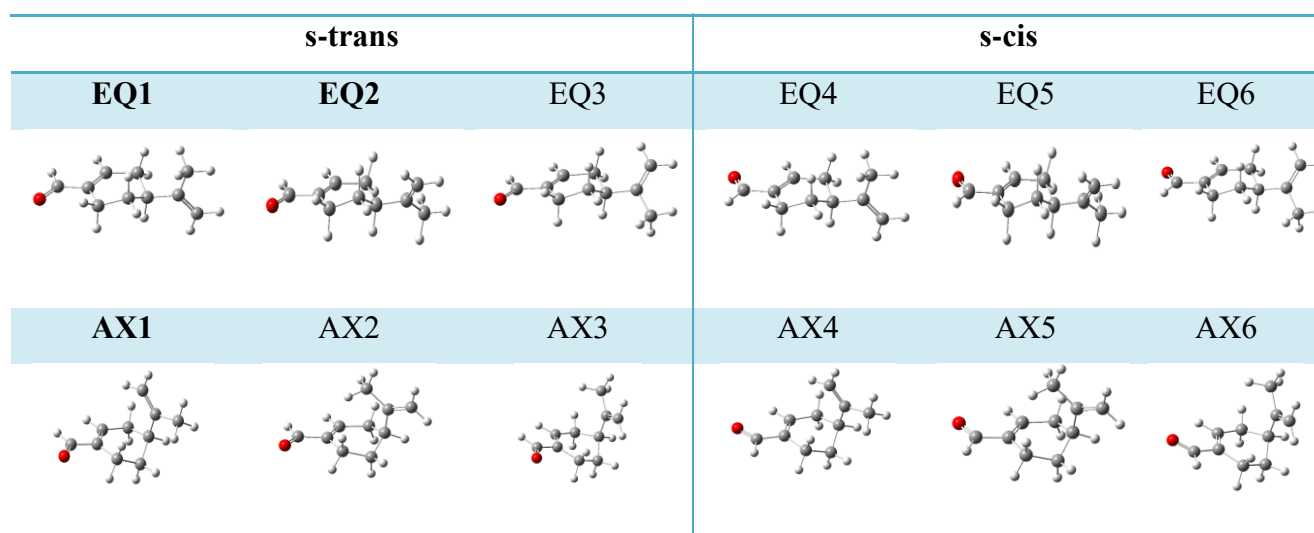


Figure 2: Depiction of the theoretical structures

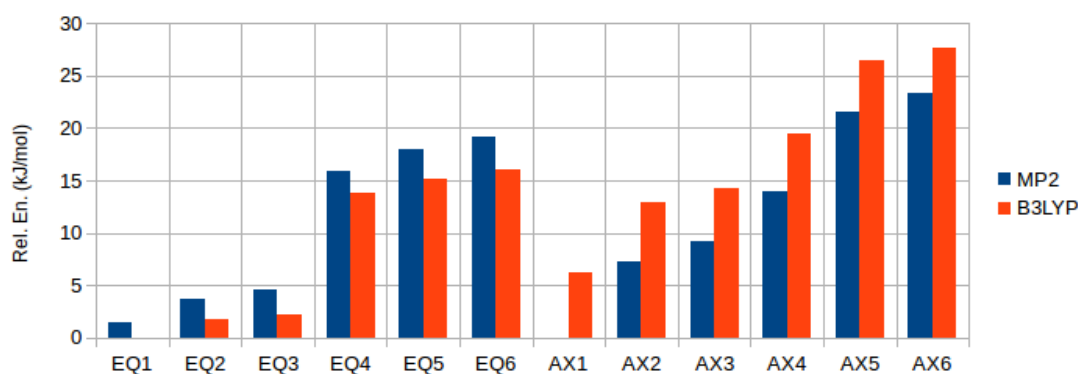


Figure 3: Comparison of the conformers relative energies, calculated at B3LYP and MP2 theory levels.

Table1: Spectroscopic parameters calculated at MP2/6-311++G(d,p) theory level.

	EQ1	EQ2	EQ3	EQ4	EQ5	EQ6
A (MHz)	2926.18	2950.89	2865.97	2888.04	2845.01	2905.17
B (MHz)	537.12	547.49	551.09	535.97	550.81	544.12
C (MHz)	510.65	491.96	495.3	507.87	489.79	492.35
μ_a (D)	2.89	2.98	2.86	2.74	2.7	2.85
μ_b (D)	1.52	1.7	1.41	1.48	1.15	1.56
μ_c (D)	0.63	0.45	0.36	0.16	0.52	0.22
ΔE_c (cm ⁻¹)	118.6	307.1	376.9	1334.7	1505.8	1605.7
	AX 1	AX2	AX3	AX4	AX5	AX6
A (MHz)	1882.34	1993.49	1754.06	2051.01	2086.42	1721.99
B (MHz)	725.5	705.01	749.45	690.22	695.39	753.39
C (MHz)	690.65	689.75	718.16	672.7	669.3	709.91
μ_a (D)	2.77	0.13	2.9	2.14	1.65	2.66
μ_b (D)	2.03	3.29	2.09	0.58	2.37	1.49
μ_c (D)	0.7	0.34	0.74	2.76	0.08	0.83
ΔE_c (cm ⁻¹)	0	612.1	769.6	1168.4	1806.6	1956.6

Table 2: Spectroscopic parameters calculated at B3LYP/6-311++G(d,p) theory level.

	EQ1	EQ2	EQ3	EQ4	EQ5	EQ6
A (MHz)	2942.13	2964.36	2892.23	2890.02	2853.8	2923.53
B (MHz)	531.68	541.47	546.96	531.24	544.63	540.28
C (MHz)	505.4	487.51	487.64	503.33	486.3	485.56
μ_a (D)	3.28	3.38	3.26	3.15	3.14	3.3
μ_b (D)	1.68	1.89	1.48	1.46	1.09	1.61
μ_c (D)	0.63	0.39	0.39	0.26	0.6	0.14
ΔE_c (cm ⁻¹)	0	139.7	178.5	1152.3	1270.7	1339.3
	AX1	AX2	AX3	AX4	AX5	AX6
A (MHz)	2021.98	2135.09	1939.23	2165.07	2177.35	1892.45
B (MHz)	673.6	658.63	684.8	655.11	657.94	683.42
C (MHz)	647.06	647.02	639.88	633.13	636.3	637.96
μ_a (D)	3.26	2.76	3.4	3.6	2.8	3.18
μ_b (D)	2.13	2.18	2.37	1.68	1.54	1.16
μ_c (D)	1.13	0.86	0.91	0.66	0.17	1.37
ΔE_c (cm ⁻¹)	522.5	1077.2	1185.4	1633.4	2209.1	2313.7

Experimental section

Commercial sample of PERY was purchased from Sigma-Aldrich and used without any further purification. It is a liquid at room temperature with boiling point of 104-105°C and vapor pressure of 10 mmHg. PERY was placed in a bespoke heating reservoir attached to the nozzle at temperature of 79°C. PERY was seeded in neon gas at backing pressures of ca. 5 bars. Typical molecular pulses of 1100 μs were used to produce the supersonic jet in vacuum chamber. The spectra were recorded using broadband microwave spectroscopy employing the chirped-pulse spectrometer (PJ-CP-FTMW) in the frequency range from 2-8 GHz at King' College Department. Microwave chirped pulses of 4 μs were applied with a delay of 1400 μs with respect to the start of the molecular pulse. Molecular relaxation signals were collected for 15 μs using the digital oscilloscope and converted into the frequency domain through a fast Fourier-transform algorithm. The resolution is ca. 110 kHz.

Rotational spectrum

The broadband spectrum of PERY was recorded in the 2-8 GHz frequency range by PJ-CP-FTMW (figure 4). The rotational spectrum appears very rich of lines reflecting the presence of several species. The most intense lines of the spectrum were identified as belonging to the EQ1 and EQ2 species. Guided from experimental rotational constants values, previously determined from Moreno *et al.*, for the EQ1 and EQ2 species, the fittings of these species were completed, including new transitions lines observed in the 2-8 GHz frequency range. The rotational spectrum of EQ1 species is constituted from transitions obeying all three selection rules while in that of EQ2 only μ_a -type and μ_b -type transitions were assigned. In both cases, transitions from J up to 8 and K_a up to 4 were identified.

Afterwards based on the values of the theoretical rotational constants and those of electric dipole moment components reported in table 1 the spectrum of AX1 species was assigned. For this species a -type, b -type and c -type transitions with J up to 6 and K_a up to 3 were identified. All fittings were done with Pickett's SPFIT program [22], using a semirigid rotor Hamiltonian (H_R) in the A -reduction and I' representation [23]. The three obtained sets of spectroscopic parameters are reported in table 3.

While the spectrum of EQ3 was not observed. The missing of these signals is probably due to the conformational relaxation process upon supersonic expansion. A process that takes place when the

barrier connecting two different minima is less than $2kT$ [24]. In order to verify this statement, the internal rotation pathway of isopropenyl group was explored varying the corresponding dihedral angle ($C_3C_4C_9C_{10}$) by 15° steps at the B3LYP/6-311++G(d,p) level theory, whereas all the other internal coordinates were freely optimized. The calculated PES indicates that the interconversion barrier of EQ3 on EQ2 is 155 cm^{-1} justifying the lack of this species in the spectrum.

Table 3: Experimental spectroscopic parameters

	EQ1	EQ2	AX1
A (MHz)	2932.6820(9) ^a	2954.620(1)	1919.416(1)
B (MHz)	536.5552(2)	547.0088(4)	710.46348(6)
C (MHz)	510.1997(2)	491.6141(4)	678.6590(7)
D _J (kHz)	-	0.012(5)	0.15(1)
D _{JK} (kHz)			1.0(6)/
D _K (kHz)			2.7(2)
N ^b	66	71	49
σ (kHz) ^c	7	6	7
$\mu_a/\mu_b/\mu_c$ ^d	yes/yes/yes	yes/yes/no	yes/yes/yes

^a Standard error in parentheses in the units of the last digit. ^b Number of transitions. ^c Root mean square deviation of the fit. ^d Yes or no observation of *a*-, *b*-, and *c*-type transitions, respectively.

Isotopologues species

Owed to the sensitivity of the PJ-CP-FTMW, the spectra of the ^{13}C isotopologues species were observed in natural abundance. The peaks belonging to all ten ^{13}C isotopologues for the two EQ1 and EQ2 species were identified. Only the *a*-type transitions were sufficiently intense to be observed. The transitions were fitted using the same Hamiltonian of the parent species, obtaining the rotational constants relative to the species EQ1 and EQ2, reported in table 4. For the EQ2 isotopologues, the value of the centrifugal distortion constant, D_J , was fixed to those of the corresponding parent species.

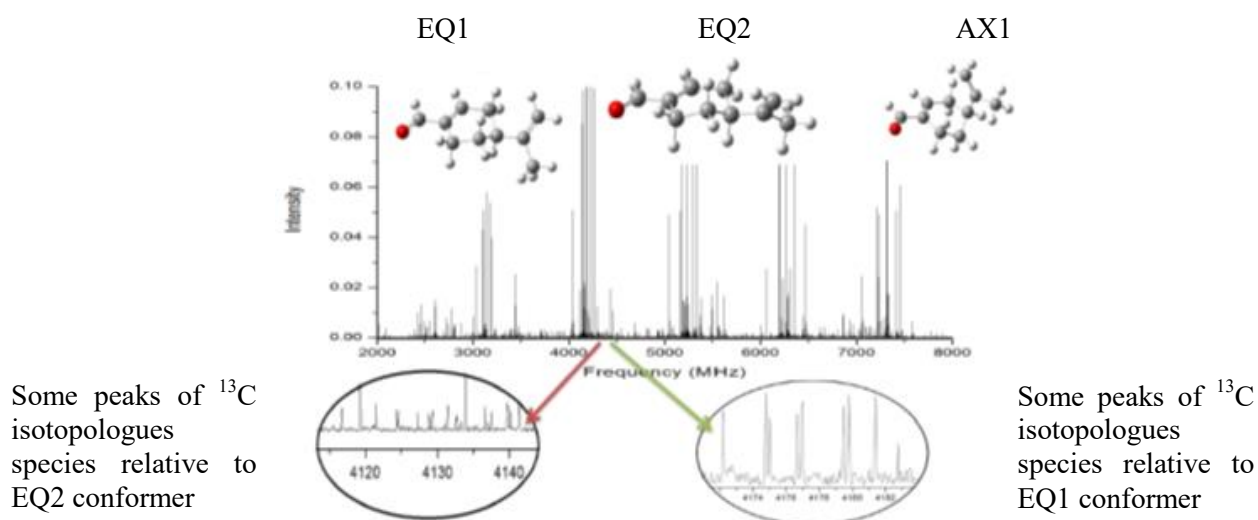


Figure 4: The broadband spectrum of perillaldehyde recorded in the 2-8 GHz frequency range, with a depiction of observed conformers.

Table4: ^{13}C isotopologues species experimental rotational constants relative to the species EQ1 and EQ2.

	EQ1					EQ2				
	A(MHz)	B (MHz)	C (MHz)	N ^b	σ (kHz) ^c	A (MHz)	B (MHz)	C (MHz)	N	σ (kHz)
$^{13}\text{C}_1$	2932(2) ^a	534.9037(7)	508.6769(7)	15	7	2953.5(6)	545.2791(7)	490.1900(8)	13	7
$^{13}\text{C}_2$	2900(2)	536.0271(8)	508.7984(7)	14	7	2924.4(9)	546.3910(8)	490.4251(9)	12	5
$^{13}\text{C}_3$	2903(2)	536.3894(7)	509.1422(7)	14	7	2925.6(9)	546.7206(8)	490.7653(9)	13	3
$^{13}\text{C}_4$	2930(2)	535.8088(7)	509.5930(7)	14	4	2952.7(6)	546.2551(7)	491.0519(9)	12	6
$^{13}\text{C}_5$	2908(2)	536.4573(7)	509.4614(8)	14	7	2928.0(7)	546.9686(8)	490.838(1)	10	7
$^{13}\text{C}_6$	2909(2)	535.8362(7)	508.8949(8)	13	5	2931.6(6)	546.1531(7)	490.4011(9)	13	7
$^{13}\text{C}_7$	2925(2)	530.8750(7)	504.9874(8)	13	8	2950.4(9)	541.1070(9)	486.7527(8)	13	5
$^{13}\text{C}_9$	2929(2)	532.7347(7)	506.7512(7)	14	7	2953.5(6)	543.0484(9)	488.4127(8)	12	7
$^{13}\text{C}_{10}$	2909(2)	529.1264(8)	504.2027(7)	14	7	2926.2(9)	540.9289(9)	486.2780(8)	13	4
$^{13}\text{C}_{11}$	2902(2)	530.2141(7)	505.2058(8)	14	6	2930(1)	539.800(1)	485.6184(9)	10	5

^a Standard error in parentheses in the units of the last digit. ^b Number of transitions. ^c Root mean square deviation of the fit.

Experimental structure

Owed to the availability of the rotational constants for the parent species and all ten ^{13}C isotopologues, the experimental structure of EQ2 was determined.

The substitution geometry (r_s) was found by Kraitchman's equations implemented in KRA program [25]. It is compared to the equilibrium one (r_e) calculated at the MP2/6-311++G(d,p) level in table

6. The r_s coordinates carry the errors suggested by Costain [26] to provide a realistic account of the uncertainties from vibration-rotation effects. The method returns one imaginary value for the c coordinate of C₂ atom and this was set to zero. The structure confirms clearly the assignment to EQ2 conformer and it also agree well with theoretical equilibrium structure.

The experimental structure of EQ1 was not determined because the rotational constant A of the ¹³C isotopologues species was not well determined.

Table 6: Comparison between experimental substitution (r_s absolute values in Å) and theoretical equilibrium (r_e , Å) principal axis system coordinates of the C atom for the observed conformers of EQ2

	C ₁		C ₂		C ₃		C ₄		C ₅	
	r_s	$r_e b$	r_s	r_e	r_s	r_e	r_s	r_e	r_s	r_e
a Å	1.713(5) ^a	1.719	0.94(1)	0.931	0.53(2)	0.569	1.083(8)	1.105	0.26(4)	0.287
b Å	0.24(3)	0.241	1.27(1)	1.276	1.22(1)	1.215	0.0(1)	0.026	1.249(8)	1.248
c Å	0.0(1)	0.072	0.40(3)	0.443	0.45(3)	0.451	0.32(3)	0.2889	0	0.132
	C ₆		C ₇		C ₉		C ₁₀		C ₁₁	
	r_s	r_e	r_s	r_e	r_s	r_e	r_s	r_e	r_s	r_e
a Å	1.151(8)	1.166	3.175(4)	3.181	2.590(3)	2.600	3.164(4)	3.164	3.437(1)	3.438
b Å	1.106(8)	1.101	0.47(3)	0.447	0.18(5)	0.149	1.14(1)	1.139	0.953(5)	0.934
c Å	0.35(2)	0.321	0.17(8)	0.058	0.18(5)	0.090	0.63(2)	0.625	0.745(7)	0.724

^aCostain's errors expressed in units of the last decimal digits. ^bFrom MP2/6-311++G(d,p) geometry.

Discussions

The experimental rotational constants for the three observed species are in very good agreement with those calculated ones. As it can be seen in table 7, the percentage differences ($\Delta\%$) between the sets of experimental and theoretical rotational constants are very small, especially when the geometries are determined at MP2/6-311++G(d,p) theory level.

However the two calculations methods showed discrepancies on the stability of the conformers of the axial or equatorial family.

To clarify this point an estimate of the relative energy (ΔE cm⁻¹) between the conformers can be obtained experimentally, employing the Boltzmann formula:

$$\frac{N_1}{N_0} = e^{-\frac{\Delta E}{kT}}$$

where k , T and N_1/N_0 are the Boltzmann constant, the absolute temperature of the sample, and the relative abundance of the conformers, respectively.

The relative abundances can be estimated by comparing the experimental intensity of nearby rotational transitions:

$$\frac{N_1}{N_0} \approx \frac{I_1 \mu_0^2 \gamma_1}{I_0 \mu_1^2 \gamma_0}$$

where I , μ , and γ are the peak intensity, the electric dipole moment value and the integrated (?) intensity of the considered transitions.

Using this formula it was found that the ratio between the populations of EQ1 and EQ2 is: $N(EQ1)/N(EQ2) \approx 2$, namely the EQ1 conformer population inside the sample is almost twice the EQ2 population.

By this ratio the estimated relative energy of the conformer EQ2 respect to EQ1 is $\Delta E = 122 \text{ cm}^{-1}$. This value is in better agreement with the B3LYP predicted value (139 cm^{-1}) with respect to MP2 value (188 cm^{-1}).

While the estimated ratio of population between EQ1 and AX1 is $N(EQ1)/N(AX1) \approx 5$, from which it is determined a relative energy of the conformer AX1 respect to EQ1 equal to 407 cm^{-1} . This result is in agreement with the B3LYP datum that predicted the EQ1 form more stable than AX1 by 552 cm^{-1} .

However it must be taken into account that this analysis assumes that the supersonic expansion populates only the ground vibrational of each conformer and there is no conformational relaxation between conformers. Indeed the measures of intensities depends strongly from experimental factors and are not so accurate as the frequencies measurements.

Table7 : Percentage differences ($\Delta\%$) between the sets of experimental and theoretical rotational constants.

	EQ1		EQ2		AX1	
	MP2	B3LYP	MP2	B3LYP	MP2	B3LYP
ΔA (%)	0.2	0.3	0.1	0.3	2	5
ΔB (%)	0.1	1	0.9	1	2	5
ΔC (%)	0.09	0.9	0.06	0.8	1.7	4.7

Conclusion

The conformational space of s-(-)-perillaldehyde was investigated by its rotational spectrum recorded by PJ-CP-FTMW operating in the frequency range 2-8 GHz. In the spectrum, two

equatorial and one axial conformers, EQ1, EQ2 and AX1 were identified. In addition, owed to the high sensitivity of PJ-CP-FTMW, the spectra of all ten ^{13}C isotopologues of parent species EQ1 and EQ2 were observed in natural abundance. The assignment of these spectra allowed to determine the r_s coordinates for the EQ2 form. The experimental rotational constants were in very good agreement with those calculated at MP2/6-311++G(d,p) theory level. Instead, the conformational species stability was better predicted from B3LYP/6-311++G(d,p) calculations.

References

- [1] F. Chiron, J. Calchat, R Garry, J. Pilichowski, Lacoste, *J. Photochem. Photobiol., A Chem*, 1997, 111
- [2] A. Calogirou, B. Larsen, D. Kotzias, *Atmos. Environ*, 1999, 33
- [3] F. Nunnes, M. Veloso, P. Pereira, J. De Andrade, *Atmos. Environ*, 2005, 39
- [4] K. Wagner, I. Elmadfa, *Ann. Nutr. Metab*, 2003, 47
- [5] V. Dembitsky, *Lipids*, 2006, 41, 1
- [6] P. Crowell, Z. Ren, S. Lin, E. Vedejs, M. Gould, *Biochem. Pharmacol.*, 1994, 47 (8)
- [7] G. Ruberto, M. Baratta, *Food Chem*, 2000, 69
- [8] P Geady, D. Wansley, D. Logan, *J Nat. Prod.*, 2002, 65, 7
- [9] H. Ozer, M. Sokmen, Gulluce, Adiguzel, Sahin et al., *J Agric. Food Chem.*, 2007, 55, 3
- [10] A. Wei, T. Shibamoto, *J. Agric. Food Chem*, 2007, 55, 5
- [11] Crowell, Z. Ren, S. Lin, E. Vedejs, M. Gould, *Biochem. Pharmacol.*, 1994, 47, 8
- [12] J. Neill, S. Shipman, L. Alvarez-Valtierra, A. Lesarri, Z. Kisiel, and B. Pate, *J. Mol. Spectrosc*, 2011, 269
- [13] D. Loru, M. Bermudez, M. Sanz, *J. Chem. Phys.*, 2016, 145
- [14] J. Moreno, F. Urena, J. Gonzales, T. Huet, *Chem. Phys. Lett.*, 2009, 473
- [15] T. Balle, W. Flygare, *Rev. Sci. Instrum.*, 1981, 52
- [16] J. Grabow, W. Stahl, H. Dreizler, *Rev. Sci. Instrum.*, 1996, 67
- [17] S. Melandri, W. Caminati, L. Favero, A. Millemaggi and P. Favero, *J. Mol. Struct.*, 1995, 352/353
- [18] S. Melandri, G. Maccaferri, A. Maris, A. Millemaggi, W. Caminati, and P. Favero, *Chem. Phys. Lett.*, 1996, 261
- [19] C. Calabrese, A. Maris, L. Evangelisti, L. Favero, S. Melandri, W. Caminati, *J. Phys. Chem. A.*, 2013, 117
- [20] M.J. Frisch, G.W. Trucks, H.B. Schlegel, G.E. Scuseria, M.A. Robb, J.R. Cheeseman, G. Scalmani, V. Barone, B. Mennucci, G. A. Petersson, H. Nakatsuji, M. Caricato, X. Li, H.P. Hratchian, A.F. Izmaylov, J. Bloino, G. Zheng, J.L. Sonnenberg, M. Hada, M. Ehara, K. Toyota, R. Fukuda, J. Hasegawa, M. Ishida, T. Nakajima, Y. Honda, O. Kitao, H. Nakai, T. Vreven, J.A. Montgomery Jr., J.E. Peralta, F. Ogliaro, M. Bearpark, J.J. Heyd, E. Brothers, K.N. Kudin, V.N. Staroverov, T. Keith, R. Kobayashi, J. Normand, K. Raghavachari, A. Rendell, J. C. Burant, S.S. Iyengar, J. Tomasi, M. Cossi, N. Rega, J. M. Millam, M. Klene, J.E. Knox, J.B. Cross, V. Bakken, C. Adamo, J. Jaramillo, R.

Gomperts, R.E. Stratmann, O. Yazyev, A.J. Austin, R. Cammi, C. Pomelli, J. Ochterski, R.L. Martin, K. Morokuma, V.G. Zakrzewski, G.A. Voth, P. Salvador, J.J. Dannenberg, S. Dapprich, A.D. Daniels, O. Farkas, J.B. Foresman, J.V. Ortiz, J. Cioslowski, D. Fox, Gaussian 09, Revision D.01, Gaussian, Inc., Wallingford, CT

[21] Acrolein: C. Blom, G. Grassi, A. Bauder, *J. Am. Chem. Soc.*, 1984, 106

[22] H. M. Pickett, *J. Mol. Spectr.*, 1991, 148

[23] J.K.G. Watson, in *Vibrational Spectra and Structure*; Durig, J.R., Ed.; Elsevier: Amsterdam, 1977; Vol. 6, pp 1-89.

[24] R. Ruoff, T. Klots, T. Emilson, H. Gutowski, *J. Chem. Phys.*, 1990, 93

[25] J Kraitchman, *Am. J. Phys.* 1953, 21

[26] C. Constain, G. Srivastava, *J. Chem. Phys.* 1961, 35

CHAPTER 6

MILLIMETER WAVE SPECTRUM OF THE ACRYLONITRILE-METHANOL WEAKLY BOUND MOLECULAR COMPLEX

Introduction

The rotational spectrum of a molecular system is highly sensitive to variations of atoms masses distribution. The interpretation of these spectra by appropriate Hamiltonians, single or coupled, allows to determine the structures unambiguously, the involved conformational and tautomeric equilibria, to identify the isotopic species and the possible large amplitude motions. Large amplitude motions manifest themselves directly in the spectrum generating hyperfine structures. The resolution of these structures allows to model the potential energy surface governing these motions.

In this work the cluster between acrylonitrile (ACN) and methanol (MET) has been characterized by rotational spectroscopy and ab initio calculations. The importance of this study is twofold. On one side this investigation provides a picture of orientation between the two molecular subunits from which the intermolecular forces that govern their stability can be inferred; the other hand the spectroscopic parameters, needed to verify the possible presence in the planetary atmosphere of the species, can be obtained.

Several MET clusters have been investigated by rotational spectroscopy. These studies show that the MET hydroxyl group has amphoteric behavior: it acts as a proton donor when the binding partner is aniline [1], while it acts as a proton acceptor when it is bound to water [2], phenol [3] and HCl [4]. In the homodimers (MET)₂ [5], and in the heterodimers MET-formamide [6] and MET-formaldehyde [7], it has both functions. In all the cases the spectra manifested clear tunneling effects. Two sets of rotational transitions (A and E) due to the internal rotation of methyl group were assigned separately. In addition for the MET-formaldehyde complex also the large amplitude motion of formaldehyde corresponding to a rotation around its C₂ axis was observed.

Regarding ACN clusters, few rotational studies are available. However several rotational studies on clusters involving other nitriles such as HCN and CH₃CN (acetonitrile) have been performed. In the examples reported in the literature, HCN is generally a proton donor, whereas CH₃CN acts as a proton acceptor by electron pair located at the nitrogen atom. The studies on the complexes of CH₃CN include both H atom donors, such as HF [8], HCl [9], HCN [10], HCCH [11] and H₂O [12], and Lewis acid electron acceptors, such as BF₃ [13], SO₃ [14] and F₂ [15], binding the nitrogen lone

electron pair. In all these examples the observed rotational spectrum is that originating from a symmetric top and in the case of the complex with water two tunneling components related to the motion of water were observed.

In an our already published work entitled “Millimeter wave spectrum of weakly bound complex: structure, dynamics and implication for astronomical search” [16] the 1:1 adducts between ACN and water isotopologues (DOH, DOD, H₁₈OH) were characterized. During the analysis of this spectrum, the presence of lines doublets with intensity ratio 3:1 was noted. They constitute, a typical manifestation of the exchange motion of the two equivalent hydrogen nuclei around the water C₂ symmetry axis, that being fermions have spin statistical weight ratio 3:1. The interpretation of this hyperfine structure allowed the identification of the complex structure characterized by a planar ring shaped geometry in which the two subunits are held together by two hydrogen bonds: a main OH_{HOH}—N_{ACN} interaction and a weaker O_{HOH} —HC_{ACN} interaction. A similar dynamic and structural behavior was observed also for the benzonitrile –water cluster [17]. This study constitutes a benchmark for future astrophysical investigations. At the best of our knowledge, molecular complexes have not still been detected in the interstellar medium. The main reasons could be both whether these complexes are not formed in the planetary atmosphere or their abundances are so low such to not be observed. However it is not possible to exclude their existence. For instance, in an our previous work [16], we proposed a possible mechanism for the formation of ACN-H₂O. Indeed the enhancing sensibility of new radio-telescopes could allow their detection at very low concentration. From an astrophysical point of view, both ACN and MET are defined ‘weed’ because their large abundance in the interstellar medium. Therefore, we believe that also the formation of their complex could be possible. In particular ACN has been identified in the Orion KL region [18, 19] and toward the Sagittarius B2(N) molecular nebula [20, 21]. In the latter environment even excited states of ACN were detected [22]. ACN has also been identified in the carbon rich star IRC+102163 and in the cold dark cloud TMC-1 [23]. ACN might also function as starting materials in reaction sequences resulting in the formation of larger molecules detected in different astronomical objects. While MET was first detected by Barrett toward Sgr B2 and Sgr A [24], then in dark cloud as TMC-1 [25] and L183 [26]. In 1991 Barrett observed the thermal emission of MET toward Orion-KL [27]. It was also observed towards all Galactic star forming region in the such W3(OH) [28] NGC 7538-IRSI [29] and W51 [30]. MET deuterated isotopologues was detected toward IRAS 16293-2422 [31].

Experimental section

ACN and MET were purchased from Sigma-Aldrich (purity >99%) and used without further purification. Both compounds were cooled by a mixture of ice and NaCl. A stream of argon at a pressure of about 600 kPa was passed above both ACN and MET, which were kept in two separate containers. We used a concentration of ACN and MET in the gas mixture of about 3.4% and 2.0%, respectively. The mixture was then expanded from a stagnation pressure of 39.5 kPa to about 0.5 Pa through a 0.35 mm diameter pinhole nozzle. These settings have been found as optimal for the formation of the 1:1 complex in our experiments. The rotational spectrum was recorded in the 59.6-74.4 GHz frequency range by a free-jet Stark modulated millimeter wave absorption spectrometer. The details of this spectrometer are given in ref. 32, 33, 34.

Computational methods

Full geometry optimizations and subsequent harmonic frequency calculations were performed to characterize the stationary points. All calculations were run at level MP2/aug-cc-pVTZ using the Gaussian09 program package [35].

Results

Before collecting the rotational spectrum, different geometries of the two monomers were considered by optimization procedures. Five complex structures differing for both the kind of the interactions involved and the orientation of MET with respect to plane of ACN were found to be energetic minima. A depiction of the five structures is reported in table 1, together with the spectroscopic constants, the electric dipole moment components and relative energy values. In four conformations ACN and MET form a ring-shaped structure in which the two units are held together through two hydrogen bonds: a main $\text{OH}_{\text{MET}}\cdots\text{N}_{\text{ACN}}$ interaction and a weaker $\text{O}_{\text{MET}}\cdots\text{HC}_{\text{ACN}}$ interaction. In the most stable forms (ACN-MET3 and ACN-MET4) this bond involves the terminal alkene H atom, whereas in the higher energy forms (ACN-MET1 and ACN-MET5) it involves the non-terminal alkene H atom. In ACN-MET3 and ACN-MET1 the methanol methyl group is coplanar to the plane of ACN, whereas in ACN-MET4 and ACN-MET5 the methyl group lies out of plane.

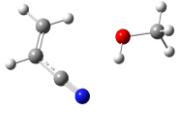
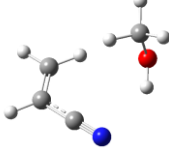
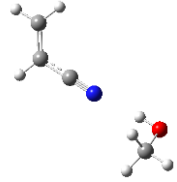
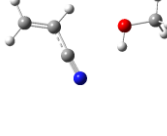
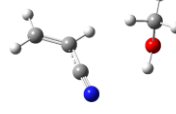
The geometry of the complex ACN-MET2 is quite different from others four. In this case the two units interact through by a single near linear hydrogen bond of the kind $\text{HO}_{\text{MET}}\cdots\text{N}_{\text{ACN}}$ with the methanol oriented in gauche respect to the ACN plane.

Rotational spectrum analysis

The broadband spectrum was recorded in the 59.6-74.4 GHz frequency range by a free-jet Stark modulated millimeter wave absorption spectrometer.

Based on the calculated rotational constants and dipole moment components reported in table 1, the species ACN-MET3 was identified. The spectrum showed rotational transitions doublets arising from the methyl internal rotation coupling to overall molecular rotation.

Table1: Calculated spectroscopic parameters for ACN-MET clusters:

	ACN-MET3	ACN-MET4	ACN-MET2	ACN-MET1	ACN-MET5
					
A (MHz)	5051	4262	16502	6079	4908
B (MHz)	1670	2176	826	1395	1768
C (MHz)	1265	1609	813	1143	1434
D _J (kHz)	1.04	4.32	1.15	0.96	4.85
D _{JK} (kHz)	5.61	-1.48	-107.54	0.01	-21.92
D _K (kHz)	2.93	4.54	1.41	81.75	86.65
d ₁ (kHz)	-0.33	-1.20	0.39	-0.29	-1.34
d ₂ (kHz)	-0.08	-0.09	-0.14	-0.04	0.00
χ _{aa} (MHz)	0.26	0.58	-3.55	1.36	1.29
χ _{bb} (MHz)	-2.07	-2.38	1.72	-3.20	-3.09
χ _{cc} (MHz)	1.80	1.80	1.83	1.85	1.80
ΔE (cm ⁻¹)	0	18.6	290.7	326.8	365.8
μ _a (D)	0.91	1.80	5.74	0.44	1.56
μ _b (D)	2.11	2.41	1.61	2.36	2.48
μ _c (D)	0	1.42	0.79	0	0.92

In molecules or molecular clusters containing a methyl group, three equivalent minima on the potential energy surface are generated by internal rotation of methyl group. Due to the tunneling effect, the vibrational energy levels split in two torsional sublevels, one non-degenerate and another doubly degenerate. For a molecule with no overall symmetry, these torsional sublevels can be classified according to the symmetry species of the methyl point symmetry group C_{3v}, so the two sub-levels are labeled as A and E, respectively. Since the electric dipole moment in these systems belongs always to symmetry species A and allowed transitions can occur only between two sublevels of the same degeneracy: A→A and E→E, rotational transitions doublets are observed within of these spectra.

A first assignment was performed for rotational transitions of the torsional sublevel A, that follows the usual selection rules for a pseudo rigid rotor, obtaining a preliminary set of experimental rotational constants. The fitting was done using a Watson's S-reduced semirigid rotor Hamiltonian implemented in SPFIT program [36, 37].

The problem of internal rotation was resolved by XIAM program of Hartwig and Dreizler [38]. The software allows the simultaneous analysis of internal rotation and nuclear quadrupole couplings. Using as input data the rotational constants previously determined and the theoretical parameters of internal rotation such as the potential barrier (V_3) showed in figure 1, the moment of inertia of the methyl top (I_α) and the angles between the internal rotation axis (C-O) of the CH_3 top and the principal axis of inertia ($\langle \text{OC}, g$; where $g=a, b, c$). From the analysis, the rotational and quartic centrifugal distortion constants, the potential barrier and the angle $\langle \text{OC}, a$ were obtained, while I_α was held fixed. All parameters are reported in table 2. No splitting due to the ^{14}N nuclear quadrupole interaction was resolved by our instrument. No evidence of others conformers was found. The missing of signal due to other conformers could be ascribed to relaxation processes upon supersonic expansion as consequence of low interconversion barriers between conformers ($<2kT$) especially when the argon is used as carrier gas [39].

Table 2: Experimental spectroscopic parameters

A (MHz)	5007.97(6) ^a	$[\text{F}_0]^{\text{d}}$ GHz	154.834
B (MHz)	1628.67(2)	I_α ($\text{u}\text{\AA}^2$) ^e	3.264
C (MHz)	1239.43(3)	V_3 (cm^{-1})	216.25(2)
D_J (kHz)	1.54(3)	δ (rad)	2.916(1)
D_{JK} (kHz)	6.5(1)	ε (rad)	0
D_K (kHz)	2.8(3)	$\langle \text{OC}, a \rangle$ ($^\circ$) ^f	167.09
d_1 (kHz)	0	$\langle \text{OC}, b \rangle$ ($^\circ$)	90.00
d_2 (kHz)	0	$\langle \text{OC}, c \rangle$ ($^\circ$)	77.09
N^{b}	47	σ (kHz) ^c	89

^a Standard error in parentheses in the units of the last digit. ^b Number of transitions. ^c Root mean square deviation of the fit. ^d Value in squared brackets is fixed to the theoretical value. ^e Inertial moment of methyl top. ^f Angle between the O- CH_3 bonds and the principal inertial axis.

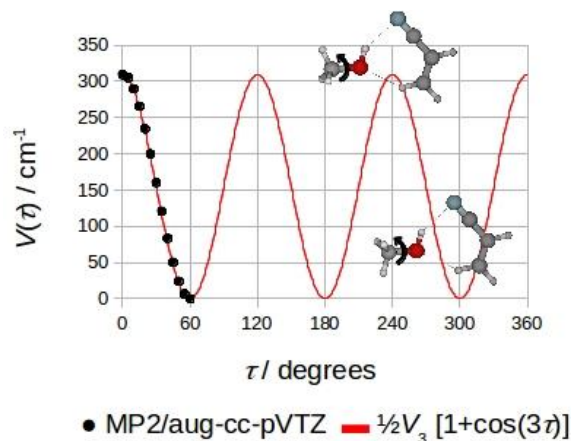


Figure 1: Potential energy path for the methyl internal rotation in ACN-MET

Discussions

From the analysis of the rotational spectrum, information on the structure can be deduced. The absence of μ_c -type transitions suggests the presence of a symmetry plane along ab axis.

Furthermore, from the rotational constants the planar momentum of inertia can be calculated by the expressions:

$$P_{aa} = h/16\pi^2(-1/A+1/B+1/C)$$

$$P_{bb} = h/16\pi^2(1/A-1/B+1/C)$$

$$P_{cc} = h/16\pi^2(1/A+1/B-1/C)$$

These parameters are very useful because describe the extension of the masses along the inertial axes ($P_{gg} = \sum_i m_i g_i^2$, m_i being the mass and g_i the g -coordinate of the i -th atom).

In particular the determination of P_{cc} provides a direct information on the planarity of structure. In our case, it was determined an experimental P_{cc} of $1.65 \text{ u}\text{\AA}^2$, that it is a value very close to zero, suggesting that all heavy atoms of the complex lie on the plane ab . The discrepancy from zero is attributable to two hydrogen atoms of the MET that lie out of the plane as was observed in bare MET [40]. The theoretical and experimental planar momenta of inertia of all structures are reported in table 3.

Table 3: Theoretical and experimental planar momenta of inertia of all clusters

	ACN-MET3	ACN-MET4	ACN-MET2	ACN-MET1	ACN-MET5	EXP.	MET state-A
$P_{aa} / \text{u}\text{\AA}^2$	360.8	601.4	301.0	207.15	267.7	308.575	18.89
$P_{bb} / \text{u}\text{\AA}^2$	81.5	20.0	98.5	93.52	84.7	99.229	2.377
$P_{cc} / \text{u}\text{\AA}^2$	1.6	10.6	1.6	25.04	18.2	1.685	1.583

Nature of the interactions

The structure identified in the spectrum corresponds to the most stable species, having a higher binding energy, obtained from ab initio calculations.

The atoms in molecules (AIM) quantum theory [41], implemented in the Multiwfn program [42], was used to analyse the nature of the H-bonding interaction in the complexes. According to the AIM analysis, the hydrogen bond is the result of electron densities of the lone pair and hydrogen atom, which results in a charge transfer from donor to the acceptor atom. Thus it can be adequately described by the topological properties of the electron density at the critical points (CP) where the gradients of density vanish. The relationship between hydrogen bond energy E_{HB} and potential energy density $V(r_{CP})$ at corresponding CP can be approximately described as: $E_{HB}=1/2V(r_{CP})$. The binding energies calculated for the five structures by MP/aug-cc-pVTZ (B.E.) and those ones obtained by AIM quantum theory, the hydrogen bonds distances (r) and angles (ϑ) are reported in table 4.

Two CPs were located for the four structures ACN-MET3, ACN-MET4, ACN-MET1 and ACN-MET3 between $H_{MET}-N_{ACN}$ and $O_{MET}-HC_{ACN}$ (alkene terminal H or non-terminal H) confirming the cyclic nature of the complex, while in ACN-MET2 only a CP is present.

Table 4: The binding energies calculated for the five structures by MP/aug-cc-pVTZ (B.E.) and those one obtained by AIM quantum theory, the hydrogen bonds distances (r) and angles (ϑ) are reported

		ACN-MET3	ACN-MET4	ACN-MET2	ACN-MET1	ACN-MET5
	<i>B.E.</i> (kJ/mol)	26.3	26.0	22.8	22.4	21.9
$H_{MET}-N_{ACN}$	r (Å)	2.226	2.323	2.035	2.412	2.543
	ϑ (°)	147.508	141.466	172.478	135.049	131.088
	<i>Eint</i>	13.036	10.546	23.373	9.735	8.895
$O_{MET}-HC_{ACN}$ (alkene terminal H or non-terminal H)	r (Å)	2.366	2.413	-	2.59	2.644
	ϑ (°)	142.218	141.271	-	113.633	113.940
	<i>Eint</i>	8.561	8.589	-	6.127	6.384

Methyl rotation barrier trend

The methyl group internal rotation can be used as a probe to explore chemical environment around it. Dramatic changes in the barrier value are observed depending to the electronic distribution and steric hindering around the methyl group. In the ACN-MET3 complex, the methanol methyl rotation barrier is determined to be 219 cm^{-1} , smaller than that in bare methanol (375.6 cm^{-1}) [40]. This is fairly consistent with results obtained for other MET hydrogen bonded

complexes. For example, the V_3 was measured to be 60-65, 74, 170, 215, 231 and 240 cm^{-1} for $\text{H}_2\text{O-MET}$ [2], HCl-MET [4], phenol-MET [3], aniline-MET [1], $\text{NH}_2\text{CHO-MET}$ [6], HCHO-MET [7], respectively. This trend was initially explained as a consequence of the complexation due to hydrogen bonds. A correlation between the bond strength and the barrier decrease was proposed for instance from Howard [43]. However expanding our bibliographic searches to other methanol complexes such as Ar-MET [44], $\text{SO}_2\text{-MET}$ [45] and $\text{CO}_2\text{-MET}$ [7] it was noted that the V_3 barrier lowers dramatically independently from the hydrogen bonds presence. Thus the cause of this trend have to be searched elsewhere. As discussed from Fraser [46], the V_3 decrease in these complexes can be only apparently attributable to the rotation of the methyl group but in reality there is another motion that affects on the methyl group dynamic. Preliminary calculations suggest that the overall methyl group is involved in an out of plane motion.

Conclusion

The weakly bound 1:1 complex between acrylonitrile and methanol has been investigated in the 59.6-74.4 GHz frequency range using a Free jet Absorption millimeter wave spectrometer and ab initio calculations. The structure identified in the spectrum corresponds to a planar cyclic structure held together through two hydrogen bonds. The nature of this interaction was investigated by AIM quantum theory. Finally a consistent declining value of methanol V_3 respect to that one monomer was observed.

References

- [1] M. Haeckel, W. Stahl, *J. Mol. Spectrosc.*, 1999, 198 (2)
- [2] P. Stockman, A. Geoffrey, A. Blake, F. Lovas, R. Suenram, *J. Chem. Phys.*, 1997, 107
- [3] A. Westphal, C. Jacoby C. Ratzer, A Reichelt, M. Schmitt, *Phys. Chem. Chem. Phys.*, 2003, 5
- [4] X. Tan, Ioannis, I. Ioannou, R. Kuczkowski, *J. Mol. Struct.*, 1995, 356
- [5] F. Lovas, H. Hartwig, *J. Mol. Spectrosc.*, 1997, 185
- [6] F. Lovas, R. Suenram, G. Fraser, C. Gillies, J. Zozom, *J. Chem. Phys.*, 1987 88 (2)
- [7] V. Ilyushin, F. Lovas, D. Plusquellic, *J. Mol. Spectrosc.*, 2006, 239
- [8] J. Bevan, A. Legon, D. Millen, S. Rogers, *Proc. R. Soc. London Ser. A*, 1980, 370
- [9] A. Legon, D. Millen, H. North, *J. Phys. Chem.* 1987, 91
- [10] N. Howard, A. Legon,, *J. Chem. Soc. Faraday Trans. 2*, 1987, 83
- [11] N. Howard, A. Legon,, *J. Chem. Phys.* 1986, 85
- [12] F. Lovas, J. Sobhanadri, *J. Mol. Spectrosc.* 2015, 307
- [13] M. Dvorak, R. Ford, R. Suenram, F. Lovas, *J. Am. Chem. Soc.*, 1992, 114
- [14] W. Burns, J. Phillips, M. Canagaratna, . Goodfriend, Leopold, *J. Phys. Chem. A*, 1999, 103

- [15] G. Cotti, S. Cooke, C. Evans, J. Holloway, A. Legon, *Chem. Phys. Lett.* 1996, 260
- [16] C. Calabrese, A. Vigorito, A. Maris, S. Mariotti, P. Fathi, W. Geppert, S. Melandri, *J. Phys. Chem A*, 2015, 119
- [17] S. Melandri, D. Consalvo, W. Caminati, P. Favero, *J Chem. Phys.* 1999, 111
- [18] L. Johansson, C. Andersson, J. Elldér, P. Friberg, A. Hjalmarson, B. Hoglund, W. Irvine, *Astron. and Astrophys.*, 1984, 130
- [19] A. Lopez, B. Tercero, Z. Kisiel, A. Daly, C. Bermudez, H. Calcutt, N. Marcelino, S. Viti, B. Drouin, Medvedev, *Astron. and Astroph.*, 2014, 572, A44
- [20] F. Gardner, G. Winnewisser, *Astrophys. J.* 1975, 195
- [21] A. Remijan, J. Hollis, F. Lovas, D. Plusquellic, P. Jewell, *Astrophys. J.* 2005, 632, (1)
- [22] A. Nummelin, P. Bergman, *Astron. and Astrophys.* 1999, 341
- [23] H. Matthews, T. Sears, *Astrophys. J.* 1983, 272
- [24] A. Barrett, R. Martin, P. Myers, P. Schwartz, *Astroph. J.*, 1972, 178
- [25] P. Friberg, A. Hjalmarson, S. Madden, W. Irvine, *Astron. and Astroph.*, 1988, 195, (1-2)
- [26] C. Walmsley, W. Batrla, H. Matthews, K. Menten, *Astron. and Astroph.*, 1988, 197, (1-2)
- [27] K. Menten, C. Walmsley, C Henkel, T. Wilson, *Astron. and Astroph.*, 1988, 198, (1-2)
- [28] E. Sutton , A. Sobolev, S. Ellingsen, D. Cragg , D. Mehringer , A. Ostrovskii, P. Godfrey, *Astroph. J.*, 2001, 554
- [29] L. Allamandola, S Sandford, A. Tielens, T. Herbst, *Astrophys. J.*, 1992, 399
- [30] S. Etoaka, M. Gray, G. Fuller, *Not. Roy. Astron. Soc.*, 2012, 423
- [31] B. Parise, F. Du, F.-C. Liu, A. Belloche, H. Wiesemeyer, R. Güsten, K. Menten, H. Hübers, B. Klein *Astron. and Astroph.*, (2012), 542, L5
- [32] S. Melandri, W. Caminati, L. Favero, A. Millemaggi and P. Favero, *J. Mol. Struct.*, 1995, 352/353
- [33] S. Melandri, G. Maccaferri, A. Maris, A. Millemaggi, W. Caminati, and P. Favero, *Chem. Phys. Lett.*, 1996, 261
- [34] C. Calabrese, A. Maris, L. Evangelisti, L. Favero, S. Melandri, W. Caminati, *J. Phys. Chem. A.* 2013, 117
- [35] M.J. Frisch, G.W. Trucks, H.B. Schlegel, G.E. Scuseria, M.A. Robb, J.R. Cheeseman, G. Scalmani, V. Barone, B. Mennucci, G. A. Petersson, H. Nakatsuji, M. Caricato, X. Li, H.P. Hratchian, A.F. Izmaylov, J. Bloino, G. Zheng, J.L. Sonnenberg, M. Hada, M. Ehara, K. Toyota, R. Fukuda, J. Hasegawa, M. Ishida, T. Nakajima, Y. Honda, O. Kitao, H. Nakai, T. Vreven, J.A. Montgomery Jr., J.E. Peralta, F. Ogliaro, M. Bearpark, J.J. Heyd, E. Brothers, K.N. Kudin, V.N. Staroverov, T. Keith, R. Kobayashi, J. Normand, K. Raghavachari, A. Rendell, J. C. Burant, S.S. Iyengar, J. Tomasi, M. Cossi, N. Rega, J. M. Millam, M. Klene, J.E. Knox, J.B. Cross, V. Bakken, C. Adamo, J. Jaramillo, R. Gomperts, R.E. Stratmann, O. Yazyev, A.J. Austin, R. Cammi, C. Pomelli, J. Ochterski, R.L. Martin, K. Morokuma, V.G. Zakrzewski, G.A. Voth, P. Salvador, J.J. Dannenberg, S. Dapprich, A.D. Daniels, O. Farkas, J.B. Foresman, J.V. Ortiz, J. Cioslowski, D. Fox, Gaussian 09, Revision D.01, Gaussian, Inc.,

Wallingford, CT

- [36] H. Pickett, *J. Mol. Spectrosc.* 148 (1991) 371-377.
- [37] J. Watson, in *Vibrational Spectra and Structure*; Durig, J.R., Ed.; Elsevier: Amsterdam, 1977; Vol. 6, pp 1-89.
- [38] H. Hartwig, H. Dreizler, *Z. Naturforsch.* 51A (1996) 923-932.
- [39] R. Ruoff, T. Klots, T. Emilson, H. Gutowski *J. Chem. Phys.* 1990, 93
- [40] M. Lees, J. Baker, *J. Chem., Phys.* 1968, 48
- [41] E. Espinosa, E. Molins, C. Lecomte, *Chem, Phys. Lett.* 1998, 285
- [42] T. Lu, F. Chen, *J. Comp. Chem.* 2012, 33
- [43] B. Ouyang, B. Howard, *Phys. Chem. Chem. Phys.*, 2009, 11
- [44] X. Tan, L. Sun, R. Kuczkowski *J. Mol. Spectrosc.*, 1995, 171
- [45] L. Sun, X. Tan, J. Jin Oh, R. Kuczkowski, *J. Chem. Phys.* 1995, 103 (15)
- [46] G. Fraser, F. Lovas, R. Suenram, *J. Mol. Spectrosc.* 1994, 167

CHAPTER 7

MICROSOLVATION OF BIOMOLECULES

Water is ubiquitous in biological environments and it plays a wide variety of roles in biochemical processes. Water molecules maintain the macromolecular structures, activate and modulate the dynamics of the biomolecules and mediate the molecular recognition processes.

Many of these functions depend, to a greater or lesser degree, on the water ability to engage hydrogen bonds with the biomolecules. Indeed the breakage or the formation of such bonds determines the reorientation and the reconfiguration of discrete and identifiable three-dimensional structures of the biomolecules inducing alterations in their functionality.

Biomolecules are often large systems containing several and different sites available to interact with water. Information on such interactions can be obtained through the characterization of water clusters with biomolecules or model molecular systems by free or pulsed jet rotational spectroscopy investigations.

The free collisional environment created by supersonic jet provides the ideal conditions to form these clusters in isolated phase following a bottom-up approach. This means that water molecules can be sequentially added to the biomolecules in a controlled fashion without the influence of external factors. Then, the formed structures can be investigated in detail through their rotational spectra recorded by high resolution rotational spectrometer.

In this way it is possible to identify the biomolecules preferred binding sites to interact with water and to have a likely picture of the first shell of solvation of the biomolecule in natural environments. Furthermore, from formed structures, the involved intermolecular interactions and their strength can be inferred.

For instance, rotational studies of water complexes with binding as alcohols [1], phenols [2], organic acids [3], amides [4], ethers [5], aldehydes [6], the structural and energetic features of classical hydrogen bonds such as OH--O, OH--N, OH--S, NH--O and OH--X have been obtained. For these bonds, binding energies are found in the range 15-25 kJ mol⁻¹. While investigation of complexes as propane-water [7] and benzene-water [8] have allowed to characterize weaker molecular interactions such as CH--O and OH-- π . The energies exhibited from these bonds are within a few kJ mol⁻¹, approaching those of van der Waals forces, however they maintain the directional properties of classical hydrogen bond.

1) THE ROTATIONAL SPECTRUM OF MONOHYDRATE AND BIHYDRATE S-(-)-PERILLALDEHYDE

The focus of this work is the structural characterization of clusters between water and the biomolecule, s-(-)-perillaldehyde (PERY) through their rotational spectrum recorded by pulsed jet chirped-pulsed Fourier transform microwave spectrometer (PJ-CP-FTMW) working in the 2-8 GHz frequency range [9, 10]. The study of clusters at low frequencies, allows the investigation of heavy molecular systems and the large sensitivity of PJ-CP-FTMW allows observing low concentration species. For instance, water clusters with the biomolecules such as β -propiolactone-(H₂O)₁₋₅ [11], formamide-(H₂O)₂ [4] and camphor-(H₂O)₁₋₃ [12], have been characterized with success by PJ-CP-FTMW.

The results of the characterization of bare s-(-)-perillaldehyde (hereafter PERY) have been discussed in chapter 5. Substantially two equatorial conformers, labelled as EQ1 and EQ2, and one axial, namely AX1, were identified.

In this section, the monohydrates (hereafter PERY-H₂O) and dehydrates clusters (hereafter PERY-(H₂O)₂) of the species EQ1, EQ2 and AX1, investigated by PJ-CP-FTMW and ab initio calculations, are discussed.

Experimental section and calculation method

Commercial sample of PERY was purchased from Sigma-Aldrich and used without any further purification. It is a liquid at room temperature with boiling point of 104-105°C and vapor pressure of 10 mmHg.

PERY was placed in a bespoke heating reservoir attached to the nozzle at temperature of 122°, while water was placed in a reservoir located outside the spectrometer at room-temperature. The clusters were prepared by passing Neon at backing pressures of ca. 4 bars over the two reservoirs. Typical molecular pulses of 1100 μ s were used to produce the supersonic jet in vacuum chamber. The spectra were recorded using broadband microwave spectroscopy employing the chirped-pulse spectrometer (PJ-CP-FTMW) in the frequency range from 2-8 GHz at King' College Department. The detailed description of the experimental setup can be found in ref. 9 and 10. The resolution is ca. 110 kHz.

Full geometry optimization and evaluation of the Hessian matrix of the dimers and trimers was carried out at the MP2/6-311++G(d, p) theory level. The usual binding energy and those corrected for the basis set superposition error (BSSE) [13] by means of the counterpoise method were calculated. All calculations were performed with the Gaussian09 program package [14].

Results of PERY-H₂O

Regarding PERY-H₂O, different orientations of the water around to three observed conformers of bare PERY, EQ1, EQ2 and AX1, were considered in optimization procedure.

A depiction of the minimum structures is reported in figure 1. All conformations showed a ring-shaped structure in which the two subunits are held together through two intermolecular bonds: a main hydrogen bond, C=O_{PERY}--H_{H₂O}, and a weaker interaction between the CH_{PERY}--O_{H₂O}. In the structures, EQ1-W1, EQ2-W1 and AX1-W1, this bond involves the carbaldehyde group H while in EQ1-W2, EQ2-W2 and AX1-W2 it involves two ring H's. The spectroscopic parameters relative to the six structures and the corresponding relative energy values, are reported in table 1.

Guided by the values of the theoretical rotational constants, which are directly related to the molecular mass distribution, and those of the electric dipole moment components, which give rise to the selection rules and intensities of rotational transitions, the spectra of three species EQ1-W2, EQ1-W1 and EQ2-W1 were identified. The most intense spectrum belongs to the species EQ1-W2. In this case, *a*-type and *b*-type transitions with *J* up to 10 and *K_a* up to 3 were identified. While for species EQ1-W1 and EQ2-W1 only *a*-type spectra were observed. Transitions with *J* up to 10 and *K_a* up to 3 were identified for the species EQ1-W1 while for the species EQ2-W1 transitions with *J* up to 9 and *K_a* up to 3 were observed. The obtained experimental spectroscopic parameters are reported in table 1. [15,16]

Other conformations were searched long, but they were not found. In particular the configuration EQ2-W2 was expected but it was not observed. Probably this species relaxes on a more stable conformation, a process that takes place upon supersonic expansion, when the interconversion barrier between conformers is less than $2kT$ [17].

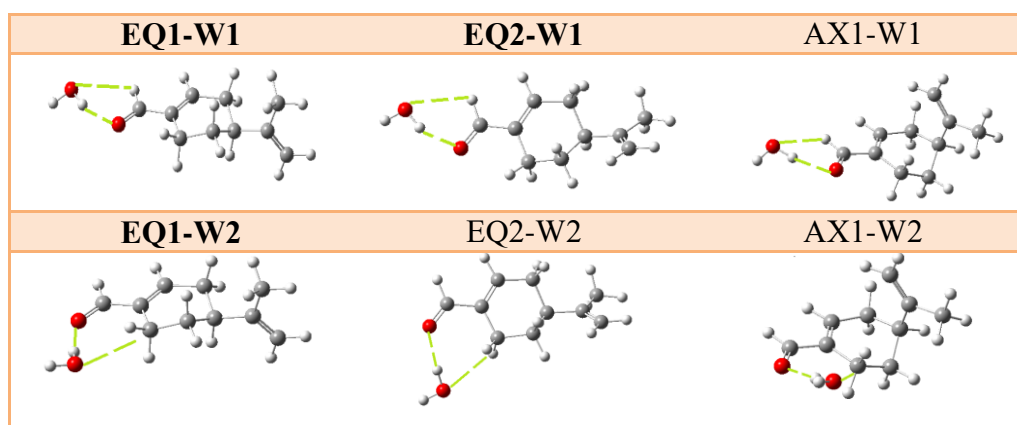


Figure 1: Depiction of the theoretical structures for PERY-H₂O clusters

Table 1: Theoretical and experimental spectroscopic parameters, relative energy and binding energies for PERY-H₂O clusters.

Calc.	EQ1_ W1	EQ2_ W1	AX1_ W1	EQ1_ W2	EQ2_ W2	AX1_ W2	Exp.	EQ1_ W1	EQ2_ W1	EQ1_ W2
A (MHz)	2750	2721	1767	1608	1634	1138	A (MHz)	2778(3) ^a	2746(1)	1614.39(2)
B (MHz)	318	323	399	427	424	632	B (MHz)	316.6911(5)	320.6735(6)	418.3800(3)
C (MHz)	307	300	393	374	371	503	C (MHz)	305.5936(5)	298.6852(5)	363.1279(4)
μ_a (D)	1.1	3.3	3.8	1.1	1.9	1.6	D_j (kHz)	0.017(2)	-	0.041(2)
μ_b (D)	3.4	0.0	0.2	3.1	2.7	2.7	D_{JK} (kHz)	-0.33(7)	0.12(8)	0.124(5)
μ_c (D)	0.4	0.7	0.2	0.1	0.6	0.0	N^b	30	21	54
ΔE_c (cm ⁻¹)	346	525	191	189	368	0	σ (kHz) ^c	5	8	6
ΔE_0 (cm ⁻¹)	265	448	169	90	280	0				
D_e (kJ/mol)	26	26.1	26.4	27.8	27.9	28.7				
D_e +BSSE (kJ/mol)	20.2	20.2	20.5	20.9	20.8	21.2				
P_{cc} (uÅ ²)	62.33	33.45	133.76	72.82	68.74	120.04	P_{cc} (uÅ ²)	61.985 [61.835]*	34.011 [33.472]	64.625 [61.835]

* Values of the monomer conformational species (EQ1, EQ2 and AX1). ^a Standard error in parentheses in the units of the last digit. ^b Number of transitions. ^c Root mean square deviation of the fit.

Results of PERY-(H₂O)₂

For PERY-(H₂O)₂, different geometries of the trimer formed between the two water molecules and the species, EQ1, EQ2 and AX1, were considered in optimization procedure. Several geometries were predicted to be energetic minima. The common features of these structures are: the water molecules interact between them to form a dimeric chain and this chain is always anchored to PERY by its carbonyl group. For the rest, the conformations can be split out into two groups. In a first group, indicated as “internal ring”, the water dimer lies above and below the ring plane and a second group, named “external ring”, in which the water dimer is about at the PERY ring height. A depiction of the structures is reported in figure 2.

Based on the values of rotational constants and dipole moment components, obtained from calculations, a prediction of the spectra was done for each one of these structures.

Two conformations of the “external ring” group, named EQ1-TWO-W and EQ2-TWO-W, were identified in the spectrum. In the two structures, the water dimer closes a ring with the aldehyde group of the EQ1 and EQ2 species through two intermolecular interactions: a main hydrogen bond, C=O_{PERY}--H_{H2O}, and a weaker interaction between the (C=O)_{PERY}--O_{H2O}. Only μ_a -type transitions

were observed in both cases. The obtained spectroscopic parameters are reported in table 3 and there compared with those obtained at MP2/6-311++G(d, p) theory level.

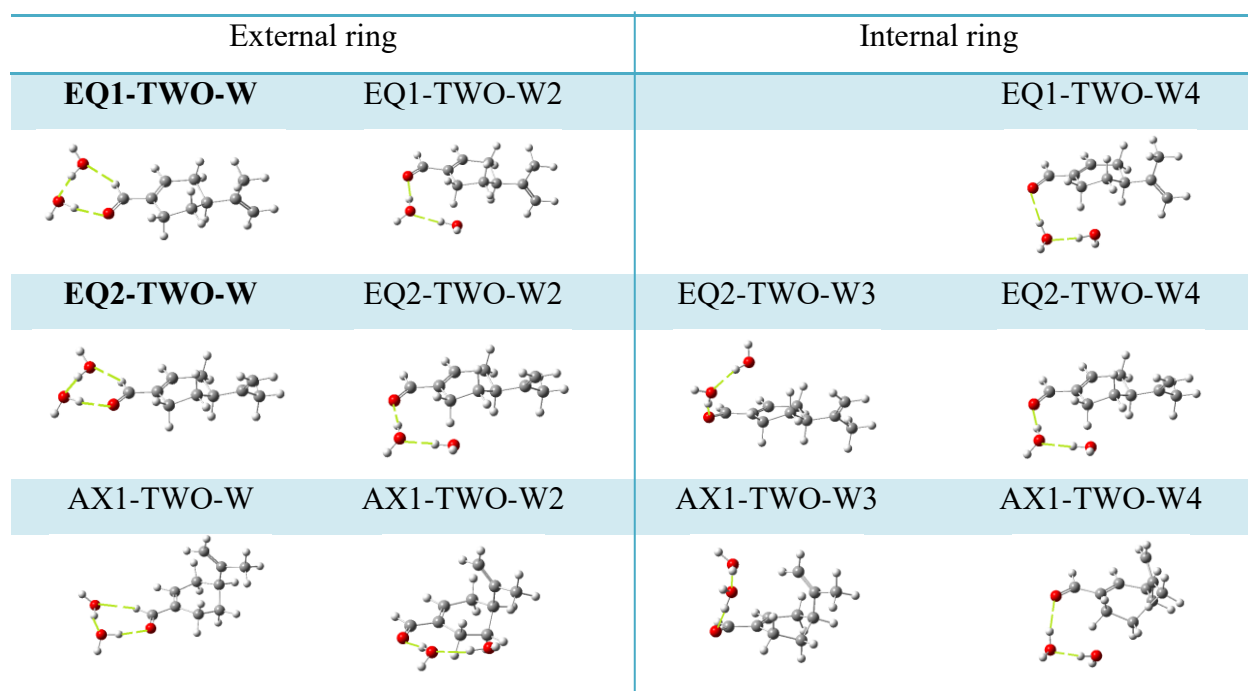


Figure 2: Depiction of the theoretical structures for PERY-(H₂O)₂ clusters.

Table 3: Theoretical and experimental spectroscopic parameters for PERY-(H₂O)₂, relative energy and binding energies for PERY-H₂O clusters.

	Theor.	Exp.	Theor.	Exp.
	EQ1-TWO-W	EQ1-TWO-W	EQ2-TWO-W	EQ2-TWO-W
A (MHz)	1782.53	1781.4(3) ^a	1755.07	1756.0(2)
B (MHz)	252.38	251.0348(5)	254.89	253.4826(5)
C (MHz)	234.12	232.7916(5)	230.62	229.3005(5)
D _j (kHz)	0.011	0.012(2)	0.012	0.013(2)
N ^b	-	29	-	28
σ (kHz) ^c	-	6	-	6
μ _a (D)	2.16	yes	2.16	yes
μ _b (D)	0.08	no	0.36	no
μ _c (D)	0.2	no	0.31	no
P _{cc} (uÅ ²)	63.669	62.965	39.647	38.770
ΔE (cm ⁻¹)	531.3	-	706.5	-
ZPE (cm ⁻¹)	511.8	-	693.1	-
B.E. (kJ/mol)	68.2	-	68.3	-
BSSE (kJ/mol)	51	-	51	-

^a Standard error in parentheses in the units of the last digit. ^b Number of transitions. ^c Root mean square deviation of the fit.

Table 4: Percentage differences ($\Delta\%$) between the sets of experimental and theoretical rotational constants.

	EQ1-W1	EQ1-W2	EQ1-W2	EQ1-TWO-W	EQ2-TWO-W
$\Delta A(\%)$	1	0.42	0.89	0.06	0.05
$\Delta B(\%)$	0.48	2.08	0.61	0.53	0.55
$\Delta C(\%)$	0.40	2.88	0.41	0.57	0.57

Discussions

From the analysis of the rotational spectrum, structural information on clusters PERY-H₂O and PERY-(H₂O)₂ can be deduced. A piece of the information results from the planar momentum of inertia P_{cc} , that is determinable directly from the rotational constants by the expression $P_{cc} = h/16\pi^2(1/A+1/B-1/C)$.

This value, describing the extension of the masses along the ab inertial axes ($P_{cc} = \sum_i m_i c_i^2$, m_i being the mass and c_i the c -coordinate of the i -th atom), provides a direct information on the planarity of structure. From the comparisons of clusters P_{cc} values with those of the species, EQ1 and EQ2, are obtained indications of the water position in the ab plane of the clusters.

For the clusters EQ1-W1, EQ2-W1, and EQ1-W2 are determined P_{cc} values equal to 61.985, 34.011 and 64.625 (uÅ²), respectively, while for the EQ1 and EQ2 species P_{cc} values are 61.835 and 33.472 (uÅ²), respectively. The similarity between P_{cc} values of EQ1-W1 and EQ1 suggests that in the cluster EQ1-W1, the water O is in the cluster ab plane. The small discrepancies between the P_{cc} values are ascribable to the out of plane water non-bonded hydrogen position.

While in the cases of EQ2-W1 and EQ1-W2, the difference between the clusters/monomer P_{cc} implicates that water O it is out of the ab plane of the monomer.

The same reasoning can be done for the clusters EQ1-TWO-W and EQ2-TWO-W. For these systems the P_{cc} values are 62.965 and 38.770 (uÅ²), respectively, to compare, with those of EQ1 (61.835 uÅ²) and EQ2 (33.472 uÅ²). So, the nearness between the P_{cc} of EQ1-TWO-W and EQ1 indicates that the two O's of the two water are in the ab plane of the cluster. The discrepancy between the two P_{cc} values can be attributed to the non-bonded hydrogen atoms of water adopting an up-down configuration.

While for EQ2-TWO-W the two values cluster/monomer P_{cc} not are similar then the two O's of the two water are out of the ab plane of the cluster.

The obtained experimental rotational constants for all species of PERY-H₂O and PERY-(H₂O)₂ are in very good agreement with theoretical those ones, suggesting that the experimental geometries are very similar to calculated those ones. The percentage differences ($\Delta\%$) between the sets of experimental and theoretical rotational constants are reported in table 4.

In summary, monohydrated and dehydrated clusters of the biomolecule, s-(-)-perillaldehyde have been observed.

For PERY-H₂O, three conformations, EQ1-W1, EQ2-W1 and EQ1-W2, were identified. The three species show a ring-shaped geometry in which the two subunits are held together through two intermolecular bonds: a main hydrogen bond, C=O_{PERY}--H_{H2O}, and a weaker interaction between the CH_{PERY}--O_{H2O}. In the structures EQ1-W1, EQ2-W1 this bond involves the carbaldehyde group H while in EQ1-W2 it involves two ring H's. Among the three species, EQ1-W2 has the spectrum more intense, corresponding also to that with higher calculated binding energy.

Whereas for PERY-(H₂O)₂, two configurations EQ1-TWO-W and EQ2-TWO-W were identified. In both configurations, the water dimer closes a ring with the aldehyde group of the EQ1 and EQ2 species. The two subunits are held through two intermolecular interactions: a main hydrogen bond, C=O_{PERY}--H_{H2O}, and a weaker interaction between the (C=O)H_{PERY}--O_{H2O}. These structures can be considered as the result of H₂O addition to the heterodimers configuration EQ1-W1 and EQ2-W1.

While, no cluster involving the conformer AX1 of PERY was observed.

Since the experimental and theoretical rotational constants are very similar, the theoretical internal coordinates were used to evaluate possible structural changes in the observed clusters.

If the structures of the heterodimers EQ1-W1/EQ2-W1 and heterotrimers EQ1-TWO-W/EQ2-TWO-W are compared, it can be seen that the addition of water to EQ1-W1 and EQ2-W1 species to form EQ1-TWO-W and EQ2-TWO-W, respectively, implicates some structural changes in the hydrogen bonds network.

The angle <C=O--H passes from 102.59°/103.29° in the heterodimers to 110.16°/110.12° in the heterotrimers while, the angle indicating the linearity of the hydrogen bond, <O--HO switches from 156.21°/156.66° to 163.78°/163.78°, respectively.

Another difference concerns the hydrogen bond length (O--H). This distance passes from 1.95/1.95 (Å) in the heterodimers to 1.85/1.85 (Å) in the heterotrimers. This shortening is an evidence of the existence of cooperative effects in hydrogen bond complexes, an effect already observed in other cases like (H₂O)₃ [18], HCl-(H₂O)₂ [19], 2-pyridone-(H₂O)₂ [20], formamide-(H₂O)₂ [4], camphor-(H₂O)₂ [12], and azetidone-(H₂O)₂ [21].

References

- [1] P. Stockman, G. Blake, F. Lovas, R. Suenram, *J. Chem. Phys.*, 1997, 107
- [2] S. Melandri, A. Maris, P. Favero, W. Caminati, *Chem. Phys.*, 2002, 283
- [3] G. Feng, L. Favero, A. Maris, A. Vigorito, W. Caminati, R. Meyer, *J. Am. Chem. Soc.*, 2012, 134
- [4] S. Blanco, J. Lopez, A. Lesarri, J. Alonso, *J. Am. Chem. Soc.*, 2006, 128
- [5] W. Caminati, A. Dell'Erba, S. Melandri, P. Favero, *J. Am. Chem. Soc.*, 1998, 120
- [6] F. Lovas, C. Lugez. *J. Mol. Spectrosc.* 1996, 179
- [7] D. Steyert, M. Elrod, R. Saykally, F. Lovas, R. Suenram, *J. Chem. Phys.* 1993, 99, (10)
- [8] S. Suzuki, P. Green, R. Bumgarner, S. Dasgupta, W. Goddard et al., *Science*, 1992, 257
- [9] J. Neill, S. Shipman, L. Alvarez-Valtierra, A. Lesarri, Z. Kisiel, and B. Pate, *J. Mol. Spectrosc.*, 2011, 269
- [10] D. Loru, M. Bermudez, M. Sanz, *J. Chem. Phys.*, 2016, 145
- [11] C. Perez, J. Neill, M. Muckle, Zalensky, et al. *Angew. Chem.*, Int. Ed. 2015, 54
- [12] C. Perez, A. Krin, A. Steber, J. Lopez, Z. Kisiel, M. Schnell, *J. Phys. Chem., Lett.*, 2016, 7, 154-160
- [13] S. Boys, F. Bernardi, *Mol. Phys.* 1970, 19
- [14] M.J. Frisch, G.W. Trucks, H.B. Schlegel, G.E. Scuseria, M.A. Robb, J.R. Cheeseman, G. Scalmani, V. Barone, B. Mennucci, G. A. Petersson, H. Nakatsuji, M. Caricato, X. Li, H.P. Hratchian, A.F. Izmaylov, J. Bloino, G. Zheng, J.L. Sonnenberg, M. Hada, M. Ehara, K. Toyota, R. Fukuda, J. Hasegawa, M. Ishida, T. Nakajima, Y. Honda, O. Kitao, H. Nakai, T. Vreven, J.A. Montgomery Jr., J.E. Peralta, F. Ogliaro, M. Bearpark, J.J. Heyd, E. Brothers, K.N. Kudin, V.N. Staroverov, T. Keith, R. Kobayashi, J. Normand, K. Raghavachari, A. Rendell, J. C. Burant, S.S. Iyengar, J. Tomasi, M. Cossi, N. Rega, J. M. Millam, M. Klene, J.E. Knox, J.B. Cross, V. Bakken, C. Adamo, J. Jaramillo, R. Gomperts, R.E. Stratmann, O. Yazyev, A.J. Austin, R. Cammi, C. Pomelli, J. Ochterski, R.L. Martin, K. Morokuma, V.G. Zakrzewski, G.A. Voth, P. Salvador, J.J. Dannenberg, S. Dapprich, A.D. Daniels, O. Farkas, J.B. Foresman, J.V. Ortiz, J. Cioslowski, D. Fox, Gaussian 09, Revision D.01, Gaussian, Inc., Wallingford, CT
- [15] H. M. Pickett, *J. Mol. Spectrosc.*, 148 (1991) 371-377.
- [16] J.K.G. Watson, in *Vibrational Spectra and Structure*; Durig, J.R., Ed.; Elsevier: Amsterdam, 1977; Vol. 6, pp 1-89
- [17] R. Ruoff, T. Klots, T. Emilson, H. Gutowski, *J. Chem. Phys.*, 1990, 93
- [18] a) F. Keutsch, J. Cruzan, R. Saykally, *Chem. Rev.*, 2003, 103; b) K. Liu, M. Brown, J. Cruzan, R. Saykally, *J. Phys. Chem. A*, 1997, 101; c) F. Keutsch, R. Saykally, *Proc. Natl. Acad. Sci., U.S.A.*, 2001, 98
- [19] a) Z. Kisiel, E. Bialkowska, -Jaworska, I. Pszczolkowski, A. Milet, C. Struniewicz, R. Moszynski, J. Sadlej *J. Chem. Phys.*, 2000, 112; b) A. Milet, C. Struniewicz, R. Moszynski, J. Sadlej, Z. Kisiel, E. Bialkowska, -Jaworska, Pszczolkowski, *Chem. Phys.*, 2001, 271

- [20] a) A. Held, D. Pratt, *J. Am. Chem. Soc.*, 1993, 115; b) S. Mata, V. Cortijo, W. Caminati, J. Alonso, M. Sanz, J. Lopez, S. Blanco, *J. Phys. Chem. A*, 2010, 114
- [21] J. Lopez, R. Sanchez, S. Blanco, J. Alonso, *Phys. Chem. Chem. Phys.*, 2015, 17

2) MICROSOLVATATION OF HETEROCYCLIC RINGS: THE ROTATIONAL SPECTRA OF IMIDAZOLIDINONE-WATER, PYRROLIDINONE-WATER AND OXAZOLIDINONE-WATER COMPLEXES

Introduction

Many water complexes characterized from large amplitude motions between equivalent conformers have been observed by rotational spectroscopy. Useful information, concerning their dynamics can be obtained from the analysis of the hyperfine structures, due to tunnel effect, within their spectra.

Generally speaking, the tunnel effect produces the splitting of vibrational energy levels in two vibrational sublevels (namely 0 and 1), separated from an energy difference (ΔE_{01}). Intrastate ($0 \rightarrow 0$ and $1 \rightarrow 1$) or interstate transitions ($0 \rightarrow 1$ and $1 \rightarrow 0$) can take place between these sublevels leading to observation of hyperfine structures in the spectrum.

The possibility that occur intrastate or interstate rotational transitions, depends from the behavior of the electric dipole moment components along the inertial axes ($\mu_g, g=a, b, c$) during the motion.

Depending on whether, the μ_g sign is unchanged or reversed, during the motion, intrastate and interstate transitions are observed, respectively. So, owed to their identification, it is possible to infer information on the motion pathway. In addition, from ΔE_{01} , the potential energy surface governing these motions can be determined using Meyer's Flexible model [1].

The propensity of the water clusters to show tunneling splitting in their spectra depends from the combination of several factors such as: i) effect mass reduced, ii) motion hindering barrier height, iii) pathway motion and iv) resolution of the spectrometer. A review on the possible dynamics in water clusters, obtained from the analysis, of their spectra, was reported by Evangelisti et al. [2].

In this work, the dynamics and structure in water clusters with a cyclic amide series have been investigated through their spectra recorded by free-jet absorption millimeter wave spectrometer [3].

The amide (or peptide) group constitutes one of the most important binding sites for water in biological environments. This feedback governs the folding and molecular recognition processes in proteins, so the understanding of structural and energetic features of the involved interactions is of special relevance.

Rotational spectroscopy studies on molecular clusters between amide compounds and water, have revealed the key factors stabilizing these structures. For instance, the characterizations of formamide-(H₂O)_n (n=1,2) [4,5], N-methyl-formamide-H₂O [6], alaninamide-H₂O [7], 2-pyridone-(H₂O)_n (n=1,2) [8,9,10] and 2-azetidinone-water [11], have shown that the water molecule tends preferentially to form cyclic structures with the amide group, in which the two subunits are held through two hydrogen bonds: C=O--HO_{H2O} and NH--O_{H2O}, respectively.

In addition, in the formamide-water system also two less stable conformations were found. In one of them, water still forms a cyclic structure with formamide, stabilized by a hydrogen bond $C=O\cdots HO_{H_2O}$, but the second interaction is $CH\cdots O_{H_2O}$. While in the other conformation, the two units interact through a single hydrogen bond of the kind $NH\cdots O_{H_2O}$ and its spectrum shows tunneling splittings due to water internal rotation around the intermolecular bond.

In this work, the clusters between 2-imidazolidinone-water, 2-pyrrolidinone-water and 2-oxazolidinone-water (hereafter IMI-W, PYR-W and OXA-W, respectively) have been considered.

The three monomers, 2-imidazolidinone, 2-pyrrolidinone and 2-oxazolidinone, (hereafter IMI, PYR and OXA, respectively), were previously characterized. Their spectra showed rotational transitions doublings, due to the tunnel effect. These splittings reveal the existence of two twisted equivalent conformations connected by an inversion ring motion. From the resolution of the hyperfine structure, the energy differences between the two vibrational sublevels were determined: ΔE_{01} (OXA)= $0.173157(1) \text{ cm}^{-1}$, ΔE_{01} (PYR)= $0.00737(7) \text{ cm}^{-1}$, ΔE_{01} (IMI)= $0.0024495(8) \text{ cm}^{-1}$.

Experimental section

Commercial samples of IMI, PYR and OXA, were purchased from Alfa Aesar and used as received. IMI ($C_3H_6N_2O \cdot 0.5H_2O$, m.w. 95.10, 98+%) and OXA ($C_3H_5NO_2$, m.w. 87.08, 99%) appear as white crystalline solid with the melting point 55° and $84\text{-}89^\circ \text{ C}$, at ambient conditions, respectively. While PYR (C_4H_7NO , m.w. 85.11, 99%) is a liquid substance with melting point $23\text{-}25^\circ \text{C}$, at ambient conditions. IMI, PYR and OXA were located in a warmed reservoir at $120^\circ\text{-}130^\circ \text{C}$ and $85\text{-}90^\circ$, and $100\text{-}110^\circ$ respectively, while water was placed in another reservoir at room temperature. The complexes IMI-W, PYR-W and OXA-W were prepared by passing a stream of argon at a pressure of about 400 kPa over two containers. The mixtures were, then, expanded from a stagnation pressure of 45 kPa to about 0.5 Pa through a 0.35 mm diameter pinhole nozzle. These settings have been found as optimal for the formation of the 1:1 complex in our experiments. The spectra were recorded by the free-jet Stark modulated millimeter wave absorption spectrometer. Details of experimental setup are given in ref.12,13 and 14. The resolution and the estimated accuracy of the frequency measurements are about 300 kHz respectively.

Results

Before collecting the spectra, plausible geometries of the heterodimers, IMI-W, PYR-W and OXA-W, were considered in optimization procedure. All quantum mechanical computations were performed using the Gaussian 09 quantum chemistry package. [15] Calculations at the B3LYP/6-

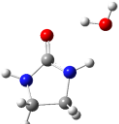
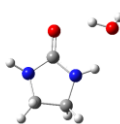
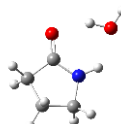
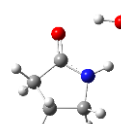
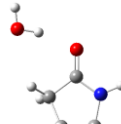
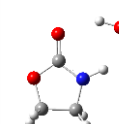
311++G(d, p) theory level have been performed to predict the rotational constants, the dipole moment components along the principal axes of inertia a , b , c , the ^{14}N quadrupole coupling constants ($I=I$) and binding energies of the obtained conformations.

The depiction of the structures with the calculations results are reported in table 1.

The three clusters, IMI-W, PYR-W and OXA-W, show two configurations of slightly different energy. The two conformers have a ring-shaped geometry in which the two subunits are held together through two hydrogen bonds: one between $\text{C}=\text{O}\cdots\text{H}_{2}\text{O}$ and another between $\text{NH}\cdots\text{O}_{\text{H}_2\text{O}}$. The two structures differ because NH group can bind $\text{O}_{\text{H}_2\text{O}}$ lone pair one side or the other.

In addition, for the system PYR-W also a less stable structure, labelled PYR-W3, was predicted to be energetic minimum. This conformation has still a cyclic structure but in this case the two subunits are held together though one hydrogen bond $\text{C}=\text{O}\cdots\text{H}_{2}\text{O}$ and weak interaction $\text{CH}_2\cdots\text{O}_{\text{H}_2\text{O}}$.

Table1: Calculated spectroscopic parameters for three clusters: IMI-W, PYR-W and OXA-W

	IMI-W1	IMI-W2	PYR-W1	PYR-W2	PYR-W3	OXA-W1	OXA-W2
							
A (MHz)	4954.09	4978.30	4763.16	4766.51	5098.16	4971.88	5002.75
B (MHz)	1672.84	1666.75	1624.49	1622.83	1426.80	1712.50	1702.13
C (MHz)	1284.70	1280.22	1248.17	1247.39	1145.17	1306.02	1299.74
μ_a (D)	3.41	3.52	2.83	2.82	4.48	2.05	2.22
μ_b (D)	1.38	1.29	1.61	1.61	0.21	3.43	3.40
μ_c (D)	1.06	0.88	0.73	0.71	0.09	0.77	1.14
ΔE (cm-1)	0	11	10	0	861	0	32
B. E. (kJ/mol)	41	41	41	41	32	40	40
χ_{aa} (MHz)	3.35	2.29	1.98	1.98	2.16	2.09	3.24
χ_{bb} (MHz)	1.82	2.51	2.01	2.01	2.23	2.63	1.85
χ_{cc} (MHz)	0.50	-4.79	-3.99	-3.99	-4.39	4.72	0.50
χ_{aa} (MHz)	3.96	2.62	-	-	-	-	-
χ_{bb} (MHz)	1.90	2.48	-	-	-	-	-
χ_{cc} (MHz)	0.22	-5.01	-	-	-	-	-
P_{cc} (uÅ)	5.37	4.985	6.185	6.148	6.010	4.899	4.55

Rotational spectra

The spectra of OXA-W and IMI-W were recorded in the 59.6-74.4 GHz frequency range while that of PYR-W was recorded in the 52-74.4 GHz frequency range by the free-jet Stark modulated millimeter wave absorption spectrometer.

Based on the predicted values of the spectroscopic constants and electric dipole moment components, the spectra of three molecular systems can be assigned both to the structures IMI-W1 or IMI-W2, OXA-W1 or OXA-W2 and PYR-W1 or PYR-W2.

The spectra of IMI-W and PYR-W were very weak. Theoretical calculations estimated for these clusters mainly μ_a and μ_b dipole moment components. However only a μ_b -type spectra with J up to 14 and K_a up to 7 were observed because μ_a -type transitions were expected at high, little populated, J levels.

No hyperfine structures due to ^{14}N quadrupole nucleus or large amplitude motions were resolved. The transitions were fitted with Pickett's SPFIT [16, 17] program, using a semirigid rotor Hamiltonian in the S -reduction and the I'' -representation [18]. The obtained rotational constants and quartic centrifugal distortions constants are reported in table 2.

The spectrum of OXA-W showed rotational transitions, split in two components of equal intensities. This hyperfine structure indicated the presence of a large amplitude motion, that connects equivalent conformations. The b -type intrastate transitions, namely $0 \rightarrow 0$ and $1 \rightarrow 1$, were identified.

The rotational transitions doublings were fit using a coupled Hamiltonian:

$$H = H_{0,R} + H_{1,R} + H_{CD} + H_{Int}$$

$$H_{Int} = \Delta E_{01} + F_{bc} (P_b P_c + P_c P_b)$$

where $H_{0,R}$ and $H_{1,R}$ are the rigid Hamiltonian relative to vibrational sublevels 0 and 1, H_{CD} is the Watson S -reduced centrifugal distortion Hamiltonian and H_{Int} is the interaction Hamiltonian between two sublevels, in which ΔE_{01} is the energy separation between the sublevels 0 and 1 and F_{bc} is the Coriolis's interaction constant, that take in account the coupling of the two sublevels. The two obtained sets rotational constants, centrifugal distortion constants, ΔE_{01} and F_{bc} are reported in table 2.

The hyperfine structure in OXA-W1 can be attributed to the water and ring inversion motions combination. For the OXA monomer had been determined a ΔE_{01} equal to $0.173157(1) \text{ cm}^{-1}$ while for the OXA-W1 complex is $0.16678(3)$. The lowering ΔE_{01} in the complex can be attributed to the reduced mass effect of the water.

While, the absence of hyperfine structure in the spectra of PYR-W1 and IMI-W1 can be explained from the fact that the tunneling splittings for the PYR and IMI monomers were much small and the presence of water has furthermore reduced these splittings.

Table 2: Experimental spectroscopic parameters for three clusters: IMI-W, PYR-W and OXA-W

	IMI-W1	PYR-W1	OXA-W1	
			v=0	v=1
A (MHz)	4969.68(2)	4770.72(1)	4991.668(9) ^a	4992.146(9)
B (MHz)	1673.39(2)	1626.31(1)	1709.72(2)	1709.29(2)
C (MHz)	1285.75(2)	1251.46(1)	1304.98(3)	1304.95(2)
$\mu_a/\mu_b/\mu_c^c$	no/ yes /no	no/ yes/ no	no/ yes/ no	
D _J (kHz)	0.57(3)	0.48(2)	0.20(3)	
D _{JK} (kHz)	-1.17(9)	-0.65(8)	0	
D _K (kHz)	5.3(3)	3.9(2)	5.2(1)	
ΔE_{01} (MHz)	-	-	5000(1)	
F _{bc} (MHz)	-	-	6.4(1)	
N ^b	18	30	35	
σ (kHz) ^c	109	72	89	
P _{cc} (uÅ ²)	5.316	6.427	4.817	

^a Standard error in parentheses in the units of the last digit. ^b Number of transitions. ^c Root mean square deviation of the fit. ^d Yes or no observation of *a*-, *b*-, and *c*-type transitions, respectively.

Conclusion

In this work the microsolvation effect on a lactams series have been investigated by free-jet absorption millimeter wave spectrometer.

This study can be considered an excellent model for explaining the water binding preferences in proteins. In three molecular systems, 2-imidazolidinone-water, 2-pyrrolidinone-water and 2-oxazolidinone-water, the water close a cycle with the amide group. The two subunits are held through two hydrogen bonds: C=O--HO_{H2O} and NH-O_{H2O}, respectively.

The results are in agreement with the theoretical calculations, performed at B3LYP/6-311++G(d, p) level theory, and the experimental evidences reported for other water clusters with binding partners containing the peptide group [4-11].

In spectrum of 2-oxazolidinone-water, the hyperfine structure arising from the water and ring inversion motions combination was observed.

References

- [1] R. Meyer, *J. Mol. Spect.*, 1979, 76
- [2] L. Evangelisti, W. Caminati, *Phys. Chem. Chem. Phys.*, 2010, 12
- [3] F. Lovas, R. Suenram, G. Fraser, C. Gillies, J. Zozom, *J. Chem. Phys.*, 1988, 88
- [4] S. Blanco, J. Lopez, A. Lesarri, J. Alonso, *J. Am. Chem. Soc.*, 2006, 128, (37)

- [5] L. Lavrich, M. Tubergen, *J. Am. Chem. Soc.*, 2000, 122
- [6] W. Caminati, J. Lopez, S. Blanco, S. Mata, J. Alonso, *Phys. Chem. Chem. Phys.*, 2010, 12
- [7] A. Maris, P. Ottaviani, W. Caminati, *Chem. Phys. Lett.*, 2002, 360
- [8] A. Held, D. Pratt, *J. Am. Chem. Soc.*, 1993, 115
- [9] S. Mata, V. Cortijo, W. Caminati, J. Alonso, M. Sanz, J. Lopez, S. Blanco, *J. Phys. Chem. A*, 2010, 114
- [11] J. Lopez, R. Sanchez, S. Blanco, J. Alonso, *Phys. Chem. Chem. Phys.*, 2015, 17
- [12] S. Melandri, W. Caminati, L. Favero, A. Millemaggi and P. Favero, *J. Mol. Struct.*, 1995, 352/353
- [13] S. Melandri, G. Maccaferri, A. Maris, A. Millemaggi, W. Caminati, and P. Favero, *Chem. Phys. Lett.*, 1996, 261
- [14] C. Calabrese, A. Maris, L. Evangelisti, L. Favero, S. Melandri, W. Caminati, *J. Phys. Chem. A.*, 2013, 117
- [15] M.J. Frisch, G.W. Trucks, H.B. Schlegel, G.E. Scuseria, M.A. Robb, J.R. Cheeseman, G. Scalmani, V. Barone, B. Mennucci, G. A. Petersson, H. Nakatsuji, M. Caricato, X. Li, H.P. Hratchian, A.F. Izmaylov, J. Bloino, G. Zheng, J.L. Sonnenberg, M. Hada, M. Ehara, K. Toyota, R. Fukuda, J. Hasegawa, M. Ishida, T. Nakajima, Y. Honda, O. Kitao, H. Nakai, T. Vreven, J.A. Montgomery Jr., J.E. Peralta, F. Ogliaro, M. Bearpark, J.J. Heyd, E. Brothers, K.N. Kudin, V.N. Staroverov, T. Keith, R. Kobayashi, J. Normand, K. Raghavachari, A. Rendell, J. C. Burant, S.S. Iyengar, J. Tomasi, M. Cossi, N. Rega, J. M. Millam, M. Klene, J.E. Knox, J.B. Cross, V. Bakken, C. Adamo, J. Jaramillo, R. Gomperts, R.E. Stratmann, O. Yazyev, A.J. Austin, R. Cammi, C. Pomelli, J. Ochterski, R.L. Martin, K. Morokuma, V.G. Zakrzewski, G.A. Voth, P. Salvador, J.J. Dannenberg, S. Dapprich, A.D. Daniels, O. Farkas, J.B. Foresman, J.V. Ortiz, J. Cioslowski, D. Fox, Gaussian 09, Revision D.01, Gaussian, Inc., Wallingford, CT
- [16] H. Pickett, *J. Mol. Spectrosc.*, 1991, 148
- [17] J. Watson, in *Vibrational Spectra and Structure*; Durig, J.R., Ed.; *Elsevier: Amsterdam*, 1977, 6